

# **OPERATIONAL RELIABILITY AND RISK EVALUATION FRAMEWORKS FOR SUSTAINABLE ELECTRIC POWER SYSTEMS**

A Thesis Submitted to the

College of Graduate and Postdoctoral Studies

In Partial Fulfillment of the Requirements

For the Degree of Doctor of Philosophy

In the Department of Electrical and Computer Engineering

University of Saskatchewan

Saskatoon, Saskatchewan, Canada

By

**Osama Aslam Ansari**

© Copyright Osama Aslam Ansari, March 2021. All rights reserved.  
Unless otherwise noted, copyright of the material in this thesis belongs to the author.

## **Permission to Use**

In presenting this thesis in partial fulfillment of the requirements for a Postgraduate degree from the University of Saskatchewan, I agree that the Libraries of this University may make it freely available for inspection. I further agree that permission for copying of this thesis in any manner, in whole or in part, for scholarly purposes may be granted by the professor or professors who supervised my thesis work or, in their absence, by the Head of the Department or the Dean of the College in which my thesis work was done. It is understood that any copying or publication or use of this thesis or parts thereof for financial gain shall not be allowed without my written permission. It is also understood that due recognition shall be given to me and to the University of Saskatchewan in any scholarly use which may be made of any material in my thesis.

Requests for permission to copy or to make other uses of materials in this thesis in whole or part should be addressed to:

Head of the Department of Electrical and Computer Engineering  
University of Saskatchewan  
57 Campus Drive  
Saskatoon, Saskatchewan, S7N 5A9  
Canada

OR

Dean of the College of Graduate and Postdoctoral Studies  
University of Saskatchewan  
116 Thorvaldson Building, 110 Science Place  
Saskatoon, Saskatchewan, S7N 5C9,  
Canada

# Abstract

Driven by a confluence of multiple environmental, social, technical, and economic factors, traditional electric power systems are undergoing a momentous transition toward sustainable electric power systems. One of the important facets of this transformation is the inclusion of high penetration of variable renewable energy sources, the chief among them being wind power. The new source of uncertainty that stems from imperfect wind power forecasts, coupled with the traditional uncertainties in electric power systems, such as unplanned component outages, introduces new challenges for power system operators. In particular, the short-term or operational reliability of sustainable electric power systems could be at increased risk as limited remedial resources are available to the operators to handle uncertainties and outages during system operation. Furthermore, as sustainable electric power systems and natural gas networks become increasingly coupled, the impacts of outages in one network can quickly propagate into the other, thereby reducing the operational reliability of integrated electric power-gas networks (IEPGNs).

In light of the above discussion, a successful transition to sustainable electric power systems necessitates a new set of tools to assist the power system operators to make risk-informed decisions amid multiple sources of uncertainties. Such tools should be able to realistically evaluate the hour- and day-ahead operational reliability and risk indices of sustainable electric power systems in a computationally efficient manner while giving full attention to the uncertainties of wind power and IEGPNs. To this end, the research is conducted on five related topics.

First, a simulation-based framework is proposed to evaluate the operational reliability indices of generating systems using the fixed-effort generalized splitting approach. Simulations show improvement in computational performance when compared to the traditional Monte-Carlo simulation (MCS). Second, a hybrid analytical-simulation framework is proposed for the short-term risk assessment of wind-integrated power systems. The area risk method – an analytical technique, is combined with the importance sampling (IS)-based MCS to integrate the proposed reliability models of wind speed and calculate the risk indices with a low computational burden. Case studies validate the efficacy of the proposed framework. Third, the importance sampling-based MCS framework is extended to include the proposed data-driven probabilistic models of

wind power to avoid the drawbacks of wind speed models. Fourth, a comprehensive framework for the operational reliability evaluation of IEPGNs is developed. This framework includes new reliability models for natural gas pipelines and natural gas-fired generators with dual fuel capabilities. Simulations show the importance of considering the coupling between the two networks while evaluating operational reliability indices. Finally, a new chance-constrained optimization model to consider the operational reliability constraints while determining the optimal operational schedule for microgrids is proposed. Case studies show the tradeoff between the reliability and the operating costs when scheduling the microgrids.

## Acknowledgements

Firstly, I am highly grateful to God Almighty, who, in His immeasurable capacity of knowledge and kindness, granted me the patience and strength to work on this thesis.

I owe my deepest gratitude to my supervisor, Dr. C. Y. Chung. Without his invaluable guidance, encouragement, and continuous support, this thesis would not have been completed. His breadth of knowledge and vast experience was crucial toward the completion of my research work.

I would like to pay my sincere gratitude to members of my advisory committee, Dr. Rajesh Karki, Dr. Nurul Chowdhury, Dr. Ha Nguyen, Dr. Shafiq Alam, and the external advisor Dr. Chanan Singh, for their valuable and useful suggestions which served to improve the quality of my thesis. I would also like to thank my graduate study professors, Dr. Ha Nguyen, Dr. Brian Berscheid, and Dr. Greg Poelzer, for broadening my knowledge on the topics of machine learning and renewable energy transition.

A very special thanks go out to all students and staff at the Smart Grid and Energy Network (SMARTGEN) Lab for creating a pleasant working environment and for several insightful technical discussions and many hours of brainstorming.

I would also like to gratefully acknowledge the financial support for my Ph.D. degree from the NSERC/SaskPower Senior Industrial Research Chair Program and the University of Saskatchewan.

Last but not least, I would like to pay special heartiest thanks to my family: my parents, my brothers, and my sister, for rendering unfailing support, endless encouragement, and unconditional love during my time as a Ph.D. student. I would not have accomplished this achievement without them.

Thank you all for your support

# Table of Contents

<b>Permission to Use .....</b>	<b>ii</b>
<b>Abstract.....</b>	<b>iii</b>
<b>Acknowledgements .....</b>	<b>v</b>
<b>Table of Contents .....</b>	<b>vi</b>
<b>List of Tables .....</b>	<b>xii</b>
<b>List of Figures.....</b>	<b>xiv</b>
<b>List of Abbreviations .....</b>	<b>xvii</b>
<b>Chapter 1      Introduction.....</b>	<b>1</b>
1.1      Motivation.....	1
1.2      Key Challenges .....	3
1.2.1      Multiple Sources of Uncertainties During System Operation .....	3
1.2.2      Computational Efficiency of Reliability and Risk Assessment Methods .....	4
1.2.3      Integration of Probabilistic Approaches in System Operation Practices .....	5
1.3      Literature Review.....	6
1.3.1      Uncertainty Modeling of Wind Generation for Operational Reliability Evaluation 6	
1.3.2      Reliability and Risk Evaluation Techniques.....	8
1.4      Research Questions .....	11
1.5      Contributions of the Thesis .....	13
1.5.1      Development of an importance-splitting based simulation framework for the operational reliability evaluation of generating systems .....	13
1.5.2      Development of a hybrid analytical-simulation framework for operational risk assessment.....	13

1.5.3	Development of a data-driven framework for the operational risk assessment of wind-integrated power systems.....	14
1.5.4	Development of a simulation framework for the operational reliability evaluation of IEGPNs.....	14
1.5.5	Development of the operational reliability-constrained optimal scheduling model for microgrids.....	15
1.6	Organization of the Thesis .....	15
<b>Chapter 2</b>	<b>Mathematical Foundations of the Operational Reliability and Risk Assessment of Power Systems .....</b>	<b>18</b>
2.1	Introduction.....	18
2.2	Probabilistic Modeling of Power Systems.....	19
2.2.1	Discrete RVs for Generators.....	20
2.2.2	Discrete RVs for Transmission Lines .....	21
2.3	Operational Reliability Evaluation Technique.....	22
2.3.1	Simulation Approach .....	22
2.4	Variance Reduction Techniques .....	25
2.4.1	Importance Sampling (IS).....	25
2.4.2	Importance Splitting.....	26
2.5	Proposed FEGS Approach .....	28
2.5.1	Selection of Intermediate Levels .....	28
2.5.2	FEGS Simulation Framework.....	29
2.5.3	MCMC for Discrete PDFs of Generating System .....	31
2.5.4	Inclusion of Uncertainties of Load and Wind Generation .....	32
2.6	Results.....	33
2.6.1	Demonstrative Case .....	33
2.6.2	Impact of Load Uncertainty .....	34

2.6.3	Impact of Wind Generation Uncertainty.....	35
2.7	Conclusion .....	35
<b>Chapter 3</b>	<b>A Hybrid Framework for Short-Term Risk Assessment of Wind-Integrated Composite Power Systems.....</b>	<b>37</b>
3.1	Abstract .....	37
3.2	Introduction.....	38
3.3	Preliminaries of the Area Risk Method .....	41
3.3.1	Conventional Generators Modeling.....	41
3.3.2	Transmission Lines Modeling.....	42
3.4	Proposed Reliability Modeling of Wind Generation .....	42
3.5	Proposed Risk Assessment Framework .....	48
3.5.1	Modified Area Risk Method .....	49
3.5.2	Evaluation of Partial Risks via CE-MCS.....	50
3.5.3	Overall Framework .....	53
3.6	Case Studies .....	55
3.6.1	Demonstrative Case .....	55
3.6.2	Computational Performance .....	57
3.6.3	Composite Power System Risk Indices .....	58
3.6.4	Daily Short-Term Risk Indices .....	60
3.6.5	Spinning Reserve Assessment .....	61
3.6.6	Sensitivity to the Wind Generation Penetration.....	62
3.6.7	Sensitivity to the CE Parameters.....	63
3.6.8	Practical Considerations.....	63
3.7	Conclusion .....	63
<b>Chapter 4</b>	<b>Data-Driven Operational Risk Assessment of Wind-Integrated Power Systems via Mixture Models and Importance Sampling.....</b>	<b>65</b>

4.1	Abstract .....	65
4.2	Introduction.....	66
4.3	The Preamble of Operational Risk Assessment.....	69
4.4	Proposed Probabilistic Modeling of Wind Power .....	71
4.5	Proposed short-term risk assessment method .....	76
4.6	Simulation Results .....	80
4.6.1	GMM Model .....	80
4.6.2	Operational risk indices for IEEE RTS.....	82
4.6.3	Computational Performance .....	83
4.6.4	Impact of Wind Farm Location.....	84
4.6.5	Operational risk indices for 3-area IEEE RTS.....	85
4.7	Conclusion .....	86
<b>Chapter 5</b>	<b>A Novel Framework for the Operational Reliability Evaluation of Integrated Electric Power-Gas Networks.....</b>	<b>88</b>
5.1	Abstract.....	88
5.2	Introduction.....	89
5.3	Reliability Model of IEPGNs.....	91
5.3.1	Reliability Model of Natural Gas Pipelines .....	92
5.3.2	Reliability Modeling of DF-NGFGs.....	95
5.4	Framework Proposed for Operational Reliability Evaluation of IEPGNs.....	96
5.4.1	Area Risk Method.....	97
5.4.2	Proposed Optimization Model for Minimum Load Curtailments.....	99
5.4.3	CE-IS based NSCMS .....	101
5.5	Simulation Results .....	102
5.5.1	Demonstrative Cases.....	104

5.5.2	Impact of Failures of Natural Gas Pipelines .....	105
5.5.3	Impacts of DF-NGFGs.....	106
5.5.4	Practical Considerations.....	106
5.5.5	Case Studies for <i>Test System B</i> .....	107
5.6	Conclusion .....	108
<b>Chapter 6</b>	<b>Operational Reliability-Constrained Scheduling of Microgrids via Cross-Entropy Importance Sampling-based Sample Average Approximation .....</b>	<b>109</b>
6.1	Abstract.....	109
6.2	Nomenclature.....	110
6.3	Introduction.....	112
6.4	Deterministic Model Formulation.....	114
6.5	Proposed Chance-Constrained Optimization Formulation .....	116
6.6	Model Reformulation via CE-IS Based SAA .....	118
6.6.1	IS-Based SAA.....	118
6.6.2	CE-IS-based SAA .....	120
6.7	Case Studies .....	122
6.7.1	Demonstrative Case .....	122
6.7.2	24-hour Day-Ahead Scheduling .....	125
6.7.3	Impacts of Target <b>PELC</b> on the Operating Costs .....	127
6.8	Conclusion .....	128
<b>Chapter 7</b>	<b>Conclusion .....</b>	<b>129</b>
7.1	Conclusion .....	129
7.2	Suggestions for Future Work.....	130
<b>Appendix A</b>	<b>Author's Vita .....</b>	<b>132</b>
<b>Appendix B</b>	<b>Author's Bibliography .....</b>	<b>133</b>

<b>Appendix C IEEE Reliability Test System (RTS).....</b>	<b>135</b>
<b>Appendix D Supplementary Data for IEPGNs .....</b>	<b>136</b>
<b>Appendix E Copyright Permission Letters.....</b>	<b>141</b>
<b>References.....</b>	<b>147</b>

## List of Tables

Table 2.1 Key differences between the long-term and short-term reliability methods .....	18
Table 2.2 Computational performance of FEGS-MCS vs. CMCS .....	34
Table 2.3 Short-term reliability indices considering load uncertainties .....	34
Table 2.4 Short-term reliability indices considering wind generation.....	35
Table 3.1 Short-term risk for different wind generation modeling methods .....	56
Table 3.2 Mean wind speed during different sub-periods .....	56
Table 3.3 Computational performance of CE-MCS vs. Crude NSMCS .....	58
Table 3.4 Short-term risk of composite power system .....	59
Table 3.5 Effects of $NCE$ and $\rho$ .....	63
Table 4.1 Operational risk indices for 24-bus IEEE RTS.....	83
Table 4.2 Operational risk indices for different location of wind farm .....	85
Table 4.3 Operational risk indices for 3-area IEEE RTS.....	85
Table 5.1 PELC and PGLC of IEPGNs for two demonstrative cases .....	104
Table 5.2 Operational reliability indices for varying gas loads and lead times.....	105
Table 5.3 Operational reliability indices with DF-NGFGs.....	106
Table 5.4 Operational reliability indices considering different operational strategies .....	107
Table 5.5 Operational reliability indices for Test System B.....	108
Table 6.1 Scheduling of dispatchable generators for demonstrative cases.....	123
Table 6.2 Scheduling of dispatchable generators for 24-hour day-ahead scheduling .....	126
Table D.1 General parameters for natural gas networks.....	136
Table D.2 CE optimization parameters.....	136
Table D.3 Optimization parameters.....	136
Table D.4 Node data .....	137
Table D.5 Pipeline data.....	137
Table D.6 Gas generation data.....	137
Table D.7 Gas storage data .....	138
Table D.8 NGFGs data .....	138

Table D.9 Parameters for the 4-state model of DF-NGFGs .....	138
Table D.10 NGFGs data .....	139

# List of Figures

Figure 1.1 Transition from traditional electric power system to modern sustainable electric power system .....	1
Figure 1.2 Interdependency between sustainable electric power systems and natural gas networks .....	2
Figure 1.3 Sources of uncertainties in power systems.....	4
Figure 1.4 Key subject areas for the thesis .....	12
Figure 2.1 Number of samples required for CMCS vs. the reliability index.....	24
Figure 2.2 Computational time for CMCS vs. the reliability index.....	24
Figure 2.3 Importance splitting process.....	27
Figure 2.4 Pictorial representation of GS .....	30
Figure 2.5 Pictorial representation of FEGS with load uncertainty.....	33
Figure 3.1 Pictorial representation of the area risk method. $T_0$ represents the initial hour. $T_h$ , $T_{2h}$ , and $T_{3h}$ represent one, two, and three hour(s), respectively, after the initial hour. ....	41
Figure 3.2 Conditional PDFs of wind speed in different sub-periods for a single initial wind speed at $T_0$ . ....	43
Figure 3.3 Conditional PDFs of wind speed in different sub-periods for different initial wind speeds at the start of those sub-periods.....	43
Figure 3.4 Partitioning of the conditional PDF of wind speed .....	47
Figure 3.5 Integrating the proposed reliability modeling of wind generation in the area risk method .....	49
Figure 3.6 Proposed hybrid framework for the short-term risk assessment .....	54
Figure 3.7 Regression analyses, (a), (b): using the approach of [46], and (c), (d): using the proposed approach.....	57
Figure 3.8 Heat map for the bus-pint short-term risk indices. This figure is generated using [78]. ....	60

Figure 3.9 Daily short-term risk. Load, wind generation and total committed capacity is scaled down by 2000 and shown in MW. Short-term risk is scaled up by 100. Grey dots indicate the committed generating units.....	61
Figure 3.10 Short-term risk indices for different spinning reserve criteria. ....	62
Figure 3.11 Short-term risk indices for varying capacities of wind generation. The condition of RTS are same as that for Table 3.4 (capacity 100%).....	62
Figure 4.1 Wind power curve with box plots of actual wind power data.....	72
Figure 4.2 Histogram of historical wind power data for a month.....	72
Figure 4.3 Clustering of historical data. $Th$ is the current time instant. $Th - Th + 1$ is the time interval for risk assessment. ....	73
Figure 4.4 Bivariate histogram for the given dataset for one of the three clusters .....	81
Figure 4.5 GMM for given dataset when MAP estimation is employed. ....	81
Figure 4.6 GMM for given dataset when MLE estimation is employed. ....	82
Figure 4.7 Bivariate Gaussian approximation to the given dataset. ....	82
Figure 4.8 The convergence behavior of the proposed method for three clusters when the initial wind generation is 0.5 p.u. The confidence interval is also plotted.....	84
Figure 4.9 The convergence behavior of the proposed method for three clusters when 3-area IEEE RTS is employed. Initial wind generation is set to 0.5 p.u. ....	86
Figure 5.1 A natural gas pipeline of length $L$ between nodes $i$ and $j$ of a natural gas network under normal operating conditions. ....	93
Figure 5.2 The natural gas pipeline of Fig. 5.1 in which a pinhole or hole failure occurs at a distance $\ell$ from node $i$ . ....	93
Figure 5.3 Gas release rate from a leak of varying diameter and distance from the starting node on a 60-km gas pipeline. ....	94
Figure 5.4 Four-state Markov model for NGFGs with dual fuel capabilities.....	96
Figure 5.5 The area risk method with NGFGs with dual-fuel capabilities.....	97
Figure 5.6 <i>Test System A</i> comprising a 6-bus power system and a 7-node gas network .....	102
Figure 5.7 <i>Test System B</i> comprising the 24-bus IEEE RTS and the 20-node Belgian Gas Network .....	103
Figure 6.1 Framework for the proposed microgrid scheduling problem.....	121
Figure 6.2 A 15-bus synthetic microgrid for case studies .....	122

Figure 6.3 Load, renewable power, committed generation, and storage power for <i>Model A</i> and <i>Model B</i> .....	124
Figure 6.4 <i>PELC</i> indices for <i>Model A</i> and <i>Model B</i> .....	124
Figure 6.5 <i>PELC</i> indices for <i>Model A</i> and <i>Model B</i> for day-ahead scheduling.....	125
Figure 6.6 Hourly load demand and DRES output for day-ahead scheduling.....	127
Figure 6.7 Variation in the total operating costs of microgrids with varying target <i>PELC</i> .....	128
Figure C.1 Modified IEEE RTS with wind generation.....	135

## List of Abbreviations

ADAM	ADaptive Multilevel splitting algorithm
ARMA	Autoregressive Moving Average
CDF	Cumulative Distribution Function
CE	Cross Entropy
CMCS	Crude Monte Carlo Simulation
DAUC	Day-Ahead Unit Commitment
DRES	Distributed Renewable Energy Sources
DER	Distributed Energy Resource
DF-NGFG	Dual-Fuel Natural Gas-Fired Generator
ED	Economic Dispatch
EENS	Expected Energy Not Supplied
ERCOT	Electric Reliability Council of Texas
FE	Fixed Effort
FS	Fixed Splitting
FEGS	Fixed Effort Generalized Splitting
FNS	Fixed Number of Successes
GMM	Gaussian Mixture Model
GS	Generalized Splitting
IEPGN	Integrated Electric-Power Gas Network
IID	Independent and Identically Distributed
IS	Importance Sampling
ISO	Independent System Operator
KDE	Kernel Density Estimation
LOLE	Loss of Load Expectation
LOLP	Loss of Load Probability
MAP	Maximum A Posteriori
MCS	Monte-Carlo Simulation

MCMC	Markov Chain Monte-Carlo
MH	Metropolis-Hastings
MILP	Mixed-Integer Linear Programming
MLE	Maximum Likelihood Estimation
MM	Mixture Model
NGFG	Natural Gas-Fired Generator
NSMCS	Non-Sequential Monte-Carlo Simulation
OPF	Optimal Power Flow
ORR	Outage Replacement Rate
PDF	Probability Distribution Function
PELC	Probability of Electric Load Curtailment
PGLC	Probability of Gas Load Curtailment
PJM	Pennsylvania-New Jersey-Maryland
RE	Relative Error
RES	Renewable Energy Sources
RTCA	Real-Time Contingency Analysis
RTS	Reliability Test System
RV	Random Variable
SAA	Sample Average Approximation
SMCS	Sequential Monte-Carlo Simulation
SO	System Operator
SOC	State-of-Charge
UC	Unit Commitment
UCR	Unit Commitment Risk
UGF	Universal Generating Function

# Chapter 1

## Introduction

### 1.1 Motivation

The increased concerns about the need to combat anthropogenic climate change and rising positive public perceptions about environmentally sustainable practices have become the primary drivers for a global paradigm shift in electric power systems. This paradigm shift is characterized by several changes in the structure and operation of existing electric power systems. On the generation side, renewable energy sources (RES), such as wind and solar energy, are being incorporated in large proportions [1]. Additionally, electric generators with a large carbon footprint, e.g., coal-fired power plants, are being eliminated from the generation mix and replaced by natural gas-fired generators (NGFGs) [2]. Consumption end of the electric power systems is also affected by these changes. For example, the adoption of distributed energy resources (DERs) by electricity consumers has increased significantly [1]. Additionally, microgrids, which are small-scale versions of electric power systems, are being deployed progressively to integrate the DERs more efficiently [3]. The amalgamation of these transitions has led to the transformation of traditional electric power systems into modern sustainable electric power systems (Figure 1.1) [4].

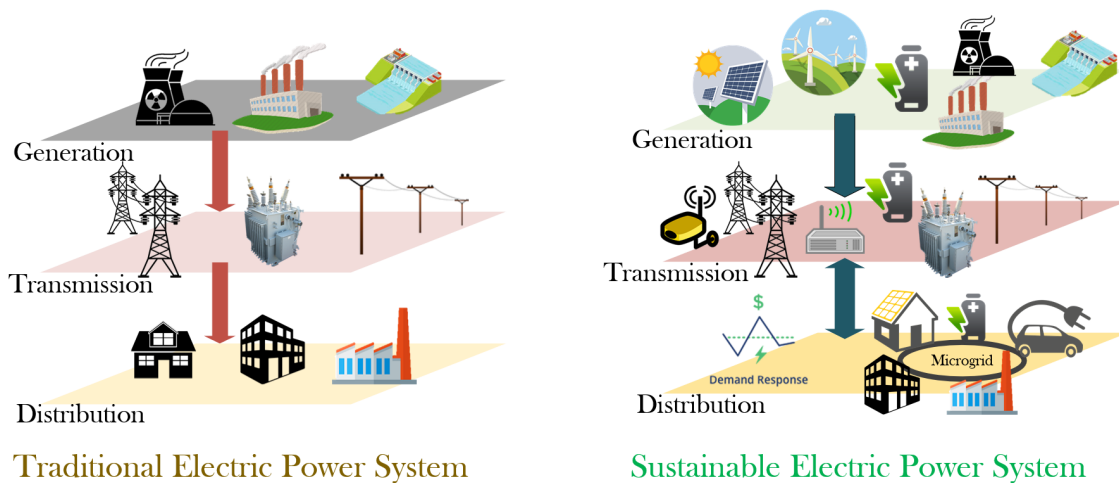


Figure 1.1 Transition from traditional electric power system to modern sustainable electric power system

The system operators (SOs) of sustainable electric power systems are faced with severe technical challenges to maintain the reliable and economic operation of these systems [5]. During system operation, the uncertainties of large-scale RES render it challenging to maintain the balance between the generation and load, thus increasing the risk of load shedding [6]. Further, additional sources of uncertainties emanating from transmission systems and distribution networks also add to the problem. Apart from the sources of uncertainties present within electric power systems, SOs also need to be aware of uncertainties originating from natural gas networks. On the one hand, the natural gas-fired generators (NGFGs) are added to electric power systems to provide flexibility and mitigate the adverse impacts of the variability of RES. On the other hand, these NGFGs rely heavily on the availability of “just-in-time” single fuel, i.e., natural gas (Figure 1.2) [7]. The impacts of component outages in natural gas networks could quickly propagate into electric power systems due to the increased interdependency between the two networks. Thus, the operational reliability of integrated electric power-gas networks (IEPGNs) could be at increased risk.

In the presence of these multiple sources of uncertainties, the existing deterministic, heuristic techniques employed by SOs for system operation become ineffective in ensuring the operational reliability of sustainable electric power systems [6]. These techniques neither respond to the probabilistic nature of sustainable electric power systems nor address the full range of risks associated with sustainable electric power systems and IEPGNs. Ergo, the existing techniques cannot assist SOs in making risk-informed decisions during system operation.

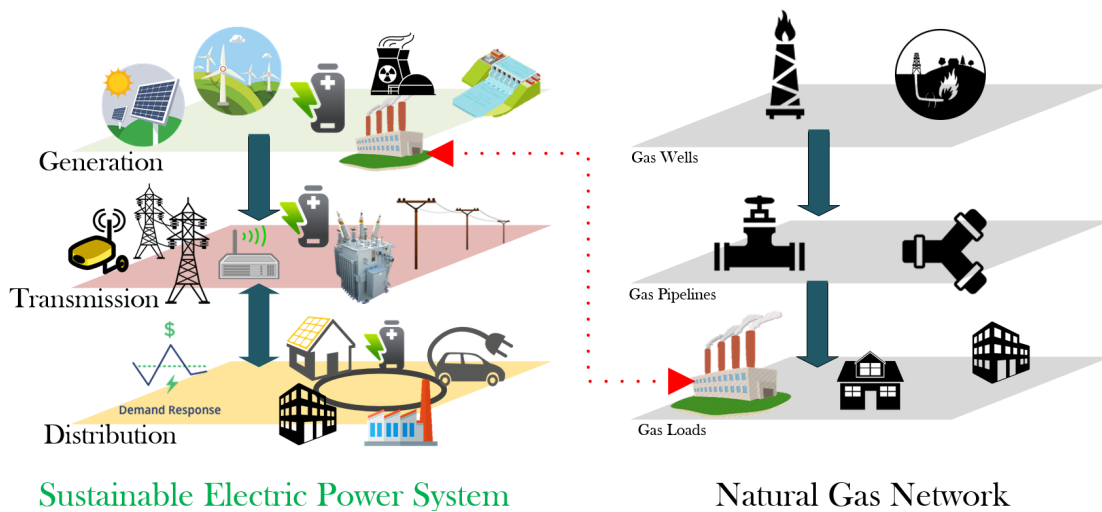


Figure 1.2 Interdependency between sustainable electric power systems and natural gas networks

The successful transition to sustainable electric power systems, therefore, necessitates the development of new probabilistic tools to evaluate the operational reliability and risk indices that can 1) model the different sources of uncertainties in the systems, 2) consider the interdependencies between electric power systems and natural gas networks, and 3) are computationally efficient for their application during system operation. Nonetheless, such comprehensive methodologies are not readily available in the existing literature. Consequently, this research aims to propose and develop computationally efficient simulation frameworks to realistically quantify the operational reliability<sup>1</sup> and risk of sustainable electric power systems and IEPGNs while fully addressing the aforementioned challenges. Furthermore, this research aims to develop a methodology for the operational reliability-constrained scheduling of microgrids, thus enabling the SOs to make risk-informed decisions while operating those microgrids. The frameworks and methodologies developed in this research would find their applications in the unit commitment (UC), economic dispatch (ED), day-ahead and hour-ahead scheduling, and operating reserve sizing processes. The inclusion of these frameworks in system operation practices would facilitate the SOs to ensure a reliable, continuous, and uninterrupted supply of electricity to consumers in sustainable electric power systems amid multiple sources of uncertainties.

## 1.2 Key Challenges

### 1.2.1 Multiple Sources of Uncertainties During System Operation

Sustainable electric power systems are inherently uncertain and stochastic. The uncertainties in sustainable electric power systems span multiple timescales and stem from different sources. Figure 1.3 depicts a list of selected sources of uncertainties originating from the generation, transmission, and load sides of an electric power system at different timescales. The uncertainties associated with random (unexpected) failures of conventional generators and transmission lines had become prominent after several large-scale blackouts, which led to the development of probabilistic tools for system planning [8]. Apart from these random outages, new sources of uncertainties originate from the imperfect forecasts of RES, DERs, and load. It is critical to consider these multiple uncertainties during systems operation (real-time, intra-day, and day-ahead

---

<sup>1</sup> In this thesis, the terms “operational reliability,” “operational risk,” “short-term reliability,” and “short-term risk” are used interchangeably, and the differences between them are indicated where deemed required.

timescales in Figure 1.3) due to two reasons. First, during system operation, the set of available remedial actions to SOs is limited compared to that in system planning. Second, the time available for SOs to deal with the adverse impacts of these uncertainties is also shorter compared to that in system planning. Consequently, the focus of this research in this thesis is on operational timescales.

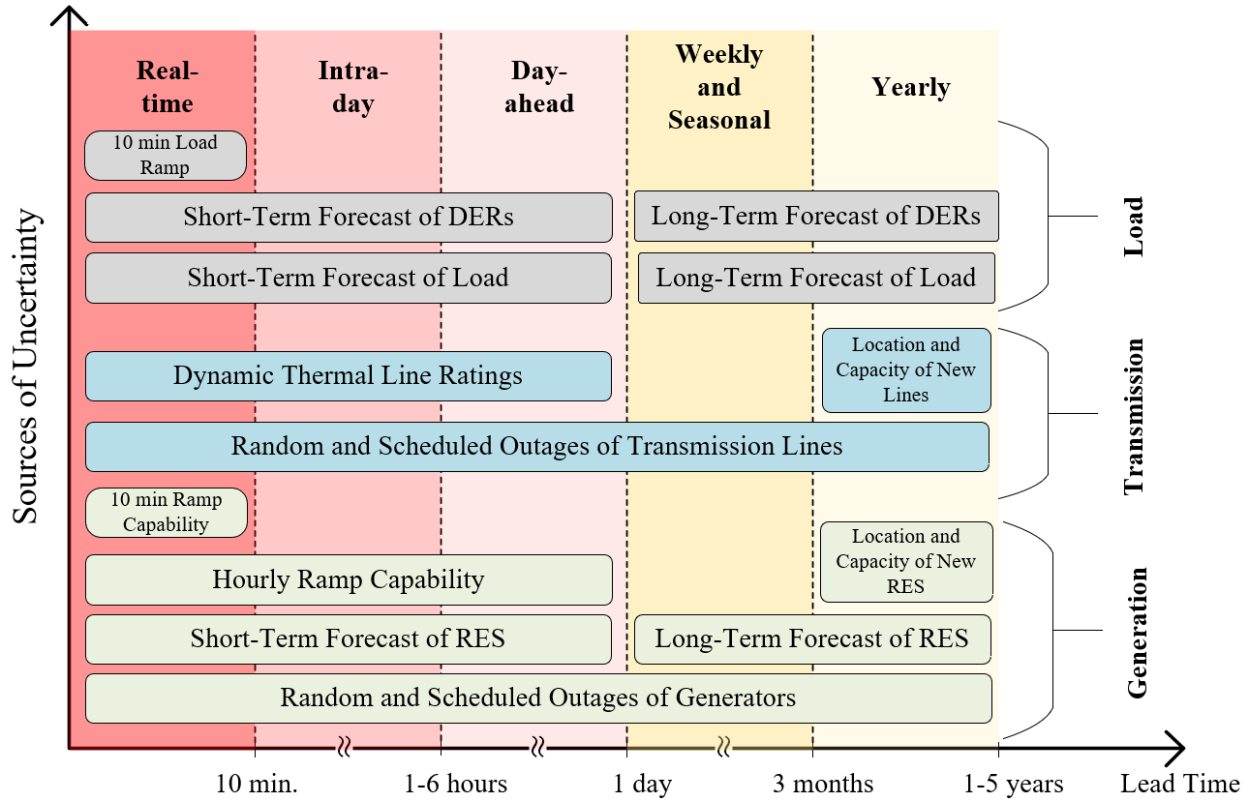


Figure 1.3 Sources of uncertainties in power systems

### 1.2.2 Computational Efficiency of Reliability and Risk Assessment Methods

The need for probabilistic tools for power systems planning and operation pre-dates the transition to sustainable power systems and the consequent inclusion of new sources of uncertainties [9]. Among several other reasons, one of the main reasons for the non-adoption of probabilistic tools has been the high requirement of computational power and intractable simulation times to evaluate operational reliability indices efficiently [10]. For planning problems, the problem of a large computational burden has been mitigated to a great extent. However, during system operation, where SOs must make decisions in a constrained time, the use of probabilistic tools is still computationally prohibitive. Consequently, simple heuristics techniques, as discussed in the next section, are employed by SOs to guarantee reliable system operation. The adoption of

probabilistic tools and methodologies during system operation warrants new techniques to reduce the computational burden.

### 1.2.3 Integration of Probabilistic Approaches in System Operation Practices

To consider the uncertainties of sustainable electric power systems during system operation, SOs have traditionally employed deterministic and heuristic techniques to ensure operational reliability. For example, one of the most common heuristic criteria during system operation is the  $N - k$  criterion. The  $N - k$  criterion specifies that the power system should be able to withstand the loss of any or largest  $k$  out of  $N$  components. The values of  $k = 1$  and  $k = 2$  are typical [11]. To ensure the operational reliability, SOs run periodic contingency analyses during normal operation of power systems to screen for contingencies that could violate the  $N - k$  criterion. Due to a large number of possible contingencies in a real-size power system<sup>2</sup>, SOs often limit the number of contingencies that could be examined. For instance, at the Saskatchewan Power Company (SaskPower), SOs perform contingency analysis for 60 different contingencies every 10 minutes to find violations of  $N - 1$  criterion [12]. SOs at the Electric Reliability Council of Texas (ERCOT) run real-time contingency analysis (RTCA) for nearly 4,500 scenarios (contingencies) every five minutes [13]. California Independent System Operator (ISO) simulates over 2,000 first-order contingences ( $N - 1$  criterion) every two minutes in the California ISO network and its neighboring areas [14]. Similarly, the Pennsylvania-New Jersey-Maryland (PJM) SO assesses 6,000 contingencies every minute [15]. Apart from running RTCA to identify security violations in the future lead time, SOs also schedule operating reserves to manage unforeseen events, such as a sudden increase in load or loss of a generator. The deterministic  $N - k$  criteria is also adopted by several SOs for this purpose [16], i.e., the amount of operating reserve is set equal to the loss of the largest online generating unit.

These deterministic and heuristic tools have worked for SOs in the past due to their simplicity and intuitiveness. However, with the new sources of uncertainties being added in sustainable power systems, such tools are ineffective [6]. For instance, consider the case of wind farms. The wind power varies continuously from the maximum rated power to the minimum rated power during a short period of time. A wind farm could lose either all its output power or a certain

---

<sup>2</sup> The total number of contingencies in a power system with  $N$  components is  $2^N$ .

percentage of its output power in the coming minutes and hours. In this scenario, the precise definition of a contingency for the wind farm is not straightforward. Moreover, different probabilities are associated with the output of wind farms that are often neglected in RTCA. Apart from the drawbacks of contingency analyses, the use of deterministic tools for the operating reserve sizing could lead to either overscheduling, which is more reliable but uneconomical, or under-scheduling, which is economical but unreliable [17].

In light of the above discussion, SOs must be equipped with probabilistic tools that can realistically capture the risks of inadequacy and outages during system operation. Such tools should also allow SOs to set acceptable levels of risk and adjust the operational decisions to satisfy the risk criteria. The focus of this research, therefore, is on the development of these comprehensive probabilistic tools for power systems operation.

## **1.3 Literature Review**

Although comprehensive research has been carried out for long-term reliability studies of power systems with RES [18], [19], the literature on operational, short-term reliability and risk assessment is not well developed. Recently, there has been increasing attention in developing probabilistic tools for power systems operation [6]. In the following sections, the current literature is broadly reviewed from two perspectives, i.e., uncertainty modeling of wind generation and reliability and risk evaluation techniques. In the individual chapters of this thesis, the literature on the specific topics of those chapters is reviewed in depth.

### **1.3.1 Uncertainty Modeling of Wind Generation for Operational Reliability Evaluation**

The first step in a reliability evaluation process is to develop reliability models of different components of an electric power system [20]. Although the reliability models for generating units and transmission lines have been well-developed, there is a dearth of suitable reliability models for RES and IEPGNs. In the following sub-sections, the uncertainty modeling of wind generation in the context of operational reliability evaluation is reviewed.

#### *1.3.1.1 Modeling Wind Speed Uncertainty*

The most common approach to model the uncertainty of wind generation in the literature of power systems reliability is to model the uncertainty of wind speed. In [21], an autoregressive

moving average (ARMA) time series for wind speed is developed using several years of historical data. The ARMA series models have been shown to perform better than other approaches, such as Markov models, for reliability and risk assessment [22]. While the ARMA series in [21] was initially proposed for long-term reliability assessment, it has been adapted to represent the uncertainty of wind speed on an operational time scale by setting up conditional probability distribution functions (PDFs) [23]. Researchers have also employed different forms of PDFs to represent wind speed uncertainty. Reference [24] adopted Burr distribution to model maximum wind speed. A two-parameter Weibull distribution is used in [25]. In [26], historical wind speed data is directly used to construct discrete PDFs for each hour. The fuzzy c-means clustering method is used in [27] to arrive at a discrete PDF model for wind speed. Researchers have also modeled wind speed as a Markov process. For example, in [28], the continuous-time Markov chain is employed to model the wind speed. However, the assumption that the wind speed follows a Markov process might not capture all of the complicated statistical features of wind speed for shorter time-steps [29].

Although the presence of a large amount of historical wind speed data increases the accuracy of these models, the models based on wind speed suffer from two main drawbacks. First, the conversion of wind speed to wind power involves the inaccuracies of the wind turbine curve [30]. Second, by concentrating on wind speed alone, the impact of other meteorological variables, such as wind direction and temperature, on the wind generation is ignored. As these factors have been shown to affect long-term reliability indices [31], it is prudent not to ignore them for short-term reliability evaluation.

### *1.3.1.2 Modeling Wind Power Uncertainty*

Instead of using wind speed, another approach is to directly model the uncertainty of wind power using historical wind power data. For instance, in [32], the Gaussian mixture model (GMM) is employed to model the PDF of wind generation. Similarly, in [33], a modified form of the Gaussian mixture model (GMM) is proposed, which takes into account the boundary characteristics of wind power PDF. The GMM models are developed using the complete historical data of wind generation. The proposed GMM models in [32] and [33] are then employed in probabilistic optimal power flow (OPF). The main advantage of directly modeling wind power uncertainty is that such models are agnostic of forecasting techniques employed by SOs. In addition, the impacts of other

meteorological variables on wind power are indirectly considered in such models. The major drawback of this approach is that these models are unable to consider the temporal correlation of wind power. In other words, the knowledge about the current wind generation (initial state) is not employed in modeling the uncertainty of wind power in the coming hours. This temporal correlation is particularly crucial for operational reliability evaluation as the reliability indices depend on the initial state of the system. Moreover, due to the limited amount of wind generation data, these models are susceptible to the problem of overfitting [34].

#### *1.3.1.3 Modeling Wind Power Forecast Error Uncertainty*

The prediction of wind power is an essential process during power system operation. As wind power prediction cannot achieve perfect accuracy, there is an error associated with the prediction. This wind power forecast error is routinely modeled to follow a Gaussian distribution [35], [36]. It has been shown that a simple Gaussian distribution is unable to capture the skewness and heavy-tail characteristics of the wind power forecast error [37]. Consequently, mixture models (MMs) have also been employed. In [38], a more flexible, versatile mixture distribution is proposed, which has been shown to outperform Gaussian, Beta, and GMM distributions. In [39], Lévy  $\alpha$ -stable distribution is adopted for wind power forecast error. Apart from parametric models, non-parametric techniques, such as quantile regression [40] and kernel density estimation (KDE) [41], are also proposed for modeling the wind power forecast error. These non-parametric models, due to their higher flexibility, are better able to capture the statistical features of the PDF of wind power forecast error.

In the existing literature, the complicated uncertainty models of wind power forecast errors have not been employed in reliability evaluation techniques. This is because the use of semi-parametric and non-parametric PDF estimation techniques poses challenges to the existing analytical and simulation techniques for operational reliability evaluation. Therefore, there is a need to develop advanced analytical and simulation techniques that can incorporate such complex PDF representations of wind power forecast error.

### **1.3.2 Reliability and Risk Evaluation Techniques**

The existing methods for the operational reliability and risk evaluation of electric power systems can be categorized into two main groups: 1) analytical methods and 2) simulation techniques.

### *1.3.2.1 Analytical Methods*

This group of methods involves developing closed-form analytical equations for reliability and risk indices. State-enumeration techniques, convolution methods, and Markov models are the most popular approaches in this group [17]. The analytical methods allow for the calculation of exact reliability indices. Moreover, their computational time is independent of the probabilities to be evaluated [42]. One of the earliest analytical methods for the operational reliability assessment is the PJM method, which was first proposed in the mid-1960s [43]. The PJM method, which is based on a state-enumeration technique, estimates the probability of a generating system just meeting or failing to meet the expected load during the lead time in which no additional generation is available. This probability is referred to as the unit commitment risk (UCR). The basic PJM method has been extended to consider de-rating of generating units [44], rapid-start generating units [45], and uncertainties of load in the lead time [17]. This extended PJM method is also referred to as the area-risk method. In [23] and [46], the area risk method is applied for wind-integrated power systems to understand the impact of wind generation on UCR. Moreover, in [10], the area risk method is also used to evaluate the well-being indices of wind-integrated power systems during system operation [47]. Researchers have also employed the area-risk method to consider energy storage [27], [48], and electric vehicles [49], [50]. State-enumeration techniques are also widely adopted in the literature. Reference [51] employs state-enumeration techniques to evaluate the operational reliability indices while considering the dynamic response and frequency control processes of power systems. Reference [52] also uses a state-enumeration technique; however, the failure rates of components under overloading conditions are also incorporated. The authors in [53] proposed the application of universal generating function (UGF) to determine short- and medium-term reliability indices.

The analytical methods suffer from several drawbacks. First, as analytical methods typically involve combinatorial computations, these methods become computationally prohibitive for large electric power systems. In fact, the computational burden increases exponentially with the increase in the number of components in electric power systems [20]. As a result, the transmission system is often neglected in such methods. This implies that the constraints and contingencies of transmission systems cannot be incorporated. Second, to ensure computational tractability, analytical methods often involve simplifications. Consequently, complex operating conditions

could not be included in the evaluation process. Third, only expected values of reliability indices could be evaluated using analytical methods. Thus, the PDFs of reliability indices, which could be useful in specific applications (such as for the evaluation of reliability costs) cannot be estimated.

#### *1.3.2.2 Simulation Techniques*

The simulation techniques offer an attractive alternative to analytical methods. The simulation methods estimate the reliability and risk indices via stochastic simulation of the actual process of the system. One such simulation method that has been extensively used in the literature is the Monte-Carlo simulation (MCS) technique [10]. MCS techniques are easy-to-implement and possess the attractive properties of ergodicity and robustness to the dimension of the problem [54]. The two main variants of MCS techniques are non-sequential MCS (NSMCS) and sequential (or chronological) MCS (SMCS). Reference [55] applies an NSMCS technique for spinning reserve assessment of composite power systems. The computational performance of NSMCS is significantly improved by adopting an importance sampling (IS) technique. In [56], the authors extend their previous work in [55] to include renewable generation. Instead of NSMCS, a quasi-sequential MCS approach is adopted, which can also consider the chronologies of load and renewable generation. In [57], a state-transition sampling-based MCS is used for the operational reliability of composite power systems. A cross entropy (CE)-based three-stage sequential IS method is proposed to improve the computational performance of MCS for short-term reliability evaluation. In [24], a combination of Latin hypercube sampling and Gibbs sampling is employed to improve computational performance. The proposed nested sampling framework is able to consider the impact of meteorological variables on the risk indices. Reference [58] adopts an importance splitting technique to estimate the reliability indices for a three-node power system; only the uncertainty of wind generation, modeled as an Ornstein-Uhlenbeck process, is considered.

Although simulation techniques are robust to the size of power systems, such techniques involve a very high computational burden for highly reliable systems. This is the case during power systems operation as the risk indices have very small values. The high computational burden either restricts the direct application of simulation techniques in power system operation or leads to compromises in modeling details.

### 1.3.2.3 *Miscellaneous Approaches*

Although analytical and simulation methods form the bulk of operational reliability evaluation methods, other techniques have also been proposed. In [59], the authors have developed a bi-level optimization model for the short-term risk assessment of transmission systems. The upper-level problem performs a binary optimization to find the worst  $N - k$  contingencies, while the lower-level problem minimizes the total load shedding for transmission contingencies. The proposed approach ignores generation outages, which are far more likely to occur than the transmission system outages during the lead time. In [60], a fast sorting technique is proposed to identify the system states based on their probabilities of occurrence. The fast sorting technique is, in essence, an extension of the state-enumeration approach.

## 1.4 Research Questions

This research aims to extend the existing literature on the operational reliability and risk assessment of sustainable electric power systems and IEPGNs to address the new challenges indicated previously. To this end, this research aims to explore the following important research questions:

- Can a computationally efficient simulation technique be developed to estimate the operational reliability indices of generating systems? Can the proposed simulation technique be able to consider both parametric and non-parametric PDF representations of wind generation?
- How can the existing analytical or simulation techniques be extended to incorporate the uncertainties of wind speed for the short-term risk assessment? How the contingencies and constraints of transmission systems be incorporated while evaluating the risk indices? What are the impacts of transmission systems on the system- and bus-level operational risk indices?
- What are the impacts of contingencies and constraints of natural gas networks on the operational reliability and risk of electric power systems? How can the different operational strategies of natural gas networks increase or decrease the short-term reliability of power systems?

- With the increasing penetration of distributed energy resources (DERs), what are the impacts of these DERs on the operational reliability of microgrids? In the presence of these DERs, how can the system operators ensure the operational reliability of microgrids? How are the operational schedules of microgrids affected by the operational reliability constraints?

To address the aforementioned research questions, Figure 1.4 depicts the key subject areas that are employed in this research. Probability theory is required to propose reliability models of components in electric power systems and IEPGNs. Reliability engineering is needed to set up equations for evaluating the reliability and risk indices. The simulation frameworks, to be used to estimate the reliability and risk indices, are based on the simulation theory. Finally, the proposed tools and frameworks are developed while giving full attention to power system operation problems.



Figure 1.4 Key subject areas for the thesis

## **1.5 Contributions of the Thesis**

Based on the research questions presented in the previous section, the thesis contributes to the existing literature in the following ways:

### **1.5.1 Development of an importance-splitting based simulation framework for the operational reliability evaluation of generating systems**

As a first contribution, a fixed-effort (FE) based generalized splitting (GS) technique is adopted for the operational reliability assessment of generating systems. FEGS is a variant of a computationally efficient MCS technique called importance splitting. FEGS is suitable for static, Non-Markovian problems that are encountered in the operational reliability assessment. To implement the FEGS technique, the Metropolis-Hastings (MH) algorithm for Markov Chain Monte Carlo (MCMC) is modified to consider the discrete random variables of electric power systems. The framework is also extended to consider the uncertainties of load demand and wind generation. Case studies on the 24-bus IEEE Reliability Test System (RTS) are performed to show the computational superiority of the proposed approach over crude MCS (CMCS), and the impacts of wind and load uncertainties on the short-term reliability of generating systems are assessed.

### **1.5.2 Development of a hybrid analytical-simulation framework for operational risk assessment**

A new framework for the short-term risk assessment of wind-integrated composite power systems via a combination of an analytical approach and a simulation technique is proposed. The proposed hybrid framework first employs the area risk method – an analytical approach, to include the detailed reliability models of different components of a power system. In this regard, a novel reliability modeling approach for wind generation for the short-term risk assessment is also proposed. Thereafter, an NSMCS technique is adopted to calculate the partial risks of the area risk method. As a result, the proposed framework is also capable of including the contingencies and constraints of the transmission system that are customarily neglected in the area risk method. The computational performance of the proposed framework is greatly enhanced by adopting the IS technique whose parameters are obtained using the CE optimization. Case studies performed on a modified 24-bus IEEE RTS validate that the detailed reliability modeling of wind generation and consideration of the transmission system are necessary to obtain more accurate short-term risk

indices. Furthermore, the computational performance of the proposed framework is shown to be higher than that of CMCS.

### **1.5.3 Development of a data-driven framework for the operational risk assessment of wind-integrated power systems**

A novel data-driven method for the operational risk assessment of wind-integrated composite power systems is proposed. First, a new approach is presented to model the uncertainties of wind power in the lead time. The proposed approach employs  $k$ -means clustering and MM to construct time-dependent PDFs of wind power. The proposed approach can capture the statistical features of wind power, such as multimodality. Later, an NSMCS technique is adopted to evaluate the operational risk indices. To improve the computational performance of NSMCS, an IS technique is applied. The IS technique is modified to include the proposed model of wind power. The method is validated on a modified 24-bus IEEE RTS and a modified 3-area IEEE RTS while employing the historical wind generation data. Simulation results verify the importance of accurate modeling of short-term uncertainty of wind power for the operational risk assessment. Further case studies have been performed to understand the impacts of transmission systems on the operational risk indices. The computational performance of the framework is also examined.

### **1.5.4 Development of a simulation framework for the operational reliability evaluation of IEGPNs**

A novel framework for the operational reliability evaluation of IEPGNS is proposed. The framework has three notable features. First, it includes a detailed reliability model of natural gas pipelines to realistically evaluate the reliability indices. Second, it models the dual-fuel capabilities of dual-fuel NGFGs (DF-NGFGs) that have been shown to improve the operational reliability of IEPGNs. Third, the linear formulation of the proposed optimization model and the adoption of CE-based IS ensures high computational efficiency of the proposed framework. The results indicate that the operational reliability indices of IEPGNs are improved when all failure modes of pipelines are considered. In addition, the impacts of dual-fuel capabilities of DF-NGFGs and the different operational strategies of system operators on operational reliability indices are also demonstrated.

### **1.5.5 Development of the operational reliability-constrained optimal scheduling model for microgrids**

A new optimization model for the operational reliability-constrained scheduling of microgrids is proposed. To this end, chance-constrained optimization is adopted to embed hourly operational reliability indices in the scheduling problem of microgrids. The explicit chance constraints in the model are reformulated using the sample average approximation (SAA). IS is then adopted to reduce the number of chance constraints and render the model tractable. The parameters of IS are obtained after making practical assumptions and using CE optimization. Case studies performed on a synthetic microgrid shows that the schedule obtained from the proposed model satisfies the operational reliability constraints set by the microgrid operator. The intra-day and day-ahead scheduling problems are solved to explain the results in detail. The impacts of target operational reliability indices set by the microgrid operator on the operating costs are also examined.

## **1.6 Organization of the Thesis**

The thesis is organized into six chapters. Sufficient details have been included in all chapters so that each chapter can be read on its own if desired. However, all of the chapters are closely linked with each other.

Chapter 1 provides the motivation behind the research work. The key challenges introduced by the transition to sustainable electric power systems are identified. Later, the literature review on the research direction is conducted. The chapter also describes the research questions that are addressed by this thesis. Further, the contributions of the thesis are summarized.

Chapter 2 focuses on the mathematical foundation of the operational reliability and risk assessment of electric power systems. This chapter also explores the fundamental drawback of using simulation techniques for operational reliability and risk assessment. The widely adopted variance reduction techniques for simulation methods are discussed. Later, a new simulation technique called the FEFS is presented for the operational reliability evaluation of generating systems. This chapter is a part of a paper titled “Short-term reliability evaluation of generating systems using fixed-effort generalized splitting,” which is published in *2020 IEEE PES General Meeting, Montreal*, 2020. As the lead author, Osama Aslam Ansari proposed, developed, and implemented the technique and carried out the simulations. He also wrote the paper. The co-

authors provided their valuable comments and suggestions for paper presentation and editing. The contents of this chapter and the aforementioned paper are related to the first contribution of the thesis.

Chapter 3 presents a novel hybrid framework to evaluate the short-term risk indices of wind-integrated composite power systems. A new approach to model uncertainty of wind speed for the short-term risk evaluation is presented. The results of case studies are examined to show the efficacy of the proposed framework. This chapter is part of a paper titled “A hybrid framework for short-term risk assessment of wind-integrated composite power systems”, which is published in *IEEE Transactions on Power Systems*. As the lead author, Osama Aslam Ansari proposed, developed, and implemented the framework and carried out the simulations. He also wrote the paper. The co-author provided his valuable comments and suggestions for problem formulation, paper presentation and editing. The contents of this chapter and the aforementioned paper are related to the second contribution of the thesis.

In Chapter 4, a novel data-driven framework for the operational risk assessment of wind-integrated power systems is presented. A data-driven approach to model the uncertainty of wind power is also proposed. Simulation results are presented to exhibit the performance of the proposed approach. This chapter is part of a paper titled “Data-driven operation risk assessment of wind-integrated power systems via mixture models and importance sampling”, which is published in *Journal of Modern Power System and Clean Energy*. As the lead author, Osama Aslam Ansari proposed, developed, and implemented the framework and carried out the simulations. He also wrote the paper. The co-authors provided their valuable comments and suggestions for paper presentation and editing. The contents of this chapter and the aforementioned paper are related to the third contribution of the thesis.

Chapter 5 presents the proposed framework for the operational reliability evaluation of IEPGNs. The proposed reliability modeling of IEPGNs is first delineated. Then, the proposed framework for the operational reliability evaluation of IEPGNs is explained. The results obtained from selected case studies are demonstrated. The importance of the proposed framework is also justified. This chapter is part of a paper titled “A novel framework for the operational reliability evaluation of integrated electric power-gas networks (IEPGNs)”, which is published in *IEEE Transactions on Smart Grid*. As the lead author, Osama Aslam Ansari proposed, developed, and implemented

the framework and carried out the simulations. He also wrote the paper. The co-authors provided their valuable comments and suggestions for paper presentation and editing. The contents of this chapter and the aforementioned paper are related to the fourth contribution of the thesis.

Chapter 6 presents the proposed optimization model for the optimal scheduling of microgrids. First, a deterministic formulation of the optimal scheduling problem for microgrids is proposed. Then, to consider hourly operational reliability constraints, a chance-constrained optimization-based model is presented. Afterward, the CE-IS-SAA technique is presented to reformulate the model and render it tractable. Case studies are then performed to show the effectiveness of the proposed model. This chapter is part of a paper titled “Operational reliability-constrained scheduling of microgrids via cross-entropy importance sampling-based sample average approximation”, which is going to be submitted to *IEEE Transactions on Smart Grid*. As the lead author, Osama Aslam Ansari proposed, developed, and implemented the framework and carried out the simulations. He also wrote the paper. The co-author provided his valuable comments and suggestions for paper presentation and editing. The contents of this chapter and the aforementioned paper are related to the fifth contribution of the thesis.

Finally, the conclusion is provided in Chapter 7. Chapter 7 also discusses the future work related to this study, which could be performed to improve the proposed tools and frameworks further.

# Chapter 2

## Mathematical Foundations of the Operational Reliability and Risk Assessment of Power Systems

### 2.1 Introduction

Power systems reliability is concerned with the presence of sufficient generation, transmission, and distribution facilities to ensure a continuous supply of electricity to consumers in the presence of unexpected failures of the power systems components, de-rating of conventional generating units, variability in the output of RES, and planned or scheduled maintenance outages [20], [17]. Power system reliability makes use of probabilistic techniques<sup>1</sup> to assess the reliability indices of a power system. Based on the period of analysis, power systems reliability can be categorized into long-term reliability assessment and short-term reliability assessment. The long-term reliability assessment techniques find their applications in power systems planning problems, e.g., generation and transmission expansion planning [17]. The widely used criteria of loss of load expectation ( $LOLE$ ) = 0.1 days/yr is a long-term reliability index that is employed by electric utilities to plan for their generating systems [61]. On the contrary, the short-term reliability measures the ability of a power system to withstand disturbances during power systems operation. The applications of short-term reliability methods are found in operational planning (e.g., UC), and real-time operation (e.g., RTCA). Table 2.1 highlights the key differences between the long-term and short-term reliability assessment methods.

Table 2.1 Key differences between the long-term and short-term reliability methods

Long-Term Reliability	Short-Term Reliability
Failure probabilities are independent of time (steady-state probabilities)	Failure probabilities are time-dependent (transient-state probabilities)
Independent of initial state of the system	Dependent on initial state of the system
Repair processes of components are modeled	Repair processes of components are ignored

<sup>1</sup> It should be noted that, in general, power system reliability includes both deterministic and probabilistic techniques. However, in this report, power system reliability implies the use of probabilistic approaches.

Long-term failure and repair rates are used	Short-term failure rates and outage replacement rate (ORR) are employed
In case of contingencies, generation re-dispatch is allowed	In case of contingencies, generation re-dispatch can be restricted
Commitment statuses of generating stations are ignored	Commitment statuses of generating stations are considered
Installed capacities of generation and transmission systems are considered	Real-time generation and transmission system capacities are included
Mostly used for off-line studies	Also useful for online studies
The methods are suitable for power systems planning	The methods are suitable for power systems operation

The reliability evaluation process, whether for the long-term or short-term reliability, involves three distinct stages:

1. reliability modeling of power systems,
2. reliability and risk assessment technique, and
3. reliability or risk indices.

As there are several differences between long-term and short-term reliability assessment techniques, the modeling approaches for the two techniques also differ. Similarly, different reliability and risk assessment techniques are adopted to consider those reliability models. In this chapter, a mathematical foundation is set for the short-term reliability evaluation methods. First, the reliability modeling of power systems for the short-term reliability and risk assessment is presented. Then, different simulation techniques are explored. Finally, a new simulation technique called the FECS is adopted to assess the short-term reliability of generating systems<sup>2</sup>.

## 2.2 Probabilistic Modeling of Power Systems

Consider a probability space  $(\Omega, \mathcal{F}, P)$  where  $\Omega$  is the sample space,  $\mathcal{F}$  is the field, and  $P$  is the probability function. The sample space  $\Omega$ , which is a collection of all possible outcomes  $(\zeta)$ , is defined as

<sup>2</sup> © 2020 IEEE. Reprinted without modifications and with permission from: O. A. Ansari, S. Mahdi Mazhari, Yuzhong Gong, and C. Y. Chung, "Short-term reliability evaluation of generating systems using fixed-effort generalized splitting," *2020 IEEE PES General Meeting, Montreal*, 2020.

$$\Omega = \left\{ \zeta_{11}^G, \dots, \zeta_{1N^1}^G, \dots, \zeta_{g1}^G, \dots, \zeta_{gN^g}^G, \dots, \zeta_{N^G 1}^G, \dots, \zeta_{N^G N^G}^G, \zeta_1^L, \dots, \zeta_l^L, \zeta_{N^L}^L : \zeta_{ij}^G \in \{0,1\}, \zeta_i^L \in \{0,1\} \right\}. \quad (2.1)$$

In (2.1), it is assumed that there are  $N^G$  generating stations and a generating station  $g$  has  $N^g$  identical generating units.  $\zeta_{ij}^G$  represents the binary status of  $j$ th generating unit at  $i$ th generating station. It is also assumed that there are  $N^L$  transmission lines.  $\zeta_i^L$  represents the binary status of  $i$ th transmission line. The binary status of 1 corresponds to a generating unit or a transmission line being available, while 0 implies that a generating unit or a transmission line is on outage. It should be noted that the different outcomes in (2.1) are defined for a given lead time ( $\Delta t$ ), which is typically one hour to one day for the short-term reliability evaluation.

### 2.2.1 Discrete RVs for Generators

Let  $n_g^G(\zeta): \Omega \rightarrow \mathbb{R}$  be a discrete RV denoting the number of generating units available during the lead time at generating station  $g$ . This definition implies that

$$n_g^G(\zeta) = \sum_{i=1}^{N^g} \zeta_{gi}^G. \quad (2.2)$$

The PDF for  $n_g^G, f_g^G(x)$ , is given by the following binomial distribution:

$$f_g^G(x) = P(\{\zeta: n_g^G(\zeta) = x\}) = \binom{N^g}{x} (1 - p_g)^x p_g^{N^g - x}, \quad (2.3)$$

where,  $p_g$  is the probability of a generating unit at  $g$ th generation station being failed during the lead time and  $x \in \{0, 1, \dots, N^g\}$ .  $p_g$  typically follows an exponential distribution [17], therefore

$$p_g = 1 - e^{-\lambda_g \Delta t}, \quad (2.4)$$

where,  $\lambda_g$  is the failure rate of a generating unit at  $g$ th generating station.

A discrete random vector ( $\mathbf{X}^G$ ) denoting the number of available generating units at all generating stations in a power system is defined as

$$\mathbf{X}^G = [n_1^G, n_2^G, \dots, n_{N^G}^G]. \quad (2.5)$$

Assuming that the outages of generating units at different generating stations are independent of each other, the PDF for  $\mathbf{X}^G$ ,  $f^G(\mathbf{X}^G)$ , can be obtained using (2.3) and is given as:

$$f^G(\mathbf{X}^G) = \prod_{g=1}^{N^G} f_g^G(x) \quad (2.6)$$

### 2.2.2 Discrete RVs for Transmission Lines

Let  $n_l^L(\zeta): \Omega \rightarrow \mathbb{R}$  be a discrete RV denoting the availability of transmission line  $l$  during the lead time. Therefore,

$$n_l^L(\zeta) = \zeta_l^L. \quad (2.7)$$

The PDF  $f_l^L(x)$  for  $n_l^L$  is given by the following Bernoulli distribution

$$f_l^L(x) = P(\{\zeta: n_l^L(\zeta) = x\}) = (1 - p_l)^x p_l^{1-x}, \quad (2.8)$$

where,  $p_l$  is the probability of  $l$ th transmission line being failed during the lead time and  $x \in \{0,1\}$ . Similar to the modeling of generators,  $p_l$  also follows an exponential distribution [17], therefore

$$p_l = 1 - e^{-\lambda_l \Delta t}, \quad (2.9)$$

where,  $\lambda_l$  is the failure rate of  $l$ th transmission line.

A discrete random vector ( $\mathbf{X}^L$ ) denoting the availability of all transmission lines in a power system is defined as

$$\mathbf{X}^L = [n_1^L, n_2^L, \dots, n_{N^L}^L]. \quad (2.10)$$

Assuming that the outages of transmission lines are independent of each other<sup>3</sup>, the PDF for  $\mathbf{X}^L$ ,  $f^L(\mathbf{X}^L)$ , can be obtained using (2.8) and is given below

$$f^L(\mathbf{X}^L) = \prod_{g=1}^{N^G} f_l^L(x). \quad (2.11)$$

---

<sup>3</sup> Note that common-mode outages are not considered in this work.

## 2.3 Operational Reliability Evaluation Technique

Let  $A$  be a set of all events that lead to load curtailment in the lead time  $\Delta t$ . That is,  $A = \{\zeta: H(\mathbf{X}(\zeta)) > 0\}$ , where  $H(\cdot)$  is a reliability measure and  $\mathbf{X} = [\mathbf{X}^G, \mathbf{X}^L]$ . The definition of  $H(\cdot)$  depends on the reliability index being evaluated and also on the scope of analysis (e.g., generating systems or composite power systems). In the operational reliability evaluation, we are interested in evaluating  $P(A)$ . If  $H(\cdot)$  represents an indicator function<sup>4</sup>, then the probability or risk  $R$  can be evaluated as,

$$R = \mathbb{E}_f[H(\mathbf{X})] = \int_{\Omega} H(\mathbf{x})f(\mathbf{x})d\mathbf{x}, \quad (2.12)$$

where,  $f(\cdot) = f^G(\cdot)f^L(\cdot)$ . Note that if  $H(\cdot)$  is a function other than the indicator function, then (2.12) is not a pure probability and it represents a risk index.

The analytical methods, as discussed in Chapter 1, evaluates (2.12) directly, e.g. through state-enumeration techniques or convolution. The integral in (2.12) is difficult to evaluate analytically for the following reasons:

1. Although  $H(\mathbf{x})$  is explicitly defined for generating systems, it is often calculated implicitly (pointwise) for composite power systems.
2. The dimension of the integral in (2.12) can become very large for large power systems.
3.  $f(\mathbf{x})$  is often a mixed discrete-continuous distribution. Therefore, closed-form solutions for (2.12) are difficult to obtain.

### 2.3.1 Simulation Approach

In the light of above discussion, simulation techniques are better suited to evaluate the integral in (2.12). In its simplest form, a large number of samples are drawn from  $f(\mathbf{x})$  and the risk index in (2.12) is estimated as  $\hat{R}$ , where

$$\hat{R} = \frac{1}{N_{\text{MCS}}} \sum_{i=1}^{N_{\text{MCS}}} H(\mathbf{x}_i). \quad (2.13)$$

---

<sup>4</sup> An indicator function is defined as  $\mathbf{I}\{y(x) \leq \alpha\} = 1$ , when  $y(x) \leq \alpha$ , and  $\mathbf{I}\{y(x) \leq \alpha\} = 0$ , when  $y(x) > \alpha$ .

In (2.13), the samples  $\{\mathbf{x}_i: i \in \{1, \dots, N_{\text{MCS}}\}\}$  are independent and identically distributed (IID) from  $f(\mathbf{x})$ . This approach is also known as crude MCS (CMCS).

Equation (2.13) can be employed to estimate any reliability index depending on the definition of  $H(\cdot)$ . However, to explain the properties of (2.14), the discussion henceforward is limited to the pure probability index. For a pure probability index,

$$H(\mathbf{x}) = \begin{cases} 1, & S(\mathbf{x}) \leq L \\ 0, & S(\mathbf{x}) > L \end{cases} \quad (2.14)$$

$$\hat{R} = \frac{1}{N_{\text{MCS}}} \sum_{i=1}^{N_{\text{MCS}}} I\{S(\mathbf{x}_i) \leq L\}, \quad (2.15)$$

where,  $L$  is the load and  $S(\cdot)$  is a performance function, e.g. sum of available generation for generating system reliability, and the available generation capacity obtained through DC-optimal power flow (OPF) or AC-OPF for composite power systems reliability. Now, in (2.15), since  $I\{S(\mathbf{x}_i) \leq L\}$  is a Bernoulli RV, the properties of (2.15) can be analyzed analytically. In particular, noticing that  $I\{S(\mathbf{x}_i) \leq L\}, \forall i$  are also IID from  $f(\mathbf{x})$ , the variance of the estimator is given by [62]

$$\text{var}[\hat{R}] = \frac{1}{N_{\text{MCS}}^2} \sum_{i=1}^{N_{\text{MCS}}} \text{var}[I\{S(\mathbf{x}_i) \leq L\}] = \frac{1}{N_{\text{MCS}}^2} (N_{\text{MCS}} \text{var}[I\{S(\mathbf{x}_1) \leq L\}]), \quad (2.16)$$

$$\text{var}[\hat{R}] = \frac{1}{N_{\text{MCS}}} R(1 - R). \quad (2.17)$$

The relative error (RE), which measures the convergence of MCS methods, is given by

$$\text{RE} = \frac{\text{std}[\hat{R}]}{\mathbb{E}_f[\hat{R}]} = \sqrt{\frac{(1 - R)}{RN_{\text{MCS}}}}. \quad (2.18)$$

Equation (2.18) is often used in MCS as a stopping criterion. The typical values of RE for generating systems and composite power systems are 1% and 5%, respectively. Equation (2.18) can also be used to obtain the number of samples required to estimate the reliability index  $R$  with a certain RE, as shown in (2.19).

$$N_{\text{MCS}} = \frac{1 - R}{RE^2(R)}. \quad (2.19)$$

Equation (2.19) clearly indicates the number of samples required for CMCS is indirectly proportional to the reliability index being estimated. Figure 2.1 and Figure 2.2 pictorially depicts the number of CMCS samples and the computational time for CMCS, respectively, when  $\alpha = 5\%$ . It is assumed that each sample takes 0.001 seconds to compute. It is clear from Figure 2.1 and Figure 2.2 that CMCS requires a large computational burden to estimate operational reliability indices of power systems.

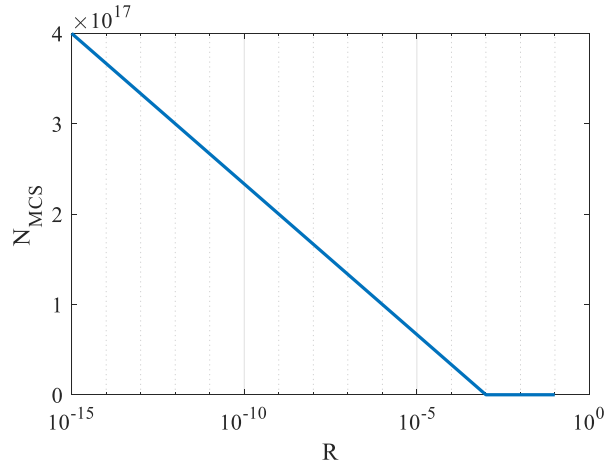


Figure 2.1 Number of samples required for CMCS vs. the reliability index.

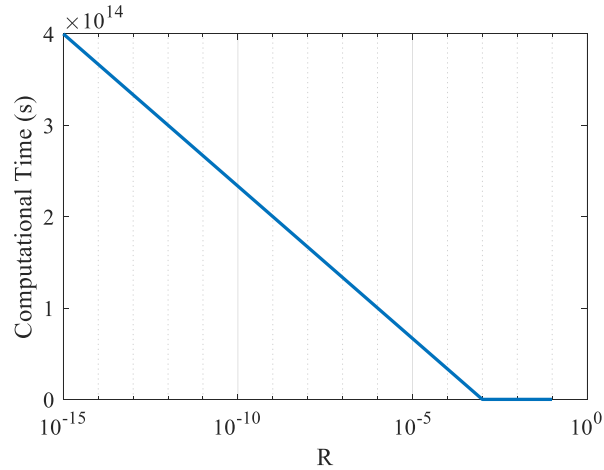


Figure 2.2 Computational time for CMCS vs. the reliability index

## 2.4 Variance Reduction Techniques

Equation (2.18) indicates that in order to reduce the number of samples required for CMCS, the variance of the estimator should be reduced. Consequently, various variance reduction techniques have been proposed [63]. The popular variance reduction techniques that have been applied to power systems reliability include control variates, antithetic variates [64], IS, stratified sampling and dagger sampling. Among these techniques, IS has been shown to achieve the highest improvement in the computational efficiency of CMCS.

### 2.4.1 Importance Sampling (IS)

IS is one of the most popular variance reduction techniques. Literature indicates that IS can achieve a considerable order of magnitude reduction in the variance of the MCS estimator [54]. Consider (2.12) again,

$$R = \mathbb{E}_f[H(\mathbf{X})] = \int_{\Omega} H(\mathbf{x})f(\mathbf{x})d\mathbf{x}. \quad (2.20)$$

The IS is based on the following reformulation:

$$R = \mathbb{E}_f[H(\mathbf{X})] = \int_{\Omega} H(\mathbf{x}) \left( \frac{f(\mathbf{x})}{f^*(\mathbf{x})} \right) f^*(\mathbf{x})d\mathbf{x} = \mathbb{E}_{f^*}[H(\mathbf{X})W(\mathbf{X})], \quad (2.21)$$

where,

$$W(\mathbf{X}) = \frac{f(\mathbf{X})}{f^*(\mathbf{X})}. \quad (2.22)$$

In essence, the IS modifies the original PDF  $f(\cdot)$  to  $f^*(\cdot)$ , which is biased to generate samples that belong to the failure event  $A$ . The new PDF  $f^*(\cdot)$  is also known as the IS density and  $W(\cdot)$  is called the likelihood ratio. The only constrain on the IS density is that  $f^*(\cdot) = 0$  when  $H(\cdot)f(\cdot) = 0$ , that is,  $H(\cdot)f(\cdot)$  is dominated by  $f^*(\cdot)$  [63].

Theoretically, it is possible to obtain an IS density that reduces the variance of the estimator to zero. This ideal IS density is obtained by minimizing the variance of (2.21) and is given as [63]

$$f^*(\cdot) = \frac{H(\cdot)f(\cdot)}{R} \quad (2.23)$$

As  $R$  is not known a-priori, (2.23) cannot be employed in practice. Therefore, the main challenge of IS is to obtain a suitable IS density, which is a good approximation to the ideal IS density. In Chapters 3, 4, and 5, IS technique is adopted as a variance reduction technique, and an iterative approach is employed to obtain the IS density, which is a close approximate of (2.23).

### 2.4.2 Importance Splitting

IS suffers from several drawbacks. The selection of optimal IS density in importance sampling is a key challenge. Sub-optimal importance sampling densities could result in erroneous estimates of reliability indices [54]. Furthermore, for high dimensional cases, IS suffers from degeneracy and may lead to variance explosion [63]. In addition, the variants of importance sampling technique typically employed in power systems literature [56] are generally suitable for PDFs belonging to exponential family, such as Beta or normal distributions. The random variables in power systems do not always follow these standard distributions.

Importance splitting offers an attractive alternative for IS. Importance splitting is a highly versatile and flexible rare-event simulation technique [65]. The basic idea behind it is to employ sequential sampling to probe regions of sample space which are of interest for rare-event simulation [66]. In short-term reliability evaluation, these regions correspond to failure regions, i.e. regions of system states which lead to load curtailment during the lead time.

The key advantages of importance splitting over IS are two-fold. First, importance splitting does not involve any change of PDFs of the underlying phenomenon, thereby avoiding the drawback of finding importance sampling density. Second, there is no restriction on the definition of  $f(\cdot)$  in (2.12).

Considering the context of the short-term reliability evaluation of generating systems, in importance splitting, the sample space is divided by a number of non-identical levels  $\{L_0, L_1, \dots, L_T\}$  with  $L_0 > L_1 > \dots > L_T$ . Let  $S(\mathbf{X})$  be the total available generation capacity during the lead time, where  $\mathbf{X} = \mathbf{X}^G$ . Each level corresponds to a hypothetically higher load demand. The final level  $L_T$  is set to the actual load demand  $L$ . Starting from  $L_0$ , which is equal to the maximum capacity of the generating system, the stochastic process is simulated until the process returns to

the starting point. During this process, the samples that have values of  $S(\mathbf{X})$  below  $L_1$  are recorded. From each of these samples, multiple new stochastic processes are simulated again until these new processes return to  $L_0$ . Similarly, further simulations are carried out starting from samples with  $S(\mathbf{X})$  values that are below  $L_2$ . The whole process continues until the region below  $L_T$  is not sufficiently explored. Fig. 2.3 pictorially depicts this importance splitting process.

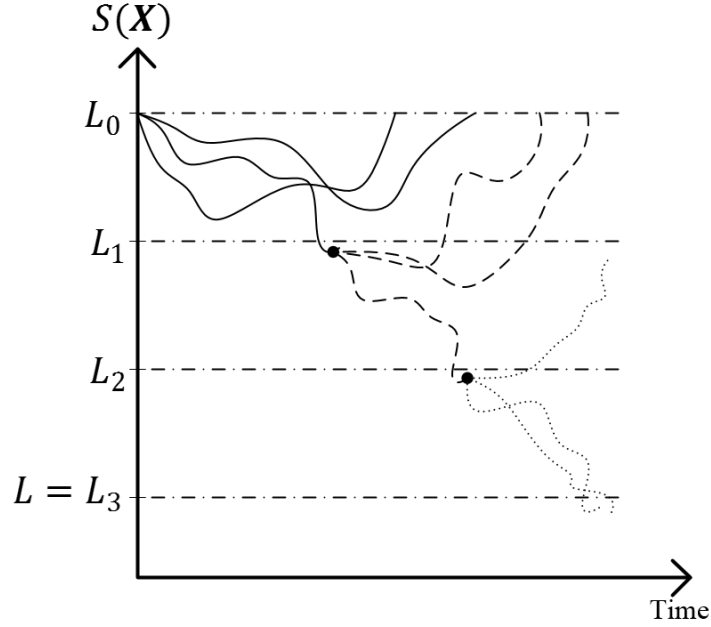


Figure 2.3 Importance splitting process

Let  $N_t$  be the number of samples that enter into the region  $S(\mathbf{X}) \leq L_t$  during  $t - 1$  simulation stage, and let  $s_t$  be the splitting factor, i.e., the number of new simulation processes, for the next stage. The conditional probability  $P(S(\mathbf{X}) \leq L_t | S(\mathbf{X}) \leq L_{t-1})$  can be estimated as

$$P(S(\mathbf{X}) \leq L_t | S(\mathbf{X}) \leq L_{t-1}) = \frac{N_t}{N_{t-1}s_t} \quad (2.24)$$

Through evaluation of these conditional probabilities at different stages or levels, the final probability  $P(S(\mathbf{X}) \leq L)$  can be evaluated by multiplying conditional probabilities.

Depending on how new processes (or trajectories) are generated, importance splitting has different variants.

#### 2.4.2.1 Fixed-Splitting (FS)

In FS splitting, at each stage, the number of new trajectories created from the samples that down-crosses  $L_t$  is fixed. This number is also known as the splitting factor [54]. As the number of new trajectories created is not dependent on the number of samples that down-crosses  $L_t$ , there is a risk of population explosion [67]. Population explosion implies that the total number of samples at each successive stage grows intractably, which leads to increased computational burden.

#### 2.4.2.2 Fixed-Effort (FE)

In FE splitting, the total simulation burden at each stage is fixed. This implies that the number of new trajectories (splitting factor) at each stage depends on the number of samples that down-crosses  $L_t$ . If there are a higher number of such samples, the splitting factor would be lower to keep the total simulated samples fixed, and vice versa. Therefore, the advantage of FE over FS is that the occurrence of population explosion can be avoided.

#### 2.4.2.3 Fixed Number of Successes (FNS)

In this variant of splitting technique, the simulation at each stage is repeated until a fixed number of samples down-crosses  $L_t$ . In other words,  $N_t$  is fixed for each stage, while  $s_t$  can be varied; this approach also avoids the population explosion problem.

## 2.5 Proposed FEGS Approach

The importance splitting techniques discussed previously are typically employed for dynamic, Markovian models [65] and thus cannot be directly adapted to evaluate (2.12). This is because (2.1) represents a static, non-Markovian problem. Botev and Kroese [67] extended the importance splitting approach to propose GS which could be directly applied to estimate (2.13). In this chapter, it is proposed to evaluate (2.12) by adapting GS.

### 2.5.1 Selection of Intermediate Levels

The efficiency of importance splitting is strongly influenced by the choice of intermediate levels  $\{L_1, \dots, L_T\}$  [65], [66]. These intermediate levels could be selected through an initial run of an importance splitting technique. As proposed in [67], in this chapter, the ADaptive Multilevel splitting algorithm (ADAM) is employed to estimate the levels. In essence, the ADAM algorithm

employs fixed values of  $P(S(\mathbf{X}) \leq L_t | S(\mathbf{X}) \leq L_{t-1})$  to estimate  $\{L_1, \dots, L_T\}$  using random populations of samples. Interested readers are referred to [67] for a detailed explanation of the ADAM algorithm.

### 2.5.2 FEES Simulation Framework

FEES is based on the concept of GS. GS extends the traditional splitting method for it to be applicable to static, non-Markovian models, such as (2.12). In essence, the key approach behind GS is to construct a Markov chain at each stage of importance splitting. Therefore, instead of simulating a dynamic process, a Markov chain is created, which has a stationary distribution given by:

$$f^t(\mathbf{X}) = \frac{f(\mathbf{X})I\{S(\mathbf{x}) \leq L_t\}}{P(S(\mathbf{X}) \leq L_t)} \quad (2.25)$$

where,  $f^t(\mathbf{X})$  is the distribution for  $t^{\text{th}}$  state of importance splitting. For reliability evaluation of generating systems,  $f(\cdot) = f^G(\cdot)$ . In essence, instead of creating multiple new trajectories from each sample that down-crosses  $L_t$ , multiple Markov chains with the number of samples equal to the splitting factor are generated. The Markov chain can be generated by employing the MCMC techniques having a Markov transition density proportional to  $f(\mathbf{X})I\{S(\mathbf{x}) \leq L_t\}$ . The seeds of these different MCMC are set to the different samples that down-crosses  $L_t$ . Notice, the similarity between (2.25) and (2.23) of IS; at the final stage  $T$ , the Markov chain has a stationary distribution of (2.23) with  $H(\cdot)$  given by  $I\{S(\mathbf{x}) \leq L\}$ .

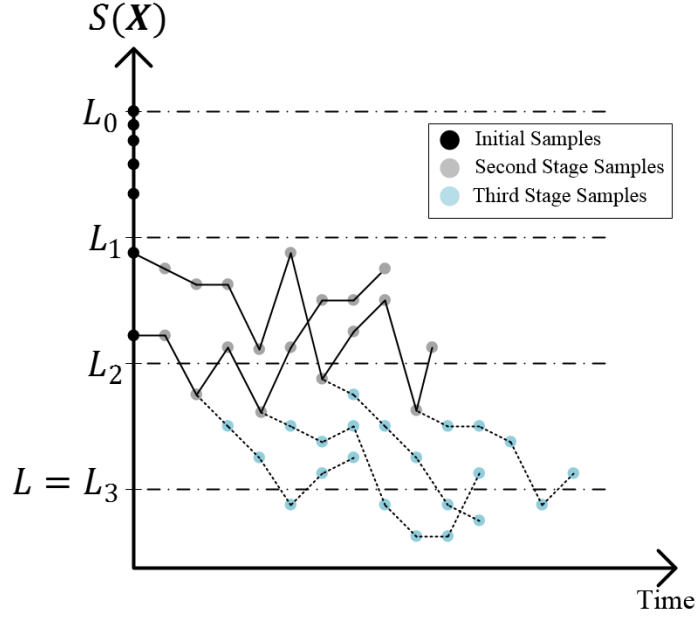


Figure 2.4 Pictorial representation of GS

Figure 2.4 depicts GS for a hypothetical case study. In this figure, three levels are indicated. The initial level  $L_0$  represents the total capacity of the generating system, while the final level  $L = L_3$  is the load demand. The time axis in Figure 2.4 corresponds to the length of Markov chain. In Figure 2.4,  $N_1$  represents the number of black dots below  $L_1$  (2 in this case) and  $N_2$  represents the number of grey dots below  $L_2$  (4 in this case).

The GS approach can be employed in both FS and FE approaches. Due to the advantages of FE mentioned previously, in this work, GS is used in conjunction with FE [54], [67]. Algorithm 2.1 details the FEFS algorithm. The implementation of FE is in step 4 of Algorithm 2.1, where different splitting factors (Markov chain's lengths) for different entrance samples are generated such that the total expected simulation burden remains  $N$  at each stage.

---

**Algorithm 2.1** FEFS Algorithm

---

**Input:** Levels  $\{L_1, L_2, \dots, L_T\}$ , fixed sample size  $N$

**Output:** Short-term reliability index in (2.12)

- 1: Set  $t = 1$ . Sample IID  $\{\mathbf{X}_1, \dots, \mathbf{X}_N\}$  from  $f(\cdot)$ . Set  $\chi_0 = \{\mathbf{X}_1, \dots, \mathbf{X}_N\}$
- 2: Select  $\chi_t = \{\mathbf{X}_1, \dots, \mathbf{X}_{N_t}\}$  from  $\chi_{t-1}$  such that for all samples in  $\chi_t$ ,  $S(\mathbf{X}) \leq L_t$ .
- 3: **For**  $t = 1$  to  $t = T$  **do**

- 4: Generate  $\{S_t^1, \dots, S_t^{N_t}\}$ , where  $S_t^i = \lfloor N/N_t \rfloor + B_i$  and  $B_i$  is a Bernoulli random variable with success probability of 0.5, such that  $\sum_i B_i = N \bmod N_t$
  - 5: From each sample  $\mathbf{X}_i$  in  $\chi_t$ , sample  $S_{ti}$  IID samples from (2.25) using MCMC with  $\mathbf{X}_i$  as the seed
  - 6: Collect all samples from step 5 to update  $\chi_t$ , which results in  $N$  samples in  $\chi_t$
  - 7: **If**  $N_t = 0$ , set  $N_{t+1} = N_{t+2} = \dots = N_T = 0$
  - 8: **End** the **for** loop
  - 9: Calculate the estimated risk  $\hat{R} = N^{-T} \prod_{t=1}^T N_t$
- 

### 2.5.3 MCMC for Discrete PDFs of Generating System

A key step in Algorithm 2.1 is to generate samples from (2.25) in step 4. This step could be realized by constructing a Markov chain whose stationary distribution is given by (2.25). This Markov chain can be generated using MCMC algorithms. In this work, the MH algorithm is adopted for MCMC. The MH-MCMC is inefficient for high dimensional problems [68]. In this chapter, a modified version of MH-MCMC is adapted for discrete PDFs of power systems. In this modified version, a new sample is accepted or rejected for each component (generating station) separately. Algorithm 2 details this component-wise discrete MH-MCMC.

---

#### Algorithm 2.2 Component-Wise Discrete MH-MCMC

---

**Input:** Initial sample  $\mathbf{X}_0 = \{n_{1,0}^G, \dots, n_{N^G,0}^G\}$  following the target distribution  $f^t(\cdot)$ , and the original distribution  $f(\cdot)$

**Output:** A population of  $N_{MC}$  samples  $\{\mathbf{X}_1, \dots, \mathbf{X}_{N_{MC}}\}$  following the target distribution  $f^t(\cdot)$

- 1: **For**  $i = 1$  to  $N_{MC}$  **do**
- 2:   **For**  $g = 1$  to  $N^G$  **do**
- 3:     Draw a candidate sample  $\delta_g$  from a uniform distribution on  $\{0, 1, \dots, N^g\}$
- 4:     Calculate the acceptance ratio  $\alpha = f_g(\delta_g)/f_g(n_{g,0}^G)$
- 5:     Accept  $\delta_g$  as  $n_{g,i+1}^G$  with probability of  $\min\{\alpha, 1\}$ , and  $n_{g,0}^G$  as  $n_{g,i+1}^G$  otherwise
- 6:   **End** the **for** loop
- 7:   Set the proposal sample  $\mathbf{X}_p = \{n_{1,i+1}^G, \dots, n_{N^G,i+1}^G\}$
- 8:   **If**  $\mathbf{X}_p = \mathbf{X}_i$ , set  $\mathbf{X}_{i+1} = \mathbf{X}_p$  and go to step 10

- 9: Evaluate  $I\{S(\mathbf{X}) \leq L_t\}$  using (2.14) and save the result
  - 10: **if**  $I\{S(\mathbf{X}) \leq L_t\} = 1$  **set**  $\mathbf{X}_{i+1} = \mathbf{X}_p$ , **else** **set**  $\mathbf{X}_{i+1} = \mathbf{X}_0$
  - 11: **Set**  $\mathbf{X}_0 = \mathbf{X}_{i+1}$
  - 12: **End the for loop**
- 

#### 2.5.4 Inclusion of Uncertainties of Load and Wind Generation

The FEGS framework presented in the previous section is developed by only considering the random outages of conventional generating stations. The uncertainties of load demand and wind generation during the lead time also impacts the short-term reliability of power systems. The previously proposed framework can be extended to include the load uncertainty and wind generation uncertainty. In particular, the definition of  $f(\cdot)$  is modified to include the PDF for load demand  $f_L(\cdot)$  and wind generation  $f_W(\cdot)$  during the lead time

$$f(\mathbf{X}) = f^G(\mathbf{X}^G)f_L(X_L)f_W(X_W) \quad (2.26)$$

where,  $X_L$  and  $X_W$  are the continuous random variable for load demand and wind generation, respectively, during the lead time, and  $\mathbf{X} = [\mathbf{X}^G, X_L, X_W]$ . The definition of  $S(\mathbf{X})$  is also modified as

$$S(\mathbf{X}) = \mathbf{X}^G(\mathbf{P}^G)^T - X_L + X_W \quad (2.27)$$

where  $\mathbf{P}^G = [P^1, P^2, \dots, P^{N^G}]$  represents the vector of capacities of a single generating unit at different generating stations. For simplicity, in this work,  $f_L(\cdot)$  and  $f_W(\cdot)$  are modeled using Gaussian distributions centered at the load demand forecast and wind generation forecast, respectively. However, it should be noted that, unlike certain IS techniques, there is no restriction on the choice of  $f_L(\cdot)$  and  $f_W(\cdot)$ .

Figure 2.5 pictorially represents the FEGS approach when only the load uncertainty is considered. Notice that the final level is always set to zero in this case.

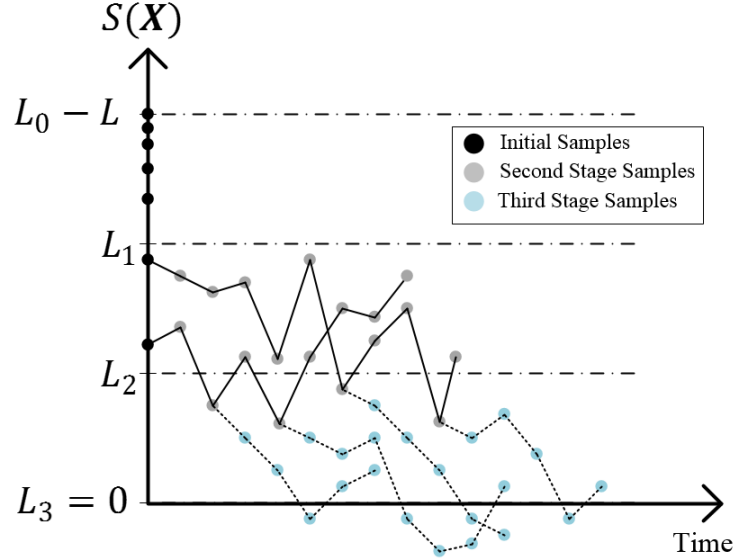


Figure 2.5 Pictorial representation of FEGS with load uncertainty

## 2.6 Results

The efficacy of the proposed FEGS approach for short-term reliability evaluation of wind-integrated power systems is numerically demonstrated. The 24-bus IEEE RTS is employed, which has a total generation capacity of 3,405 MW. The fixed sample size  $N$  in Algorithm 2.1 is set between 10,000 to 150,000. Higher values of  $N$  are used when the estimated short-term reliability indices are expected to have lower values. The lead time is set to 2 hours. All simulations are performed on a personal computer with a 3.40 GHz Intel® Core i7-4770 CPU and a 16 GB RAM. MATLAB is used to implement the proposed framework.

### 2.6.1 Demonstrative Case

In this section, the computational efficiency of the proposed FEGS approach over CMCS is demonstrated. The other variants of importance splitting are not employed for comparison as they are not applicable for the non-Markovian setting of our problem. The stopping criteria for CMCS is based on RE and is set to 10%. Table 2.2 compares the computational performance of the two approaches.  $N_S$  represents the number of times  $S(X)$  is evaluated. Higher  $N_S$  corresponds to higher computational time. As it is evident from Table 2.2, the proposed FEGS approach achieves superior computational performance compared to the CMCS. Moreover, the computational

superiority of FEGS over CMCS increases significantly with the decrease in the short-term reliability index. In Table 2.2, the slight deviation between the reliability indices estimated by the two approaches is due to the fact that an RE of 10% is used in CMCS estimations.

Table 2.2 Computational performance of FEGS-MCS vs. CMCS

Load ( $L$ ) (MW)	CMCS		FEGS-MCS	
	Risk ( $10^{-5}$ )	$N_S$	Risk ( $10^{-5}$ )	$N_S$
3100	540.31	21,500	561.24	23,000
3000	2.4964	431,400	2.3724	33,020
2900	7.1920	1,220,700	7.4240	35,568
2850	3.4896	3,250,800	3.2005	34,238
2700	1.7853	5,000,000*	1.7018	39,903

\* Maximum number of evaluations for MCS was reached and RE was 13%.

## 2.6.2 Impact of Load Uncertainty

In this section, the uncertainty of load during the lead time is also considered. The load demand forecast value is set to 2,850 MW. Table 2.3 shows the short-term reliability indices for different standard deviations of the Gaussian distribution for load demand. As expected, the results indicate that the increase in uncertainty corresponds to lower short-term reliability and higher short-term risk. A comparison of Table 2.2 with Table 2.3 indicates an increase in computational burden when load uncertainty is included.

Table 2.3 Short-term reliability indices considering load uncertainties

Standard Deviation (% of load)	FEGS-MCS	
	Risk ( $10^{-5}$ )	$N_S$
0.1	3.5344	97,736
0.5	3.9089	95,374
1	5.5137	92,131
2	6.6393	81,337
3	17.7350	88,510
5	82.407	77,961

### 2.6.3 Impact of Wind Generation Uncertainty

In this section, the impact of both load and wind generation uncertainty is studied. The standard deviation for load uncertainty is fixed to 0.1% of the forecast load demand. The standard deviation for wind generation PDF is set to 10% of the forecast value. Two cases are considered.

**Case A:** A wind farm is committed and a 155 MW generating station at bus 15 is de-committed.

**Case B:** Only conventional generators are committed and wind generation is not used.

Table 2.4 reports the results for this case study. The results indicate that, when wind generation with a forecast value of 155 MW is committed, the short-term reliability of the generation system drops. Although the maximum generation capacities of the system for both cases are identical, the uncertainty associated with wind generation increases the risk of load curtailment, thereby reducing the short-term reliability. However, at higher wind generation forecast values, the short-term reliability improves due to additional available generation capacity. These observations highlight the importance of considering wind generation uncertainties in short-term reliability evaluation.

Table 2.4 Short-term reliability indices considering wind generation

Case	Wind Generation Forecast		
	155 MW	200 MW	300 MW
Case A	$4.8159 \times 10^{-5}$	$2.0071 \times 10^{-5}$	$1.0817 \times 10^{-5}$
Case B	$3.5344 \times 10^{-5}$		

## 2.7 Conclusion

In this chapter, the mathematical foundations of operational reliability and risk assessment of power systems are presented. The drawbacks of existing analytical and simulation techniques are then analyzed. Afterward, a new approach for short-term reliability evaluation of generating systems based on importance splitting is proposed. The proposed approach employs FEGS, which is a computationally efficient MCS technique. A discrete version of component-wise MH-MCMC is presented to implement the FEGS approach. The results have shown the computational superiority of the proposed approach over CMCS. Further simulation results have indicated the

impact of uncertainties of load and wind on short-term reliability indices. The method developed in this work could be utilized by power system operators for risk-informed decision-making during system operation, such as during UC and ED.

## Chapter 3

# A Hybrid Framework for Short-Term Risk Assessment of Wind-Integrated Composite Power Systems<sup>1</sup>

### 3.1 Abstract

In this chapter, a new framework for the short-term risk assessment of wind-integrated composite power systems via a combination of an analytical approach and a simulation technique is proposed. The proposed hybrid framework first employs the area risk method – an analytical approach, to include the detailed reliability models of different components of a power system. In this regard, a novel reliability modeling approach for wind generation for short-term risk assessment is also proposed. Thereafter, a NSMCS technique is adopted to calculate the partial risks of the area risk method. As a result, the proposed framework is also capable of including the contingencies and constraints of the transmission system that are customarily neglected in the area risk method. The computational performance of the proposed framework is greatly enhanced by adopting the IS technique whose parameters are obtained using the CE optimization. Case studies performed on a modified 24-bus IEEE RTS validate that the detailed reliability modeling of wind generation and consideration of the transmission system are necessary to obtain more accurate short-term risk indices. Furthermore, the computational performance of the proposed framework is many orders higher than any other comparable methods.

---

<sup>1</sup> © 2019 IEEE. Reprinted without modifications and with permission from: O. A. Ansari, and C. Y. Chung, “A hybrid framework for short-term risk assessment of wind-integrated composite power systems,” *IEEE Trans. Power Syst.*, vol. 34, no. 3, pp. 2334-2344, May 2019 [85].

## 3.2 Introduction

The successful transition from the deterministic reliability criterion developed for traditional power systems to the probabilistic methods for modern, renewable-integrated smart grids necessitates the development of both long- and short-term risk assessment methods. Long-term risk assessment methods have been the subject of research for many decades and have been successfully developed and applied in the electric power industry for power systems planning problems [20], [17]. However, these methods are not applicable to short-term risk assessment during power systems operation owing to two main reasons. First, the long-term risk assessment methods assume the failure probabilities of power systems' components to be independent of time and operating conditions. Second, these techniques do not take into account the decisions taken during the power systems operation, e.g., in UC and ED, while evaluating the risk. Yet, the power systems operators require short-term risk indices to schedule sufficient operating or spinning reserve to account for unplanned contingencies and unexpected variability in generation and load in the coming hours [43].

The PJM method, first proposed in the mid-1960s, is one of the earliest and simplest methods to assess short-term risk for a generating system [43]. The basic PJM method aims to evaluate the probability of a generating system to just meet or fail to meet the expected load during the time in which no additional generation is available. This time is also known as the lead time, and the probability is called the unit commitment risk. Several authors have extended the basic PJM method to consider rapid-start generating units [17], load uncertainty [20], [17], wind generation [23], [46], [69], energy storage [27], [48], and electric vehicles [49] in the evaluation process. Nonetheless, as an essentially analytical approach, the basic PJM method and its variants suffer from two major drawbacks. First, these methods involve state-enumeration techniques whose complexity increases exponentially with the number of power system's component that are included in the evaluation process [20]. Second, analytical methods often incorporate certain simplifications to make the evaluation process tractable. For instance, higher-order contingencies [70] or lower probability events, such as failures of multiple transmission lines in a short time period, are neglected. Because of these reasons, the transmission system's contingencies and constraints might not be incorporated in a straightforward manner. Consequently, the effect of the

transmission system on short-term risk might not be conveniently assessed. Ergo, the bus- or load-point short-term risk indices might not be evaluated.

To address the abovementioned limitations, some authors recently proposed simulation-based approaches. In [55], the short-term risk of a composite power system is evaluated using NSMCS. The extremely poor computational performance of MCS for very low failure probabilities is mitigated by employing an IS technique. Reference [56] extends the work in [55] to consider renewable generation using quasi-sequential MCS. The variability in the output of renewable generation is modeled using some fixed scenarios, each having same occurrence probabilities. In [57], a state-transition sampling based MCS is employed to compute the short-term risk indices of a composite power system. IS is also utilized to improve the computational speed of the MCS. In [71], IS is applied to sequential MCS to consider the chronology of failure events in the short-term risk assessment. A bi-level optimization model is proposed in [59] to assess the short-term risk of a transmission system, while neglecting the outages of the generators. In [72], the credibility theory is applied to model the failure probabilities of power systems' components under different weather and operational conditions. Then, the short-term risk is evaluated considering the proposed fuzzy model of failure probabilities. In [68], the computational performance of NSMCS for risk assessment is improved using the subset simulation. Despite the worthy contributions of these works, renewable sources, particularly wind generation, are either not considered at all [55], [57], [71], [59], [72] or insufficiently modeled [56], [68]. However, the uncertainty introduced by highly variable renewable sources coupled with the limitations of the transmission system can have a measurable impact on the short-term risk of composite power systems.

Analytical approaches can allow for detailed reliability modeling of wind generation in short-term risk assessment [23], [46], whereas simulation techniques are robust and can consider the transmission system as well as different operational characteristics of a power system [55], [71]. The purpose of this work is therefore to propose a hybrid framework that makes use of the aforesaid advantages of analytical and simulation techniques to duly evaluate the short-term risk of a wind-integrated composite power system.

To suitably assess the impact of wind generation on short-term risk, a novel reliability modeling approach for wind generation is first proposed. The proposed modeling approach employs conditional probability distributions of wind speed, conditional probabilities, and the law of total

probability to effectively model the probable variations in the output of wind generation during the lead time. The area risk method, which is an extension of the basic PJM method, is then modified and extended to include the proposed reliability modeling approach.

Thereafter, the modified area risk method is innovatively amalgamated with the NSMCS to calculate the partial risks of the area risk method. NSMCS is selected because the requirements for computational memory and reliability data for the NSMCS are lower than other MCS techniques. To improve the computational performance of the proposed framework, the IS technique is applied to the NSMCS. In addition to the generators and transmission lines, the IS technique is directly applied to the wind speed distributions for wind generation. The parameters of the IS technique are obtained using iterative CE optimization, which is one of the most widely adopted methods to obtain the near-optimal IS parameters [63], [73].

The proposed framework is applied to a modified IEEE RTS to indicate its effectiveness in efficiently computing the short-term risk indices of a wind-integrated composite power system. The short-term risk indices are also evaluated for the commitment schedules obtained from the DAUC program to show its application in power systems operation.

The main contributions of this work are as follows:

1. A novel hybrid framework for short-term risk assessment is proposed. The framework exploits the advantages of the area risk method and NSMCS to suitably assess the short-term risk of wind-integrated composite power systems. The proposed framework can also evaluate the bus- or load-point indices.
2. To obtain accurate short-term risk indices, a new reliability modeling approach for wind generation is also proposed. This approach effectively models the uncertainty of wind generation in the operational domain through conditional distributions. Additionally, the area risk method is modified to include the proposed reliability modeling approach.
3. The computational speed of the proposed hybrid framework is greatly enhanced by adopting the CE-based IS technique for NSMCS. The IS technique is also applied to the conditional distributions of wind speed.

### 3.3 Preliminaries of the Area Risk Method

The area risk method, which is an extension of the basic PJM method, was first proposed to consider rapid start generating units in the evaluation of short-term risk [17]. The area risk method divides the given lead time into several sub-periods, and the partial risk in each sub-period is obtained using the basic PJM method. The summation of these partial risks gives the overall short-term risk for a given lead time. Consequently, the area risk method can consider the varying operational states of a power system within a lead time. As an example, Figure 3.1 pictorially depicts the area risk method for a given lead time that is divided into three sub-periods. Note that this representation only portrays the area risk method and does not necessarily represent the actual short-term risk indices.

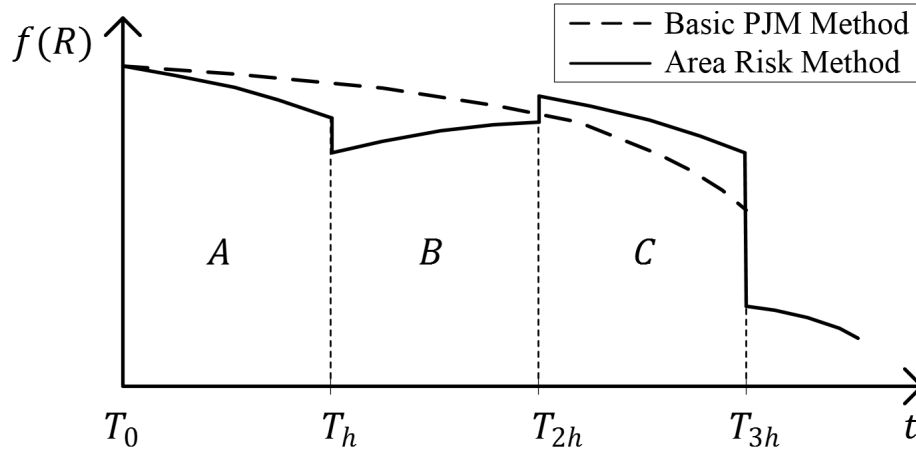


Figure 3.1 Pictorial representation of the area risk method.  $T_0$  represents the initial hour.  $T_h$ ,  $T_{2h}$ , and  $T_{3h}$  represent one, two, and three hour(s), respectively, after the initial hour.

After dividing the lead time into appropriate sub-periods, the next step is to obtain suitable reliability models of different components of a power system for each sub-period of the area risk method.

#### 3.3.1 Conventional Generators Modeling

Reliability modeling of conventional generators for short-term risk assessment is based on the assumption that the lead time is sufficiently short to ignore any repair processes [17]. Therefore, the probability of a generating unit on outage, also known as the ORR, is given by the following exponential distribution:

$$ORR_g = 1 - e^{-\lambda_g t} \approx \lambda_g t, \quad \forall g \in \{1, \dots, N^G\}, \quad (3.1)$$

where each generating station  $g$  consists of  $N^g$  identical generating units with  $ORR_g$ ,  $\lambda_g$  is the failure rate in failures per hour of a generating unit in generating station  $g$ ,  $t$  is the lead time, and  $N^G$  is the total number of generating stations in the power system. Note that because of its memoryless property, the exponential distribution inherently models the dependence of a random variable (in this case, time to fail  $t$ ) between the sub-periods [42]. In other words, the failure time of a generating unit in a certain sub-period is dependent on the generating unit's outage history in the previous sub-periods.

### 3.3.2 Transmission Lines Modeling

In the original area risk method and its variants [23], [46], [48], [49], [69], the transmission system is generally ignored. However, transmission line outages coupled with line flow limits might also result in load curtailment, which contributes to the short-term risk. Therefore, in this work, the transmission system is taken into account for accurate short-term risk evaluation. The inclusion of transmission system also allows for the calculation of bus-point indices. Similar to the modeling of conventional generators, the repair process is ignored and the exponential distribution is assumed. Consequently, the transmission lines are also modeled using ORR. For a line  $l$ :

$$ORR_l = 1 - e^{-\lambda_l t} \approx \lambda_l t, \quad \forall l \in \{1, \dots, N^L\}, \quad (3.2)$$

where  $\lambda_l$  is the failure rate in failures per hour of transmission line  $l$  and  $N^L$  is the total number of transmission lines.

## 3.4 Proposed Reliability Modeling of Wind Generation

Aptly modeling the variability of wind generation during the lead time is vital to precisely assess the short-term risk of a wind-integrated power system. The wind generation fluctuates with the wind speed that is highly irregular and variable. Hence, a single ORR, as used for conventional generators, cannot represent the wind generation's capacity outages in short-term risk assessment methods.

One approach to modeling the wind generation is through the probabilistic modeling of wind speed during the lead time. The wind speed in a short future time period strongly depends on the

initial wind speed at the start of that time period. This observation has been adopted in [23] and [46]. In particular, [46] obtains the conditional PDFs of wind speed for different sub-periods in the lead time for a given initial wind speed at the start of the lead time ( $T_0$  in Fig. 1). The initial wind speed at  $T_0$  is deterministically known, along with other operational statuses during power systems operation. The conditional PDFs are then converted to wind power PDFs using the wind turbine's power curve. Figure 3.2 represents these conditional PDFs of wind speed for a given initial wind speed at  $T_0$  in different sub-periods for an actual wind farm site. In this approach, the initial wind speeds at the start of subsequent sub-periods (i.e., at  $T_h$  and  $T_{2h}$ ) are ignored.

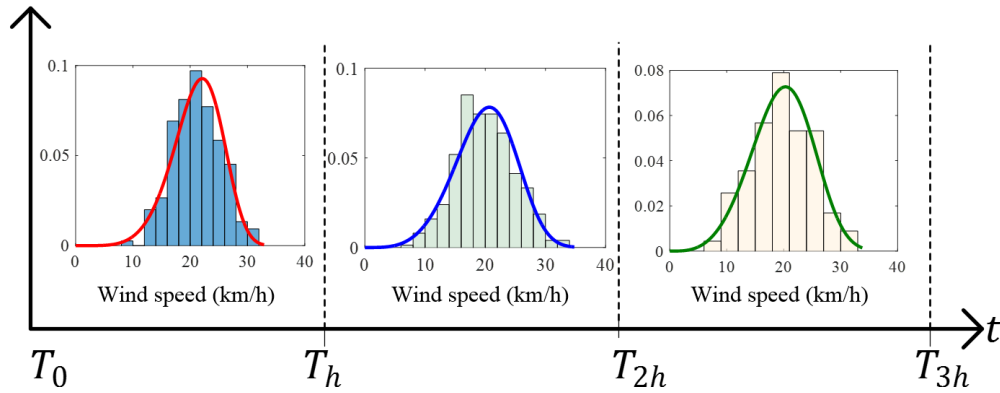


Figure 3.2 Conditional PDFs of wind speed in different sub-periods for a single initial wind speed at  $T_0$ .

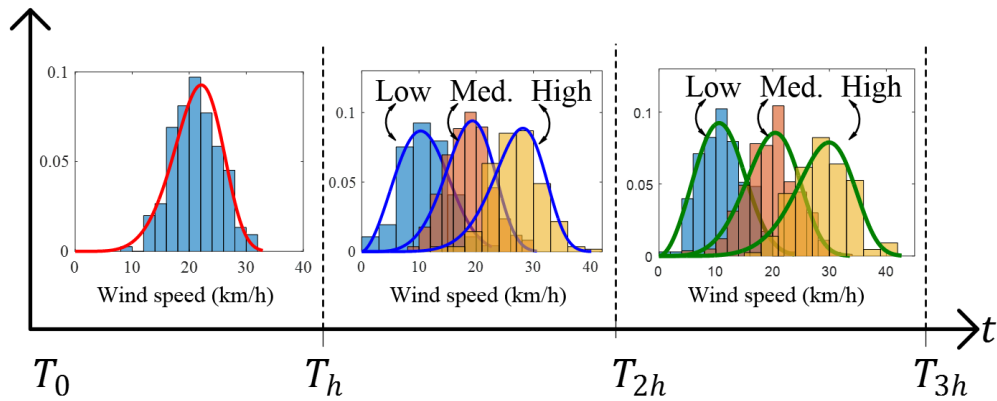


Figure 3.3 Conditional PDFs of wind speed in different sub-periods for different initial wind speeds at the start of those sub-periods.

Due to the highly volatile nature of wind speed, considering only a single wind speed PDF during each sub-period might not truly capture its spasmodic variations. Also, the wind speed PDFs

during different sub-periods can be poles apart depending on the initial wind speeds at the start of the respective sub-periods. In other words, the wind speed PDFs during different sub-periods should be conditional on the initial wind speed at the start of the respective sub-periods, and not at the start of the lead time. Figure 3.3 illustrates the abovementioned statements. For the second sub-period B ( $T_h - T_{2h}$ ), the conditional PDFs of wind speed for three arbitrarily chosen initial wind speeds (low, 10 km/h; medium, 20 km/h; high, 30 km/h) at the start of the second sub-period ( $T_h$ ) are shown. A comparison with Figure 3.2 shows that the conditional PDFs of wind speed in the second sub-period are markedly different from the one obtained by assuming a single initial wind speed at the start of the entire lead time. Similar conclusions can be drawn about the conditional PDFs of wind speed in the third sub-period C ( $T_{2h} - T_{3h}$ ). Hence, the conditional PDFs of wind speed in a sub-period must consider the probable initial wind speeds at the start of that sub-period. These probable initial wind speeds at the start of a sub-period, in turn, depend on the conditional PDF in the preceding sub-period.

To understand the impact of different modeling approaches of PDFs on the risk assessment, first, the risk is generally defined as follows [63]:

$$Risk = \int H(\mathbf{x})F(\mathbf{x})d\mathbf{x}, \quad (3.3)$$

where,  $H(\cdot)$  is a test function and will be explained later.  $F(\cdot)$  is the joint PDF of a random vector  $\mathbf{X}$ . For composite power systems,

$$F(\mathbf{X}) = f^G(\mathbf{X}^G)f^L(\mathbf{X}^L)f_P^{ws}(\mathbf{X}^w), \quad (3.4)$$

where,  $f^G(\mathbf{X}^G)$  is the PDF for random vector  $\mathbf{X}^G$ , which represents the number of available generating units in each generating station,  $f^L(\mathbf{X}^L)$  is the PDF for random vector  $\mathbf{X}^L$  representing the availability of transmission lines, and  $f_P^{ws}(\mathbf{X}^w)$  is the PDF for random vector of wind speed  $\mathbf{X}^w$  in a period P. Note that  $\mathbf{X} = [\mathbf{X}^G, \mathbf{X}^L, \mathbf{X}^w]$ .  $f^G(\mathbf{X}^G)$  and  $f^L(\mathbf{X}^L)$  can be calculated using (3.1) and (3.2), respectively. From (3.3) and (3.4), it is clear that the choice of PDFs directly affects the risk indices. Hence, a more precise determination of  $f_P^{ws}(\mathbf{X}^w)$  will expectedly result in more accurate risk indices.

Now using the above notation, according to [46],

$$f_B^{ws}(v^B) = f_{B|A}^{ws}(v^B|v^A), \quad f_C^{ws}(v^C) = f_{C|B}^{ws}(v^C|v^B), \quad (3.5)$$

where,  $f_{B|A}^{ws}(v^B|v^A)$  is the conditional PDF for sub-period B given a PDF for sub-period A, and  $f_{C|B}^{ws}(v^C|v^B)$  is the conditional PDF for sub-period C given a PDF for sub-period B. In other words, (3.5) implies that the PDFs for sub-periods B and C are assumed to be independent of the PDFs for sub-periods A and B, respectively. This independence assumption indicates the lack of information about the model.

As shown in Figure 3.3 and its corresponding discussion, a more reasonable approach is to model the PDFs for sub-periods B and C, considering their dependence on the PDFs for sub-periods A, and B, respectively. By the law of total probability, these PDFs can be obtained as

$$f_B^{ws}(v^B) = \int_{-\infty}^{\infty} f_{B|A}^{ws}(v^B|v^A) f_A^{ws}(v^A) dv^A, \quad (3.6)$$

$$f_C^{ws}(v^C) = \int_{-\infty}^{\infty} f_{C|B}^{ws}(v^C|v^B) f_B^{ws}(v^B) dv^B, \quad (3.7)$$

In this work, a systematic approach based on probabilistic techniques, is proposed to consider (3.6) and (3.7) for the short-term risk assessment. In what ensues, the proposed approach is explained by considering a lead time of 3 hours as an example. For a specific power system, the actual determination of a suitable lead time depends on the start-up times of rapid-start generating units [43]. Also, as an example, the lead time is divided into three hourly sub-periods. Note that the choice of hourly sub-periods is motivated by the typical one-hour intervals considered in the UC programs. However, the systematic approach presented here is generally applicable to any length of lead time and for any number of sub-periods.

Referring to Figure 3.1, as a first step, using the known initial wind speed ( $v^{\text{ini},A}$ ) at the start of the lead time, i.e. at the start of sub-period A, the conditional PDF of wind speed for sub-period A,  $f_A^{ws}(v^A)$ , is obtained using Algorithm 1. In Algorithm 3.1, for  $f_A^{ws}(v^A)$ , the given hour is  $T_0$  and the  $h$ th hour is  $T_h$ .

---

**Algorithm 3.1** Algorithm for Wind Speed Conditional PDFs

---

---

**Input:** Mean and standard deviation of historical hourly wind speeds, ARMA series of wind speed, and initial wind speed of a given hour

**Output:** Conditional Weibull PDF of wind speed for the next  $h$ th hour

- 1: Simulate the ARMA series of wind speed using historical hourly wind speed data for a large number of simulation years  $N$  ( $\sim 5000 - 10,000$  years) [23], let  $\Lambda$  be the set of simulated wind speed values, then  $\Lambda = \{v_s^{t,\eta}, t \in \{1, \dots, 8760\}, \eta \in \{1, \dots, N\}$ , where  $v_s^{t,\eta}$  is the simulated wind speed in hour  $t$  and year  $\eta$ .
  - 2: Define an interval  $\Delta v$  (e.g., 1 km/h) around the initial wind speed of the given hour
  - 3: Group all those simulated wind speed values of the next  $h$ th hour, provided that the simulated wind speed values of the given hour lie in the interval around the initial wind speed, i.e.,  $\Psi = \{v_s^{T_0+h,\eta} : v_0^{T_0} - \frac{\Delta v}{2} \leq v_s^{T_0,\eta} \leq v_0^{T_0} + \frac{\Delta v}{2}\}, \eta \in \{1, \dots, N\}$ , where  $\Psi \subset \Lambda$  is the set of grouped simulated wind speed values  $v_s^{T_0+h}$  of  $h$ th hour,  $v_s^{T_0}$  is the simulated wind speed values of given hour,  $v_0^{T_0}$  is the initial wind speed at given hour  $T_0$
  - 4: Fit a Weibull PDF to the set  $\Psi$ , i.e.,  $f_h^{ws}(\cdot) = \text{Weib}(a, b)$ , where  $a$  is the scale parameter and  $b$  is the shape parameter.
- 

Next, the PDF for the first sub-period A is divided into  $N^p$  partitions. The midpoints of these partitions are assumed to be estimates of initial wind speeds for the start of sub-period B i.e., at  $T_h$ . These midpoints are obtained using (3.8)–(3.10):

$$p_i^A = \underline{v}^A + i \left( \overline{v}^A - \underline{v}^A \right) / N^p, \quad \forall i \in \{1, \dots, N^p - 1\}, \quad (3.8)$$

$$v_j^{\text{ini},B} = \frac{p_{j-1}^A + p_j^A}{2}, \quad \forall j \in \{2, \dots, N^p - 1\}, \quad (3.9)$$

$$v_1^{\text{ini},B} = \frac{\underline{v}^A + p_1^A}{2}, \quad v_{N^p}^{\text{ini},B} = \frac{p_{N^p-1}^A + \overline{v}^A}{2}, \quad (3.10)$$

where  $p_i^A$  and  $v_j^{\text{ini},B}$  are the partitioning points of  $f_A^{ws}(v^A)$  and the estimated initial wind speeds, respectively.  $\overline{v}^A$  and  $\underline{v}^A$  are the maximum and minimum observed wind speed values of  $v^A$  in sub-period A, respectively.

Each of these estimated initial wind speeds have associated occurrence probabilities that can be calculated using (3.11)–(3.13):

$$P(v_j^{\text{ini},B}) = \int_{p_{j-1}^A}^{p_j^A} f_A^{ws}(v^A) dv^A, \quad (3.11)$$

$$P(v_1^{\text{ini},B}) = \int_0^{p_1^A} f_A^{ws}(v^A) dv^A, \quad (3.12)$$

$$P(v_{N^p}^{\text{ini},B}) = \int_{p_{N^p-1}^A}^{\infty} f_A^{ws}(v^A) dv^A, \quad (3.13)$$

where  $P(v_j^{\text{ini},B})$  is the probability of initial wind speed  $v_j^{\text{ini},B}$ . Note that  $\sum_{j=1}^{N^p} P(v_j^{\text{ini},B}) = 1$ .

Figure 3.4 depicts these estimated initial wind speeds using the conditional PDF of wind speed for sub-period A with  $N^p = 3$ . For this case, these three initial wind speeds might correspond to low, medium and high initial wind speed scenarios, having corresponding occurrence probabilities as illustrated by the shaded region in the figure.

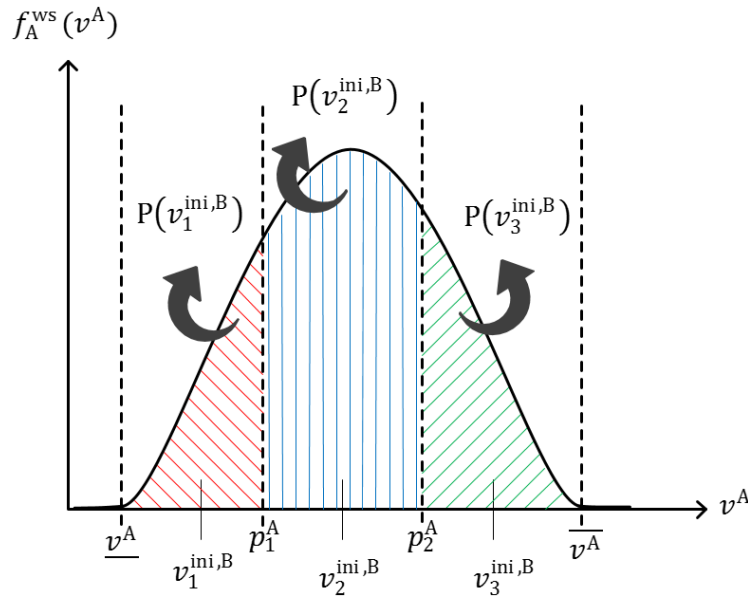


Figure 3.4 Partitioning of the conditional PDF of wind speed

Now, for each of these estimated initial wind speeds, conditional PDFs of wind speed for sub-period B are obtained using Algorithm 3.1. In this case, the initial hour is set to the start of sub-period B ( $t_h$ ) and the  $h$ th hour is set to the end of sub-period B ( $t_{2h}$ ). As a result, a total of  $N^P$  conditional PDFs ( $\{f_{B,1}^{ws}, \dots, f_{B,N^P}^{ws}\}$ ) are obtained that represent the variability of wind speed for this sub-period. This statement can be interpreted as follows. As the uncertainty of wind speed increases with future time, multiple PDFs are employed to represent this increased uncertainty. Moreover, each of these conditional PDFs also have occurrence probabilities given by (3.11)–(3.13).

By following a similar approach, the estimates of initial wind speed at the start of sub-period C ( $v_j^{\text{ini},C}$ ) can be obtained by further dividing each of the  $N^P$  conditional PDFs of sub-period B into  $N^P$  partitions. However, this division would result in  $N^P \times N^P$  estimates of initial wind speed and conditional PDFs for sub-period C, thereby requiring  $N^P \times N^P$  computations of partial risks. To circumvent the problem of high computational burden and intractability, first a surrogate conditional PDF of wind speed for sub-period B is estimated using the initial wind speed at the start of sub-period A via Algorithm 3.1. Afterward, this surrogate conditional PDF is divided into  $N^P$  partitions resulting in  $N^P$  estimated initial wind speeds for the start of sub-period C. Then, the conditional PDFs of wind speed for sub-period C ( $\{f_{C,1}^{ws}, \dots, f_{C,N^P}^{ws}\}$ ) are obtained using these estimated initial wind speed values via Algorithm 3.1. As a result, the conditional PDFs for sub-period C are still dependent on the initial wind speeds at the start of sub-period C, while the number of conditional PDFs remains  $N^P$ . The whole process can be repeated for any number of sub-periods of the area risk method and for any  $N^P > 1$ .

### 3.5 Proposed Risk Assessment Framework

In this section, the proposed framework for the short-term risk assessment of wind-integrated composite power systems is explained. The key ingredients of the proposed framework are the modified area risk method considering the proposed reliability modeling of wind generation and the IS-based NSMCS. The short-term risk index considered in this chapter is the probability index, i.e., the probability of load curtailment. Nonetheless, the framework can be easily extended to evaluate other risk indices, such as expected power not supplied and expected number of load curtailments.

### 3.5.1 Modified Area Risk Method

The area risk method needs to be adapted to consider the proposed reliability modeling of wind generation. Note that, for each sub-period B and C,  $N^P$  partial risks, corresponding to  $N^P$  conditional PDFs of wind speeds, must be evaluated. Also, because each of these  $N^P$  partial risks represent disjoint events, the law of total probability can be applied to obtain the net partial risks. For sub-periods B and C, the net partial risks are given by (3.14)–(3.15), and the total risk is then evaluated by (3.16):

$$R_B = \sum_{j=1}^{N^P} P(v_j^{\text{ini},B}) \cdot PR_j^B - R_A, \quad (3.14)$$

$$R_C = \sum_{j=1}^{N^P} P(v_j^{\text{ini},C}) \cdot PR_j^C - R_B, \quad (3.15)$$

$$R = R_A + R_B + R_C, \quad (3.16)$$

where  $PR_j^B$  is the partial risk in sub-period B considering the  $j$ th conditional PDF of wind speed  $v^B$ . Similarly,  $PR_j^C$  represents the partial risk in sub-period C considering the  $j$ th conditional PDF of wind speed  $v^C$ .  $R_A$ ,  $R_B$ , and  $R_C$  are the net partial risks for sub-periods A, B, and C, respectively.  $R$  is the total risk for the entire lead time. Equations (3.14) and (3.15) can be viewed as discrete approximations to (3.6) and (3.7), respectively. Fig. 5 pictorially represents the modification to the area risk method for  $N^P = 3$ .

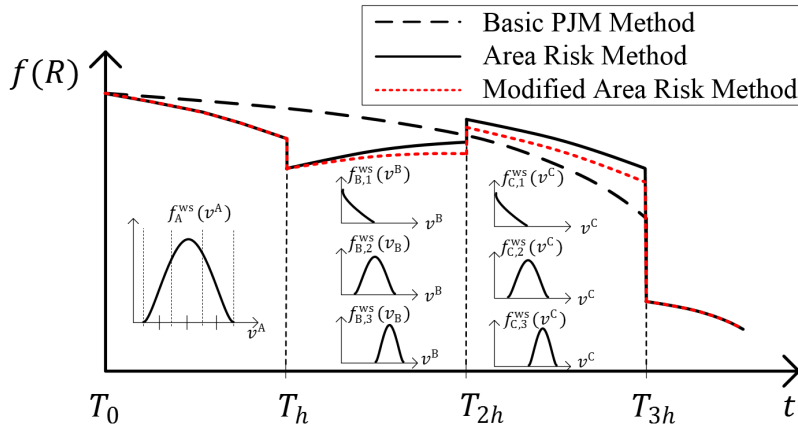


Figure 3.5 Integrating the proposed reliability modeling of wind generation in the area risk method

### 3.5.2 Evaluation of Partial Risks via CE-MCS

The routinely employed approach to evaluate the partial risks in the area risk method is to use a capacity outage probability table (COPT), which is, in essence, an analytical method. As mentioned in the Section 3.2, analytical methods are not appropriate for composite power system risk assessment. Therefore, a more prudent approach is to employ a simulation technique such as NSMCS. Simulation techniques are robust to system size and can also consider a wide range of operational characteristics. Therefore, this work proposes a fusion of the area risk method with NSMCS to adequately assess the short-term risk of a composite power system.

Using crude NSMCS, the  $j$ th partial risk for any sub-period P can be evaluated as

$$PR_j^P = \frac{1}{N^{\text{sim}}} \sum_{k=1}^{N^{\text{sim}}} H(\mathbf{X}_k; L), \quad (3.17)$$

where  $\mathbf{X}_k = [\mathbf{X}_k^G, \mathbf{X}_k^L, \mathbf{X}_k^W]$ ,  $\mathbf{X}_k^G = [n_k^1, \dots, n_k^g, \dots, n_k^{N^G}]$ ,  $\mathbf{X}_k^L = [\zeta_k^1, \dots, \zeta_k^l, \dots, \zeta_k^{N^L}]$ , and  $\mathbf{X}_k^W = [v_k^1, \dots, v_k^w, \dots, v_k^{N^W}]$ .  $\mathbf{X}_k^G$  and  $\mathbf{X}_k^L$  are the  $k$ th samples following  $B(\mathbf{X}; \mathbf{N}^g, \mathbf{ORR}_G)$  and  $B(\mathbf{X}; \mathbf{1}, \mathbf{ORR}_L)$ , respectively, where  $B(\cdot; \cdot, \cdot)$  stands for the binomial distribution [18].  $\mathbf{ORR}_G$  and  $\mathbf{ORR}_L$  are vectors of ORRs for the generating stations and transmission lines, respectively.  $n_k^g$  represents the number of available generating units in generating station  $g$  having a total of  $N^g$  generating units.  $\mathbf{N}^g$  is a vector of the number of generating units  $N^g$ .  $\zeta_k^l$  is 1 if line  $l$  is available and 0 if it is on outage.  $v_k^w$  is the  $k$ th wind speed sample following the  $j$ th conditional PDF of the wind speed of wind farm  $w$ ,  $f_{P,j}^{ws,w}(\mathbf{X}_k^W)$ .  $N^W$  is the number of wind farms.  $N^{\text{sim}}$  is the number of samples. Note that  $R_A$  in (3.16) can also be calculated using (3.17).

In (3.17),  $H(\mathbf{X}_k; L)$  is a test function that evaluates whether or not the sample  $\mathbf{X}_k$  leads to load curtailment. For the short-term risk assessment of a generating system,

$$H(\mathbf{X}_k; L) = \begin{cases} 0 & S(\mathbf{X}_k) \geq L \\ 1 & S(\mathbf{X}_k) < L' \end{cases} \quad (3.18)$$

where  $S(\mathbf{X}_k)$  represents the summation of available generation capacity associated with state  $\mathbf{X}_k$ , and  $L$  is the load. For composite power systems, the definition of  $S(\mathbf{X}_k)$  is modified, as the transmission system should also be considered to determine the load curtailment. In this regard, the DC representation of transmission system is adopted in this work. The DC-OPF is employed to evaluate the load curtailment at each bus for each state  $\mathbf{X}_k$ . If no load curtailment occurs at any

bus,  $S(\mathbf{X}_k)$  is the same as that obtained for the generating system. However, if the load curtailment is non-zero,  $S(\mathbf{X}_k)$  is given by:

$$S(\mathbf{X}_k) = \sum_{b=1}^{N^B} l_b, \quad (3.19)$$

where  $l_b$  is the load served at bus  $b$  and  $N^B$  is the total number of buses in the system.  $l_b$  is obtained using the DC-OPF.

A fundamental downside of the crude NSMCS is the large computational burden when the events to be assessed are rare i.e. for *rare event simulation* [63]. This is the case in the short-term risk assessment as the probability of load curtailment in a short lead time is often very small (around  $\sim 10^{-4}$ ). Also, because  $N^P$  partial risks are required to be evaluated for each of sub-periods B and C, the direct application of the crude NSMCS is computationally prohibitive. Hence, in this work, the IS technique is applied to improve the computational performance of the crude NSMCS. The IS is a variance reduction technique in which the original probability distributions are distorted to increase the occurrences of failure events, thereby accelerating the convergence rate of simulation. In this case, IS modifies  $B(\cdot; \mathbf{N}^g, \mathbf{ORR}_G)$  and  $B(\cdot; \mathbf{1}, \mathbf{ORR}_L)$  to  $B(\cdot; \mathbf{N}^g, \mathbf{ORR}_G^*)$  and  $B(\cdot; \mathbf{1}, \mathbf{ORR}_L^*)$ , respectively. In addition, in this work, the original conditional PDF of the wind speed is distorted from  $f_{P,j}^{ws,w}(\cdot)$  to  $f_{P,j}^{ws,w,*}(\cdot)$ .  $f_{P,j}^{ws,w}(\cdot)$  is a Weibull distribution with two parameters  $(a_w, b_w)$ ; however, only the scale parameter  $(a_w)$  is modified. These distorted PDFs, also known as the IS densities, are then used to obtain the new samples  $\mathbf{X}_k$ . The partial risk is then evaluated by the following unbiased estimator:

$$PR_j^P = \frac{1}{N^{\text{sim}}} \sum_{k=1}^{N^{\text{sim}}} H(\mathbf{X}_k; L) W(\mathbf{X}_k), \quad (3.20)$$

where  $W(\mathbf{X}_k)$  is the likelihood ratio and given by:

$$W(\mathbf{X}_k) = W_G(\mathbf{X}_k) W_L(\mathbf{X}_k) W_W(\mathbf{X}_k), \quad (3.21)$$

$$W_G(\mathbf{X}_k) = B(\mathbf{X}_k^G; \mathbf{N}^g, \mathbf{ORR}_G) / B(\mathbf{X}_k^G; \mathbf{N}^g, \mathbf{ORR}_G^*), \quad (3.22)$$

$$W_L(\mathbf{X}_k) = B(\mathbf{X}_k^L; \mathbf{1}, \mathbf{ORR}_L) / B(\mathbf{X}_k^L; \mathbf{1}, \mathbf{ORR}_L^*), \quad (3.23)$$

$$W_W(\mathbf{X}_k) = \prod_{w=1}^{N^W} (f_{P,j}^{ws,w}(\mathbf{X}_k^W) / f_{P,j}^{ws,w,*}(\mathbf{X}_k^W)). \quad (3.24)$$

Different methods can be employed to obtain the IS densities [63], [73]. The most widely used approach is the CE optimization, which minimizes the Kullback-Leibler divergence between the optimal IS densities and the approximated IS densities. In this work, the CE optimization is adopted to find the IS densities for generators, transmission lines, and wind speed. Interested readers are referred to [73] for a detailed discussion on the CE optimization and to [74], [75], [76] for its initial application to the long-term risk assessment of power systems. For the sake of simplicity, the CE optimization is presented here as Algorithm 3.2, without detailing each step.

The combination of the CE optimization with NSMCS will be referred to, henceforward, as the CE-MCS.

---

**Algorithm 3.2** CE Optimization

---

**Input:** Original ORRs of generating units and transmission lines, Weibull PDF of wind speed and load  $L$

**Output:** Distorted ORR of generating units and transmission lines, and distorted Weibull PDF of wind speed

- 1: Set the number of samples for CE optimization ( $N^{\text{CE}}$ ), and other CE parameters ( $\rho, \alpha, m^{\text{max}}$ )
- 2: Obtain the original vectors of ORRs and  $f_{P,j}^{ws,w}(\cdot)$
- 3: Set iteration counter  $m = 1$ ,  $\mathbf{ORR}_G^m = \mathbf{ORR}_G$ ,  $\mathbf{ORR}_L^m = \mathbf{ORR}_L$ , and  $f_{P,j}^{ws,w,m}(\cdot) = f_{P,j}^{ws,w}(\cdot)$
- 4: **for**  $m = 1$  to  $m = m^{\text{max}}$  **do**
- 5:     Obtain samples  $\mathbf{X}_p = [\mathbf{X}_p^G, \mathbf{X}_p^L, \mathbf{X}_p^W]$ , where  $p = \{1, \dots, N^{\text{CE}}\}$ , following  $B(\cdot; \mathbf{N}^g, \mathbf{ORR}_G^m)$ ,  $B(\cdot; \mathbf{N}^g, \mathbf{ORR}_L^m)$ , and  $f_{P,j}^{ws,w,m}(\cdot)$
- 6:     Evaluate the performance function  $S(\mathbf{X}_p)$  and arrange  $S(\mathbf{X}_p)$  in ascending order, i.e.,  $S[1] \leq S[2] \leq \dots \leq S[N^{\text{CE}}]$
- 7:     **if** ( $S[\lceil \rho N^{\text{CE}} \rceil] \geq L$ ), set  $\widehat{L}_m = S[\lceil \rho N^{\text{CE}} \rceil]$  **else** set  $\widehat{L}_m = L$
- 8:     Evaluate the test function  $H(\mathbf{X}_p; \widehat{L}_m)$  for all  $p$
- 9:     Calculate  $W_G(\mathbf{X}_p)$ ,  $W_L(\mathbf{X}_p)$ , and  $W_W(\mathbf{X}_p)$  using (5f)–(5h), also calculate  $W(\mathbf{X}_p)$  using (5e), for all  $p$
- 10:    Calculate the distorted ORRs and scale parameter:

$$ORR_g^{m+1} = \alpha \left( 1 - \frac{1}{N^g} \frac{\sum_{p=1}^{N^{\text{CE}}} H(\mathbf{X}_p; \widehat{L}_m) W(\mathbf{X}_p) n_p^g}{\sum_{p=1}^{N^{\text{CE}}} H(\mathbf{X}_p; \widehat{L}_m) W(\mathbf{X}_p)} \right) + (1 - \alpha) ORR_g^m$$

$$ORR_l^{m+1} = \alpha \left( 1 - \frac{\sum_{p=1}^{N^{CE}} H(\mathbf{X}_p; \widehat{L}_m) W(\mathbf{X}_p) \zeta_p^l}{\sum_{p=1}^{N^{CE}} H(\mathbf{X}_p; \widehat{L}_m) W(\mathbf{X}_p)} \right) + (1 - \alpha) ORR_l^m$$

$$a_w^{m+1} = \left( \frac{\sum_{p=1}^{N^{CE}} H(\mathbf{X}_p; \widehat{L}_m) W(\mathbf{X}_p) (v_p^w)^{b_w}}{\sum_{p=1}^{N^{CE}} H(\mathbf{X}_p; \widehat{L}_m) W(\mathbf{X}_p)} \right)^{1/b_w}$$

11:     **if**  $\widehat{L}_m = L$ , break the **for** loop

12:     Set  $ORR_G^* = ORR_G^m$ ,  $ORR_L^* = ORR_L^m$ , and  $f_{p,j}^{ws,w,*}(\cdot) = f_{p,j}^{ws,w,m}(\cdot)$

---

### 3.5.3 Overall Framework

The complete hybrid framework for the short-term risk assessment of wind-integrated composite power systems is given in Figure 3.6. The first step of the framework involves determining the committed generating units through a UC program. Then, the modified area risk method is utilized and the partial risk for the first sub-period is obtained using the CE-MCS presented in Section 3.5.2. Thereafter,  $N^p$  partial risks are evaluated using (3.20) for each subsequent sub-period. Finally, the total risk is evaluated using (3.16). Note that the parallel computational techniques can be applied to calculate the partial risks for all sub-periods at the same time. To this end, the framework in Fig. 6 can be slightly modified. The step for calculating the net partial risks ((3.14) and (3.15)) after evaluating partial risks for all conditional PDFs for a sub-period can be deferred, and the partial risks for all sub-periods can be calculated first. This allows steps in the larger grey rectangles in Figure 3.6 to be run on separate cores of a PC at the same time.

With regard to the evaluation of bus-point indices, the only modification required to the proposed framework is a change in the definition of test function  $H(\mathbf{X}_k; L)$ . In this case,  $H(\mathbf{X}_k; L)$  must be defined for each bus in the power system as follows:

$$PR_j^P = \frac{1}{N^{\text{sim}}} \sum_{k=1}^{N^{\text{sim}}} H(\mathbf{X}_k; L) W(\mathbf{X}_k), \quad (3.24)$$

$$H_b(\mathbf{X}_k; L_b) = \begin{cases} 0 & l_b \geq L_b \\ 1 & l_b < L_b \end{cases}, \quad (3.25)$$

where  $H_b(\mathbf{X}_k; L_b)$  is the test function for bus  $b$ ,  $L_b$  is the load demand at bus  $b$ . After defining the test function, the rest of procedure is similar, and the partial risk is calculated using:

$$PR_{j,b}^P = \frac{1}{N^{\text{sim}}} \sum_{k=1}^{N^{\text{sim}}} H_b(\mathbf{X}_k; L_b) W(\mathbf{X}_k), \quad (3.26)$$

where  $PR_{j,b}^P$  is the partial risk for bus  $b$  in sub-period  $P$  considering the  $j$ th conditional PDF of wind speed.

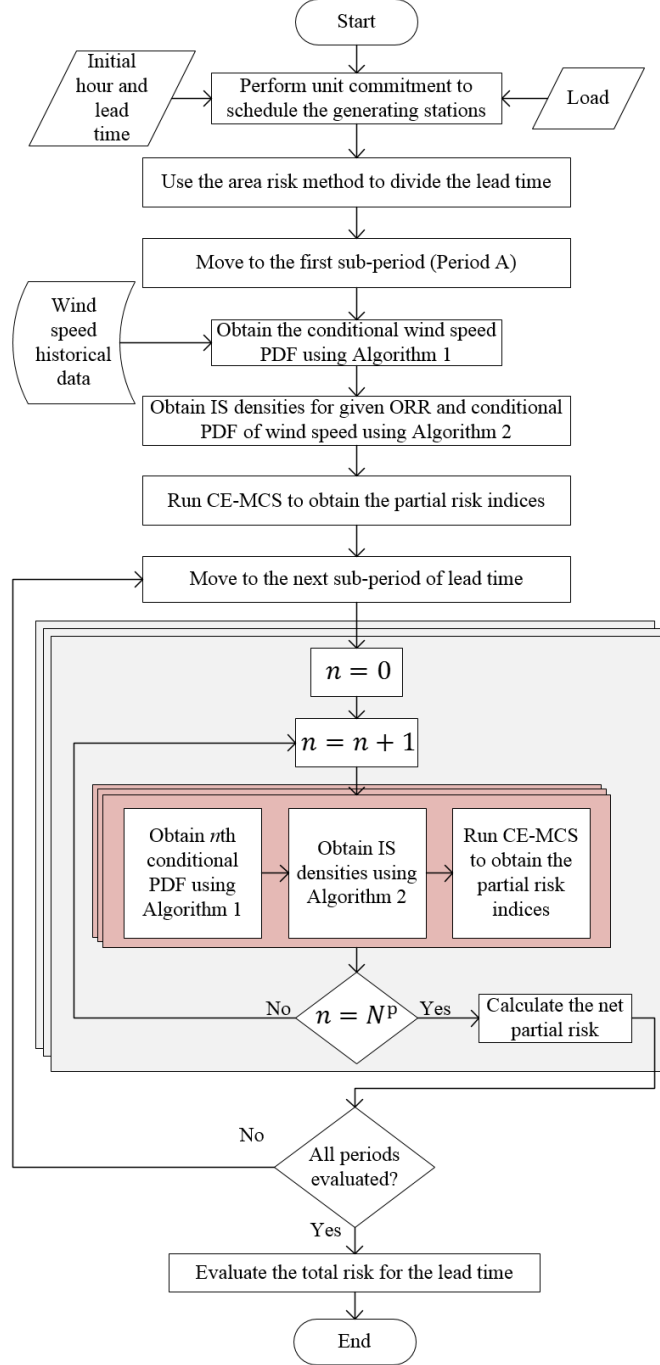


Figure 3.6 Proposed hybrid framework for the short-term risk assessment

### 3.6 Case Studies

In this section, the effectiveness of the proposed framework is demonstrated through some key simulations performed on the modified 24-bus IEEE RTS [77]. The original RTS comprises 14 generating stations with 32 generating units in total, 24 buses, 17 load points, and 33 transmission lines. The original RTS is modified by including a 1,000 MW wind farm at bus 14. Also, a 155 MW conventional generator at bus 16 is removed. For CE optimization,  $N^{\text{CE}}$  is set between 20,000 and 50,000,  $\rho$  is set between 0.01 and 0.05,  $\alpha$  is set to 0.95, and  $m^{\text{max}}$  is set to 10. These parameters are obtained from [73] and [74]. For the convergence of MCS, the minimum coefficient of variation (COV) is set to 2% for the generating system and 5% for the composite power system. In all simulations, the lead time is equal to 3 hours and  $N^{\text{P}}$  is set to 3. The ARMA series for Algorithm 1, along with the wind turbine curve, is obtained from [21]. All studies are performed for January 31 from hours 00:00 to 04:00, unless otherwise stated. Note that these specific hours are only selected for case studies. As it will be shown later, the proposed framework is generally applicable for any time of the day. All simulations are performed on a PC with a 3.40 GHz Intel® Core i7-4770 CPU and 16 GB RAM. The proposed framework is implemented in MATLAB R2015a, with GUROBI 7.0.2 used as a solver for DC-OPF.

#### 3.6.1 Demonstrative Case

To confirm the efficacy of the proposed reliability modeling approach of wind generation, the proposed framework is compared with the approaches presented in [23] and [46]. Because [23] and [46] do not consider the transmission system, it is ignored in this subsection for the sake of comparison. The load is set to the peak value of 2,850 MW, and all 31 generating units are committed to supply the load.

Table 3.1 presents the short-term risk indices for different initial wind speeds at the start of the lead time. The short-term risk indices obtained from the proposed framework lie between the ones estimated by [23] and [46]. In other words, [46] ([23]) may overestimate (underestimate) the short-term risk indices. The aforementioned observation holds for all initial wind speed values. One reason for this behavior can be elucidated with the help of Table 3.2, which depicts the mean wind speeds and corresponding occurrence probabilities for each sub-period in all three approaches when the initial wind speed is 20 km/h. For example, for sub-period B, [46] assumes a mean wind

speed of 19.94 km/h with a probability of 100%. However, there is actually a 26.39% chance that the mean wind speed during sub-period B is 25.63 km/h. Higher mean wind speeds correspond to higher wind generation and, therefore, lower risk indices. On the other hand, [23] assumes a mean wind speed of 19.71 km/h for the entire lead time and thus neglects any possible low wind speed values that might occur within different sub-periods of the lead time. Hence, the risk obtained by [23] is lower. By considering the multiple conditional PDFs during sub-periods B and C, the proposed approach accounts for the probable variations in the wind speed and, consequently, in wind generation during these sub-periods, thereby resulting in more realistic risk evaluation.

Table 3.1 Short-term risk for different wind generation modeling methods

Initial Wind Speed	Case	$R_A (\times 10^{-4})$	$R_B (\times 10^{-4})$	$R_C (\times 10^{-4})$	$R (\times 10^{-4})$
10 km/h	Proposed	0.5011	1.3768	2.7686	4.6465
	[46]	0.5011	1.9990	4.2676	6.7677
	[23]		-		4.2690
20 km/h	Proposed	0.2630	0.9939	1.7637	3.0206
	[46]	0.2630	1.2337	2.8485	4.3452
	[23]		-		2.7855
30 km/h	Proposed	0.0384	0.2735	1.1404	1.4523
	[46]	0.0384	0.2782	1.2073	1.5239
	[23]		-		1.2634

Table 3.2 Mean wind speed during different sub-periods

Case	Period A (km/h)	Period B (km/h)	Period C (km/h)
Proposed	21.15 (1) †	12.05 (0.1290)	12.43 (0.2434)
		18.72 (0.6071)	20.55 (0.6058)
		25.63 (0.2639)	27.93 (0.1508)
[46]	21.15 (1)	19.94 (1)	19.71 (1)
[23]		19.71 (1)	

To further investigate the accuracy of the proposed reliability modeling approach, the regression analyses between wind generation values of different sub-periods are exhibited in Figure 3.7. A close scrutiny of Figure 3.7 reveals two important insights. Firstly, the linear regression models in sub-periods B and C are evidently different when the initial wind power (or initial wind speed) at the start of the respective sub-periods (i.e., at  $T_h$ , and  $T_{2h}$ , respectively) are considered. This observation reinforces the point made in Section 3.3 that the wind speed PDFs of sub-periods

should be conditional on the initial wind speeds at the start of respective sub-periods. Secondly, compared to Figure 3.7(a) and Figure 3.7(b), the linear regression models in Figure 3.7(c) and Figure 3.7(d), respectively, indicate higher wind generation in those sub-periods. The higher wind generation will expectedly result in lower probabilities of load curtailment. As a result, the short-term risk indices obtained using the proposed approach are lower than those calculated from [46] in Table 3.1

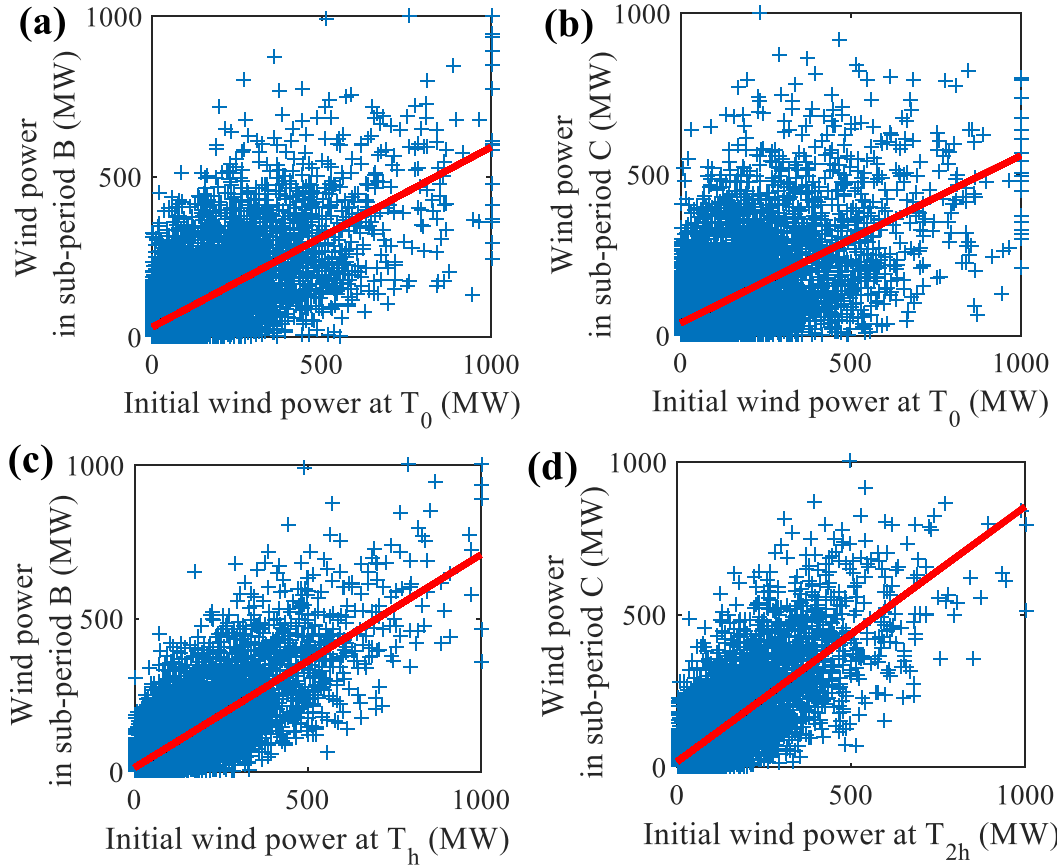


Figure 3.7 Regression analyses, (a), (b): using the approach of [46], and (c), (d): using the proposed approach

### 3.6.2 Computational Performance

From the power system operators' perspective, the computational speed of short-term risk assessment framework is of great importance in order to make timely risk-informed decisions. Ergo, in this subsection, the computational speed of the proposed framework is examined. For a COV of 2%, crude NSMCS would require nearly  $\sim 10^8$  samples to evaluate the risk which is on the

order of  $\sim 10^{-4}$  [54]. This means one complete risk evaluation for the entire lead time would require approximately  $\sim 7 \times 10^8$  samples. This, in turn, would result in extremely large computational times. Therefore, to compare the computational performances of the CE-MCS with the crude NSMCS within a suitable simulation time, the system is made less reliable by removing a 155 MW conventional generator at bus 15 and assessing the short-term risk indices of the resulting generating system. For this modified system, Table 3.3 compares the computational performances of the crude NSMCS against the CE-MCS, while considering the initial wind speed of 20 km/h. The computational performance of the CE-MCS is several orders higher than that of the crude NSMCS. The poor performance of the crude NSMCS is due to very low failure probabilities of the power system components during a short lead time.

Table 3.3 Computational performance of CE-MCS vs. Crude NSMCS

Case	Metric	Period A	Period B	Period C	Total
CE-MCS	Risk ( $\times 10^{-3}$ )	2.0373	2.2227	3.8679	8.1279
	Time (s)	0.52	3.28	48.03	51.83
Crude NSMC	Risk ( $\times 10^{-3}$ )	2.0467	2.1426	4.1050	8.2943
	Time (s)	5804.26	7872.21	7040.96	20717

### 3.6.3 Composite Power System Risk Indices

The results presented in Sections 3.6.1 and 3.6.2 clearly establish the superiority of the proposed framework, both, in terms of the proper modeling of wind generation and very high computational performance, over existing methods. In this subsection, we turn our attention to the short-term risk assessment of a wind-integrated composite power system. The contingencies in the transmission system and the line flow limits are now considered. The conditions of RTS are the same as for Table 3.1. The initial wind speed is set to 20 km/h. Table 3.4 summarizes the short-term risk indices for different capacities of the transmission system. A comparison of Table 3.1 with Table 3.4 indicates that the short-term risk indices are expectedly higher when the transmission system is included in the assessment. Interestingly, the transmission system's capacities significantly affect the short-term risk indices. With lower transmission capacities, the short-term risk indices are measurably higher. The varying capacities of the transmission system may correspond to the situation of weather-dependent transmission line ratings. Hence, through the proposed framework, power system operators can also recognize the indirect impacts of weather on short-term risk

indices. On comparing Table 3.3 with Table 3.4, it can be observed that the computational time increases when the transmission system is considered. This is due to the DC-OPF analysis which is performed for each contingency state for composite systems.

Table 3.4 Short-term risk of composite power system

Capacity	Metric	Period A	Period B	Period C	Total
100 %	Risk ( $10^{-4}$ )	0.2536	0.9387	2.0397	3.2320
	Time (s)	91.56	378.49	324.75	794.80
90 %	Risk ( $10^{-3}$ )	0.2832	0.9798	1.1557	2.4187
	Time (s)	70.60	354.36	450.81	875.77
80 %	Risk ( $10^{-3}$ )	0.4510	1.1156	1.3384	2.9050
	Time (s)	72.66	314.00	246.90	633.56

Figure 3.8 is a heat map for the short-term risk at different bus-points when the transmission capacity is 100%. Some buses do not experience any load curtailment and the short-term risk indices at those buses are zero. Also, one can conclude that, from the point of view of short-term risk, bus 18 has the highest risk of load curtailment for these particular hours. Power system operators can utilize such information to provision bus-specific preventive actions. One such action involves re-dispatching the nearby generating units or committing additional units to minimize the risk. Note that these bus-point short-term risk indices can only be obtained by including the transmission system in the assessment framework

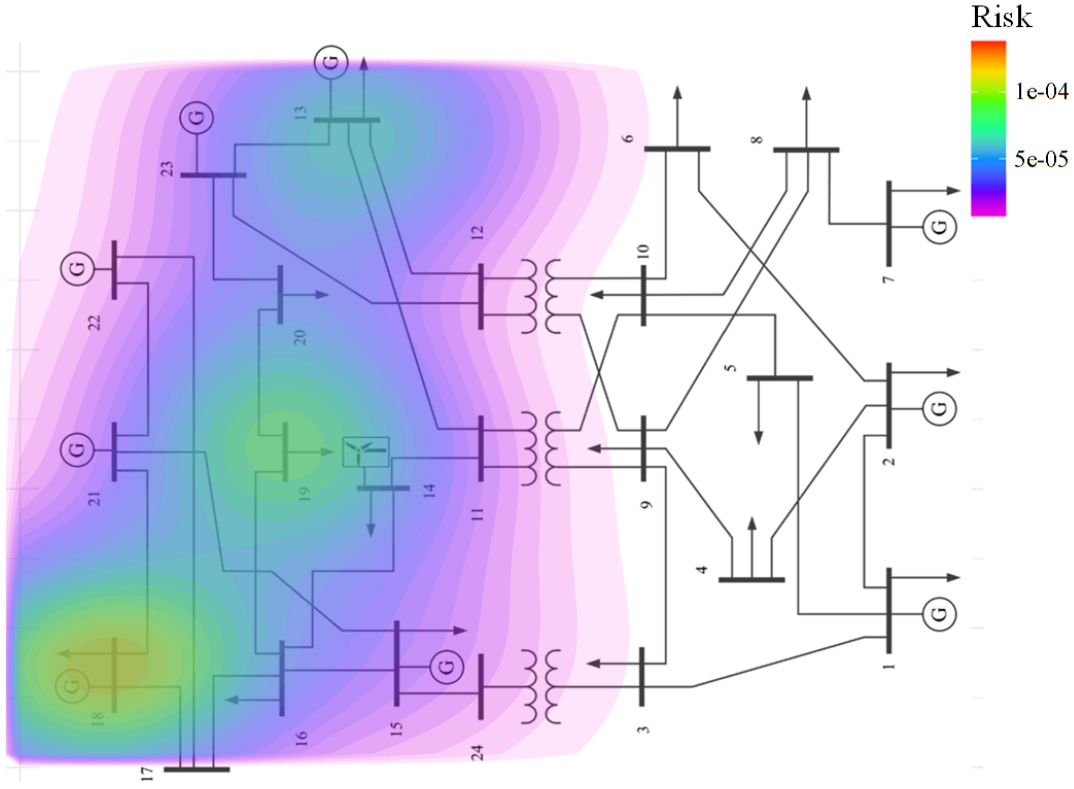


Figure 3.8 Heat map for the bus-pint short-term risk indices. This figure is generated using [78].

### 3.6.4 Daily Short-Term Risk Indices

This section evaluates short-term risk indices for an entire day. The studies are performed for April 2 and the historical mean hourly wind speeds of that day are assumed to be the initial wind speeds. Fig. 3.9 depicts the total risk for each hour of the day. Interestingly, the total risk is higher during off-peak hours as compared to on-peak hours; this is because few generating stations are committed to supply the load during off-peak hours. Furthermore, most of these committed generating stations comprise only a single unit. Hence, a single generating unit outage might result in load curtailment. On the other hand, many generating stations comprising several generating units are committed during on-peak hours. Wind generation also peaks during these hours. This observation is in stark contrast to the long-term risk assessment, in which the on-peak hours (i.e., the peak load) contribute the most to the long-term risk indices. This highlights the importance of considering the commitment decisions as well as daily variation in load and generation for short-term risk assessment.

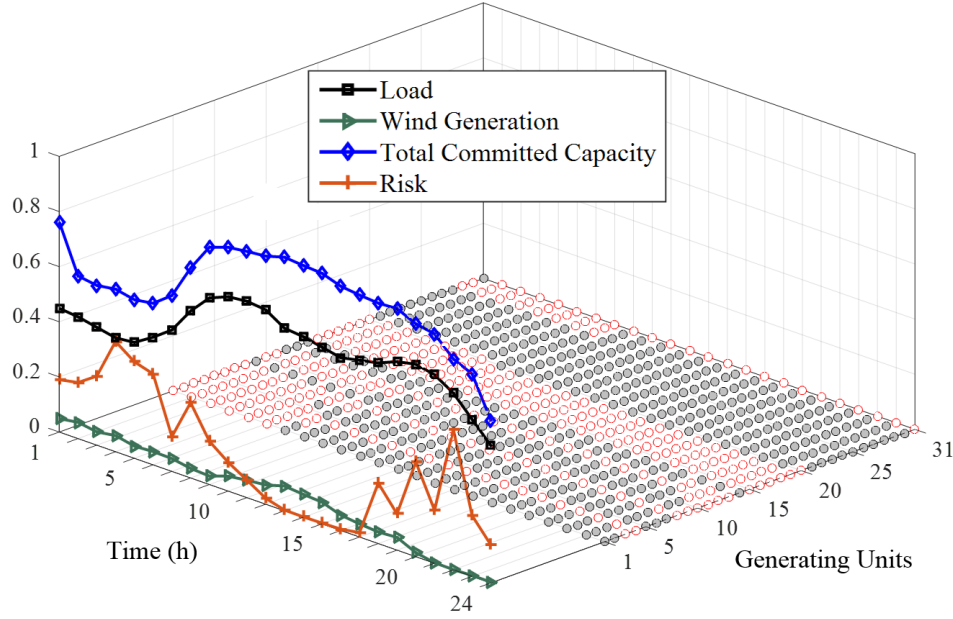


Figure 3.9 Daily short-term risk. Load, wind generation and total committed capacity is scaled down by 2000 and shown in MW. Short-term risk is scaled up by 100. Grey dots indicate the committed generating units.

### 3.6.5 Spinning Reserve Assessment

In this section, the proposed framework is applied to compare and contrast two deterministic criteria for setting the spinning reserve in power system operation. In criterion 1, the spinning reserve is equal to the capacity of the largest online generating unit, i.e. the N-1 criterion, and in criterion 2, the spinning reserve is set to a certain percentage of load (in this study, 10%) [79]. Figure 3.10 illustrates the short-term risk indices and the spinning reserve for the two criteria. As can be seen, for criterion 1, i.e. the N-1, the short-term risk indices are lower compared to criterion 2. However, the total operational costs are the opposite. For criterion 1, the DAUC costs are \$ 2.4864 M, whereas for criterion 2, the costs are \$ 2.0595 M. This shows that the reliability and costs compete with each other and that higher reliability comes at increased costs. An interesting observation is that, for criterion 1, the spinning reserve remains the same for all hours, however, the short-term risk varies noticeably. This observation demonstrates the shortfall of using inconsistent deterministic criteria for ensuring the reliability during power system operation. On contrary, the power system operators can utilize short-term risk indices to adjust the spinning reserve requirements while ensuring the reliability.

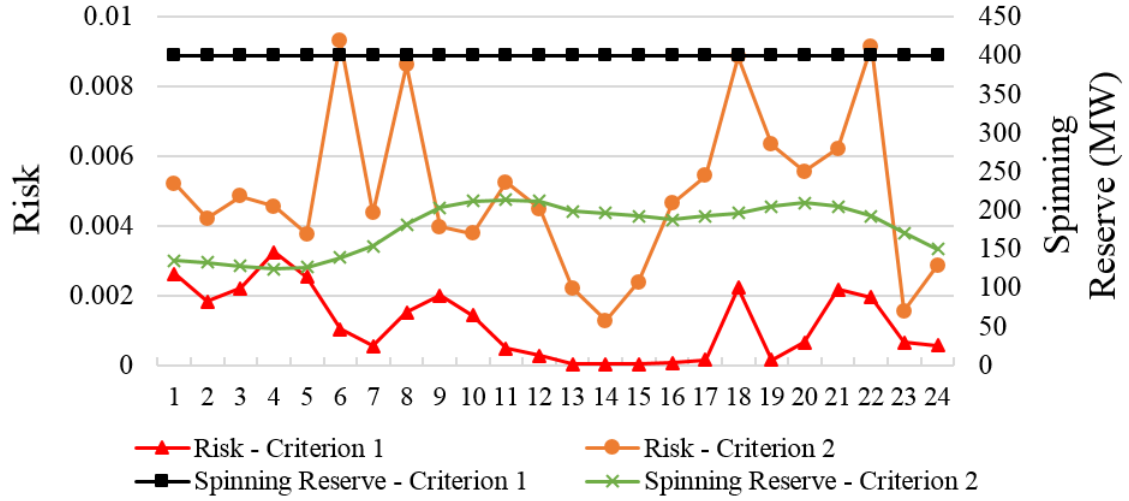


Figure 3.10 Short-term risk indices for different spinning reserve criteria.

### 3.6.6 Sensitivity to the Wind Generation Penetration

This subsection examines the effects of the penetration of wind generation on the short-term risk indices. Figure 3.11 shows that the total risk monotonically decreases with increasing capacity of the wind farm. For the first and second sub-periods, which are Period A and Period B, the decrease in risk is only marginal. A very slight increase in risk for Period B is observed when the wind farm capacity is 1,250 MW. This is due to the fact that the simulated risk indices are obtained within a certain range of true, actual values (in this case 5%). For the last sub-period, i.e., Period C, a sharp reduction in risk is observed. This observation supports the rationale of utilizing the area risk method to evaluate the partial risks and identify the sub-period(s) that contributes to the short-term risk.

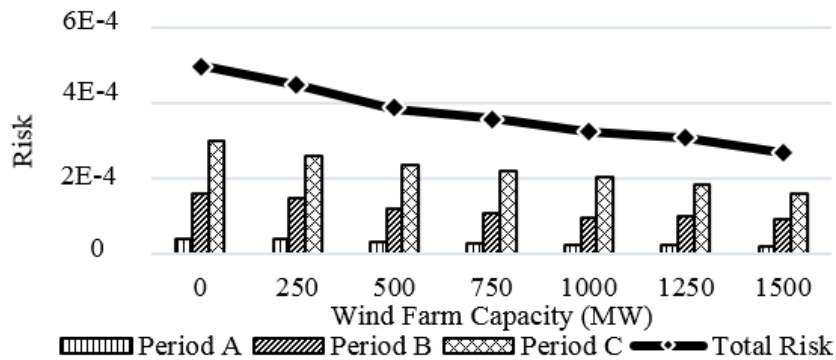


Figure 3.11 Short-term risk indices for varying capacities of wind generation. The condition of RTS are same as that for Table 3.4 (capacity 100%).

### 3.6.7 Sensitivity to the CE Parameters

This section examines the effect of parameters of CE optimization on the performance of the proposed framework. The two most important CE parameters are the number of samples for CE optimization  $N^{\text{CE}}$ , and the multi-level or rarity parameter  $\rho$  [73]. Table 3.5 shows the short-term risk indices and corresponding computational times for different values of  $N^{\text{CE}}$  and  $\rho$ , for the case study of Section 3.6.1. As can be observed, the choice of  $\rho$  can impact the computational time to a certain degree, however, the short-term risk indices remain the same.

Table 3.5 Effects of  $N^{\text{CE}}$  and  $\rho$

$N^{\text{CE}}$	Metric	$\rho = 0.01$	$\rho = 0.03$	$\rho = 0.05$
20,000	Risk ( $10^{-4}$ )	3.0080	3.0601	3.0402
	Time (s)	21.233	46.80	33.86
30,000	Risk ( $10^{-4}$ )	3.0274	3.0239	3.0565
	Time (s)	16.37	22.88	14.36
50,000	Risk ( $10^{-4}$ )	3.0773	3.0911	3.0481
	Time (s)	13.67	32.18	9.88

### 3.6.8 Practical Considerations

As mentioned in Section 3.2 and shown in Section 3.6.4 and Section 3.6.5, power system operators can utilize the short-term risk indices to evaluate the reliability of the power system in the operational domain. The short-term risk indices calculated using the proposed framework can then be used as input to the conventional power system operation methods. One such scheme for using the short-term risk indices in power system operation has been discussed in [80]. This scheme involves calculating the short-term risk indices after performing the DAUC. Then, the spinning reserve constraints are adjusted for those hours which have higher risk indices and the DAUC is performed again. This ensures that the short-term risk indices remain below a certain pre-defined level for all hours. The proposed framework developed in this framework can easily be appended to such schemes.

## 3.7 Conclusion

In this chapter, a hybrid framework for the assessment of short-term risk indices of a wind-integrated composite power system is proposed. An analytical technique, i.e., the area risk method,

is extended to appropriately consider the impact of wind generation on short-term risk indices through a new reliability modeling approach of wind generation. The modified area risk method is then combined with the CE-MCS, which is an efficient and robust simulation technique, to arrive at a novel framework for the short-term risk assessment of composite power systems.

The case studies performed on the 24-bus IEEE RTS validates the effectiveness of the proposed reliability modeling approach as well as the computational superiority of the proposed framework compared to existing methods. Further, the impacts of the transmission system and daily unit commitment on the short-term risk indices are also explored. Short-term risk indices are significantly affected by the transmission capacities and commitment decisions. Finally, the impact of wind penetration and CE parameters on the short-term risk indices are examined.

# Chapter 4

## Data-Driven Operational Risk Assessment of Wind-Integrated Power Systems via Mixture Models and Importance Sampling<sup>8</sup>

### 4.1 Abstract

The increasing penetration of highly intermittent wind generation could seriously jeopardize the operational reliability of power systems and increase the risk of outages. Thus, it becomes important to realistically evaluate the operational risk indices. To this end, this chapter proposes a novel data-driven method for operational risk assessment of wind-integrated composite power systems. First, a new approach is presented to model the uncertainty of wind power in the lead time. The proposed approach employs  $k$ -means clustering and MM to construct time-dependent probability distributions of wind power. The proposed approach can also capture the complex statistical features of wind power, such as multimodality. Later, an NSMCS technique is adopted to evaluate the operational risk indices. To improve the computational performance of NSMCS, CE-based IS technique is applied. The CE-IS technique is modified to include the proposed model of wind power. The method is validated on a modified 24-bus IEEE RTS and a modified 3-area IEEE RTS while employing the historical wind generation data. The simulation results verify the importance of accurate modeling of short-term uncertainty of wind power for operational risk assessment. Further case studies have been performed to understand the impact of the transmission system on operational risk indices. The computational performance of the framework is also examined.

---

<sup>8</sup> Reprinted without modifications and with permission from: O. A. Ansari, Y. Z. Gong, W. Liu, and C. Y. Chung, "Data-driven operation risk assessment of wind-integrated power systems via mixture models and importance sampling," *J. Modern Power Syst. Clean Energy*, vol. 8, no. 3, pp. 437-445, May 2020. [34].

## 4.2 Introduction

The penetration of wind generation in modern power systems is on the rise. According to a recent forecast by Global Wind Energy Council, by 2022, the total global installed capacity of wind generation will reach 840 GW – a 42% increase from the current level [81]. This ever-growing utilization of wind generation inevitably brings several challenges to power systems. One of the critical challenges is to improve and maintain the reliability of power systems and reduce the risk of electricity outages. In particular, during power systems operation, the short-term reliability would be significantly impacted due to either complete lack of or constrained availability of remedial resources amid unexpected variability of wind generation [23], [17], [20]. There is, thus, a pressing need to develop frameworks that can accurately assess the short-term or operational risk of wind-integrated power systems. These frameworks could then enable power system operators to take risk-informed decisions well-ahead of time to mitigate the adverse impacts of wind generation on power system reliability.

The consideration of wind generation in long-term risk assessment of power systems is well-studied [82], [83], [84]. For instance, in [82] and [83] ARMA series for wind speed are developed for reliability studies. Reference [84] formulates capacity outage probability tables while considering both the variability of wind speed and the outages of wind turbines. Nonetheless, these techniques do not apply to operational risk assessment. The main reason is that the long-term reliability models of wind speed and wind power are not appropriate to represent the time-dependent short-term uncertainty of wind power during power system operation.

For operational risk assessment of wind-integrated power systems, the existing methods can be broadly classified into two main categories: analytical methods and simulation techniques. Reference [27] formulates a discrete PDF of wind power using wind speed time series, which is then employed in an analytical technique known as the PJM method [17]. In [23] and [46], the ARMA series of wind speed is adapted to construct discrete PDFs which are conditioned on initial wind speed. These wind speed PDFs are then utilized in the area-risk method which is an extension of the PJM method. In [70], the wind speed ARMA series is directly adopted in a contingency-list based analytical method for operational risk assessment.

Analytical methods have limited applications and are not suitable for operational risk assessment of composite generation-transmission systems [20]. In this case, simulation techniques, such as MCS, provide an attractive alternative approach for operational risk assessment. In [28] the continuous time Markov chain is employed to model the wind speed. Later, the Markov chain is used in conjunction with sequential MCS for operational risk evaluation. Reference [56] employs quasi-sequential MCS where wind power is modeled using a fixed number of scenarios. The computational efficiency of MCS is enhanced by adopting the CE based IS technique. Different from pure analytical and simulation methods, in [85] a hybrid framework is proposed. The wind speed uncertainty is modeled using multiple conditional Weibull PDFs. Then the area-risk method is combined with CE-IS based NSMCS to evaluate the short-term risk indices.

A common determinant of the existing techniques in [27], [46], [70], [28], and [85] is that either discrete or parametric continuous PDFs are employed to model the short-term uncertainty of wind speed. There are two key issues with this approach. First, the process of modeling the wind speed and later converting it to wind power unavoidably includes the inaccuracy of wind power curve [86]. Second, the unimodal PDFs (e.g., Weibull and Gaussian) employed in these studies, are not well-suited to model the complicated statistical features of wind speed and wind power [41]. These features, which include the multimodality of PDF and temporal correlation, might lead to inaccurate short-term risk indices. These two issues will be discussed in depth later.

To address the problems envisaged previously, in this chapter a new approach is proposed to model the short-term uncertainty of wind power for operational risk assessment. First, k-means clustering is used to obtain sufficient historical data of wind power for fitting time-dependent PDFs. Then for each cluster, MMs are utilized to develop multivariate PDFs, which can capture the complicated statistical features of wind power. MMs are semi-parametric probabilistic models that can represent arbitrarily complex PDFs with great flexibility. Previously, GMMs have been used to model spatial correlation of wind speed in long-term reliability evaluation [87], [88]. Researchers have also employed GMMs to model the forecast error of wind power [89] and in probabilistic OPF to represent the uncertainty of wind power [33]. In contrast to [87] and [88], in this work, GMMs are adopted to construct time-dependent PDFs of wind power for specific hours in order to render them suitable for short-term reliability evaluation. The drawback of using wind speed data as discussed previously is thus also avoided. Compared to [89] and [33], as the data

available for fitting GMMs for specific hours are scarce, this work adopts maximum a posteriori (MAP) estimation for GMMs as opposed to maximum likelihood estimation (MLE). This is because MLE is susceptible to overfitting and in the case of GMMs, is also prone to singularities [90].

Afterward, using the law of total expectation, an analytical expression for integrating the proposed wind power modeling in operational risk assessment is obtained. An NSCMS technique is then adopted to evaluate the analytical expression for operational risk assessment. The computational speed of the NSCMS is greatly enhanced by employing the CE-IS technique [63], [73]. The CE-IS technique is also modified to include the proposed short-term uncertainty model of wind power. In particular, a proxy distribution is used to obtain the distorted parameters of GMMs. This ensures that the operational indices are evaluated with an acceptable computational burden. The proposed data-driven framework is tested on a modified 24-bus IEEE RTS and a modified 73-bus 3-area IEEE RTS. The actual wind power data from a wind farm in Spain is adopted for probabilistic modeling of wind power.

In summary, the main contributions of this chapter are:

1. This chapter presents a novel approach based on k-means clustering and GMMs to represent the uncertainty of wind power for operational risk assessment. The proposed approach also adopts MAP estimation to obtain GMM parameters, instead of the widely-used MLE technique to avoid overfitting and singularities.
2. Building upon the proposed probabilistic modeling of wind power, this work presents a new framework for operational risk assessment. The clustering-based GMM modeling of wind power is integrated in the operational risk assessment using the law of total expectation.
3. A NSMCS technique is adopted to estimate the risk indices. To improve the computational performance, CE-based IS is adapted. The CE-based IS is also applied to GMMs of wind power. Simulation studies are also performed on two test systems to depict the efficacy of the proposed modeling approach and the operational risk assessment framework.

### 4.3 The Preamble of Operational Risk Assessment

Consider a power system with  $N^G$  conventional generating stations,  $N^L$  transmission lines,  $N^W$  wind generating units, and  $N^B$  buses. To represent the uncertainties arising from the unplanned outages of conventional generating units, transmission lines, and wind power at time  $t$ , a random vector  $\mathbf{X}_t = [\mathbf{X}_t^G, \mathbf{X}_t^L, \mathbf{X}_t^W]$  is defined.  $\mathbf{X}_t^G = [n_t^1, \dots, n_t^s, \dots, n_t^{N^G}]$  where  $n_t^s$  is the number of available generating units in generating station  $s$ .  $\mathbf{X}_t^L = [\zeta_t^1, \dots, \zeta_t^l, \dots, \zeta_t^{N^L}]$  where  $\zeta_t^l$  represents the status of transmission line  $l$ ; it is 1 if the transmission line is available and 0 if it is on outage.  $\mathbf{X}_t^W = [g_t^1, \dots, g_t^w, \dots, g_t^{N^W}]$ , where  $g_t^w$  is the wind power of wind farm  $w$ . Using the above notation, the risk can be mathematically expressed as the following integral

$$R_t = \mathbb{E}[H(\mathbf{X})] = \int_{\Omega} H(\mathbf{x}) f_t(\mathbf{x}) d\mathbf{x}, \quad (4.1)$$

where  $R_t$  is the risk index, and  $H(\cdot)$  is the limit-state function or test function. It will be defined later in Section 4.5.  $f_t(\cdot)$  is the joint multi-variate PDF of random vector  $\mathbf{X}$ ,  $\Omega$  is the state space, and  $\mathbb{E}[\cdot]$  is the expectation operator.  $\mathbf{x}$  is a particular realization of  $\mathbf{X}$ . As can be deduced from (4.1), the choice of  $f_t(\cdot)$  significantly impacts the risk indices. A more accurate estimation of  $f_t(\cdot)$  would invariably lead to a more accurate evaluation of the risk indices [85].

Assuming that the outages of conventional generating units and transmission lines, and variability of wind power are mutually independent of each other,  $f_t(\cdot)$  can be expressed as

$$f_t(\mathbf{x}) = f_t^G(\mathbf{x}^G) f_t^L(\mathbf{x}^L) f_t^W(\mathbf{x}^W). \quad (4.2)$$

For the conventional generating units, it is assumed that each generating station  $s$  further comprises identical  $N^s$  generating units. The failure events of these generating units are also assumed to be independent of each other [17]. Therefore,  $f_t^G(\cdot)$  can be modeled as a product of binomial distributions.

$$f_t^G(\mathbf{x}^G) = \prod_{s=1}^{N^G} \text{Bin}(N^s, p_s(\Delta t)), \quad (4.3)$$

where

$$\text{Bin}(N^s, p_s(\Delta t)) = \binom{N^s}{n_t^s} (1 - p_s(\Delta t))^{n_t^s} (p_s(\Delta t))^{N^s - n_t^s}, \quad (4.4)$$

and

$$p_s(\Delta t) = 1 - e^{-\lambda_s \Delta t} \approx \lambda_s \Delta t. \quad (4.5)$$

In (4.5),  $\lambda_s$  is the failure rate of a generating unit in generating station  $s$  and  $\Delta t$  is the lead time (typically 1 hour).  $p_s(\Delta t)$  is also referred to as ORR [17].

Similar to the conventional generating units, it is assumed that the line outages are independent of each other. Ergo  $f_t^L(\cdot)$  is represented by a product of Bernoulli distributions:

$$f_t^L(\mathbf{x}^L) = \prod_{s=1}^{N^L} \text{Ber}(p_l(\Delta t)), \quad (4.6)$$

where

$$\text{Ber}(p_l(\Delta t)) = (1 - p_l(\Delta t))^{\zeta_t^l} (p_l(\Delta t))^{1 - \zeta_t^l}, \quad (4.7)$$

and

$$p_l(\Delta t) = 1 - e^{-\lambda_l \Delta t} \approx \lambda_l \Delta t. \quad (4.8)$$

Similar to the conventional generating units,  $\lambda_l$  is the failure rate of transmission line  $l$ .

Lastly, for wind power, it assumed that the spatial correlation among the wind farms is negligible. This implies that  $f_t^W(\cdot)$  can be expressed as:

$$f_t^W(\mathbf{x}^W) = \prod_{w=1}^{N^W} f_t^w(g_t^w), \quad (4.9)$$

where  $f_t^w(g_t^w)$  is the PDF for wind farm  $w$  at time  $t$ . In the next section, a new approach is presented to estimate this PDF using historical wind power data.

## 4.4 Proposed Probabilistic Modeling of Wind Power

In this section, a novel approach founded on k-means clustering and GMMs is presented to model the PDF of wind power for operational risk assessment. Before delving any further, first, the motivation behind the proposed approach is presented. As mentioned in the Section 4.2, the existing approaches in operational risk assessment are based primarily on modeling wind speed PDF. Wind power PDF is then obtained through a wind power curve [27], [85]. Figure 4.1 portrays a typical wind power curve along with box plots representing measured wind power and wind speed data for a wind farm near Swift Current, Canada. Two observations can be made from investigating this figure. First, there is a high degree of discrepancy between the wind power estimated by the wind power curve and the actual wind power. On the one hand, underestimation of wind power would correspond to higher than actual risk indices. On the other hand, overestimation of wind power would result in lower than actual risk indices. This observation implies that operational risk indices would be inaccurate if only wind speed data is used. Second, the uncertainty of wind power is substantial in the region between the cut-in and rated wind speeds. Accurate modeling of this uncertainty is essential in order to calculate precise risk indices.

The wind power also possess certain sophisticated statistical features that cannot be captured by simple parametric PDFs (e.g., Weibull, Beta, and Gaussian) often used in the existing literature on power systems reliability. One such feature is the multimodality. Figure 4.2 plots the histogram of actual wind power measured for a complete month for the same wind farm of Figure 1. From Figure 4.2, at least two modes can be easily identified. Apart from multimodality, the temporal correlation between wind power of different hours is also essential for operational risk analysis [23]. Consequently, univariate PDFs could not be adopted to capture this correlation. These complex statistical features necessitate the use of non-parametric or semi-parametric multivariate PDF estimation techniques for wind power.

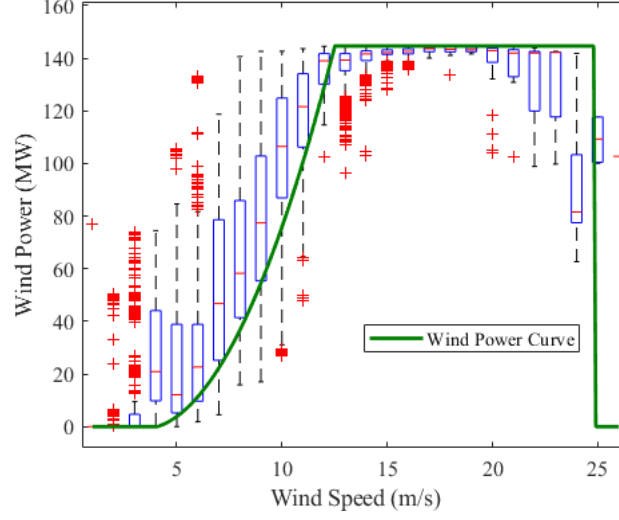


Figure 4.1 Wind power curve with box plots of actual wind power data

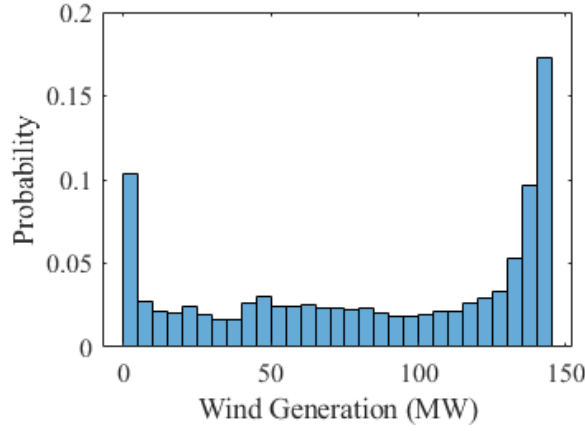


Figure 4.2 Histogram of historical wind power data for a month

In the light of the above discussion, in this work, GMMs are used to model the short-term uncertainty of wind power for specific hours of a specific day. To employ GMMs, first, additional random variables are defined. The random vector  $\mathbf{X}_t^W = [g_t^1, \dots, g_t^w, \dots, g_t^{N^W}]$  delineated in the previous section represents the wind power of wind farms during the time  $t$ . To consider the temporal dependence, consider another random vector  $\mathbf{X}_{t-1}^W = [g_{t-1}^1, \dots, g_{t-1}^w, \dots, g_{t-1}^{N^W}]$ , where  $g_{t-1}^w$  denotes the wind power of wind farm  $w$  in the current hour. It should be noted that both  $t$  and  $t - 1$  are defined for specific instances of time at a specific day. As highlighted previously, there is a strong correlation between  $g_t^w$  and  $g_{t-1}^w$ . Hence, the uncertainty of  $g_t^w$  is best represented by the conditional PDF  $f_t^w(g_t^w | g_{t-1}^w)$ . Using the concept of conditional probabilities,

$f_t^w(g_t^w|g_{t-1}^w)$  can be obtained from  $f_t^w(g_{t-1}^w, g_t^w)$ , which represents the joint density over  $g_{t-1}^w$  and  $g_t^w$ . If  $g_{t-1}^w$  is deterministically known, which is generally the case in power systems operation,  $f_t^w(g_t^w|g_{t-1}^w)$  could be directly used to evaluate risk indices. Otherwise,  $f_t^w(g_t^w)$  can be obtained by marginalizing  $g_{t-1}^w$  as

$$f_t^w(g_t^w) = \int f_t^w(g_{t-1}^w, g_t^w) dg_{t-1}^w, \quad (4.10)$$

As  $f_t^w(g_{t-1}^w, g_t^w)$  is defined for two specific hours, this PDF should be constructed using the appropriate wind power data of those specific hours. For instance, if  $t-1$  and  $t$  are hours 14:00 and 15:00, respectively, of January 3rd, all the historical data for these two hours at this day would be employed to estimate the PDF.

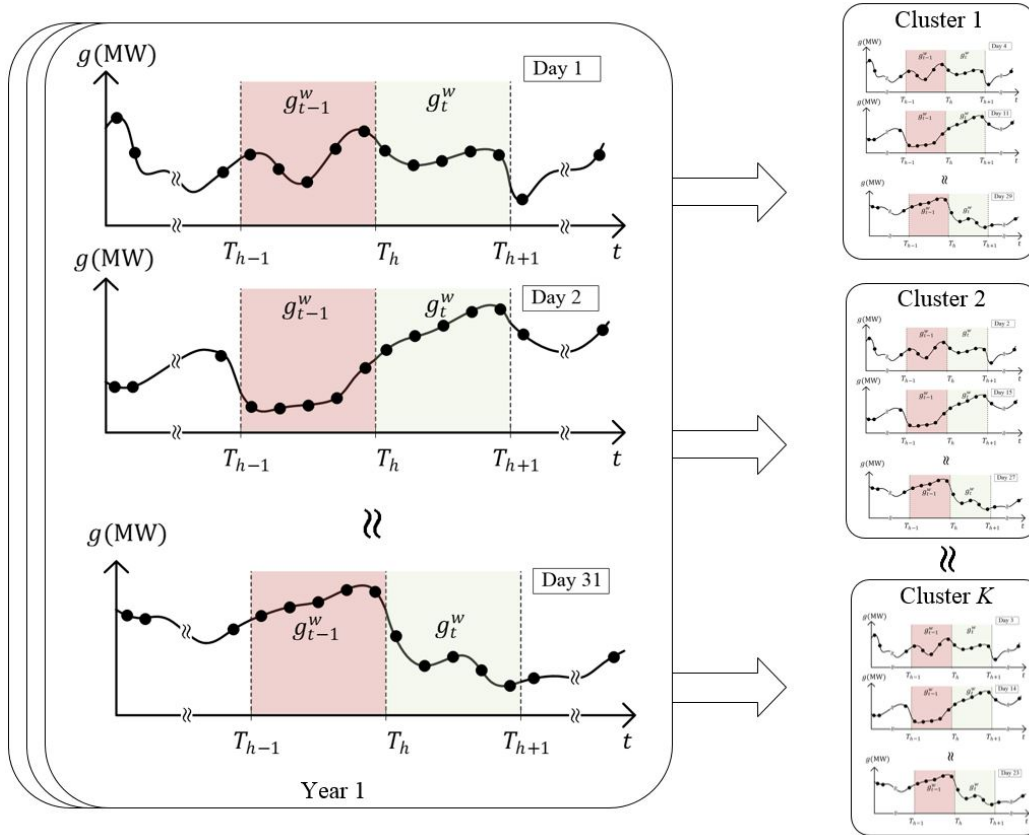


Figure 4.3 Clustering of historical data.  $T_h$  is the current time instant.  $T_h - T_{h+1}$  is the time interval for risk assessment.

In order to estimate  $f_t^w(g_{t-1}^w, g_t^w)$  for specific time periods, a substantial amount of historical data for those time periods are required. However, as only limited amount of historical data is available, in this work, a clustering approach is adopted. In particular, using  $k$ -means clustering, the historical data for a specific month under study (in the previous example, January) is grouped into clusters. Then, for each cluster, the historical data for the two particular hours (in the previous example, 14:00 and 15:00) are used to estimate the required joint PDF. The joint PDF for each cluster is associated with a probability  $\lambda_c$  which is obtained through  $k$ -means clustering. This approach ensures that sufficient data are available for fitting PDFs. The approach is pictorially depicted in Figure 4.3.

After obtaining sufficient data for specific hours of each cluster, different approaches can be utilized to estimate  $f_t^{w,c}(g_{t-1}^w, g_t^w)$  for each cluster. One such approach is the KDE which is a non-parametric technique [91]. In this work GMMs are adopted to model the PDF for the following reasons. Compared to KDE, GMMs require less data [92]. As only limited wind power data is available in practice, GMMs is a clear choice. Also, as GMMs involve parametric PDFs, they are more easy to interpret and can easily be included in the existing risk assessment frameworks. A minor drawback of GMMs is the assumption about distribution which is absent in KDE.

Using GMMs, the PDF for wind power in two particular hours is estimated as

$$\hat{f}_t^{w,c}(g_{t-1}^w, g_t^w) = \sum_{k=1}^K \pi_k \Psi_k(g_{t-1}^w, g_t^w | \theta_k), \quad (4.11)$$

where  $\Psi_k(\cdot)$  is a parametric bivariate PDF with parameters  $\theta_k$ ,  $K$  is the number of mixtures, and  $\pi_k$  is the  $k$ th mixing proportion satisfying the following conditions.

$$\sum_{k=1}^K \pi_k = 1, \quad (4.12)$$

$$0 \leq \pi_k \leq 1. \quad (4.13)$$

There are three evident advantages of using the GMM approach of (4.11). First, by employing a mixture of parametric distributions, the multi-modality of wind power PDF could be captured. Secondly, through the inclusion of  $g_{t-1}^w$ , the temporal correlation could be included in the model.

Third, as it will be explained later, by employing a mixture of bivariate PDFs essentially, the existing risk assessment frameworks could be easily modified to include (4.11) in the risk assessment framework.

In this work, the Gaussian PDF is used to model  $\Psi_k(\cdot)$ . Consequently, (4.11) can also be expressed as

$$\hat{f}_t^{w,c}(g_{t-1}^w, g_t^w) = \sum_{k=1}^K \pi_k \phi(g_{t-1}^w, g_t^w | \boldsymbol{\mu}_k, \Sigma_k), \quad (4.14)$$

where  $\phi(g_{t-1}^w, g_t^w | \boldsymbol{\mu}_k, \Sigma_k)$  denotes the Gaussian PDF with mean  $\boldsymbol{\mu}_k$  and covariance  $\Sigma_k$ . For brevity, the GMM parameters are grouped as  $\boldsymbol{\pi} = [\pi_1, \dots, \pi_K]^T$ ,  $\boldsymbol{\mu} = [\mu_1^T, \dots, \mu_K^T]^T$  and  $\boldsymbol{\Sigma}$ , which is a three-dimensional matrix of covariance matrices  $\Sigma_k$ .

The main task now is to determine, using the historical wind power data, the GMM parameters. In addition,  $K$  needs to be set. Popular techniques for determining  $K$  include the split-and-merge method [87], cross-validation, and Akaike information criterion (AIC) [88]. For a given  $K$ , the remaining GMM parameters can then be estimated by maximizing the log-likelihood of (4.14) [93]. For a given set of  $N$  bi-variate wind power data  $\{g_{t-1,i}^w, g_{t,i}^w\}$  where  $i = \{1, \dots, N\}$ , GMM parameters can be estimated using the MLE approach as

$$\boldsymbol{\pi}, \boldsymbol{\mu}, \boldsymbol{\Sigma} = \arg \max \log \prod_{i=1}^N \hat{f}_t^{w,c}(g_{t-1,i}^w, g_{t,i}^w), \quad (4.15)$$

The MLE approach for estimating GMM parameters suffers from two major shortcomings. First, given the limited amount of data, it is prone to overfitting. Second, due to the collapsing variance problem, singularities could occur [94]. Therefore, to avoid these drawbacks, in this work, the MAP approach is employed. Using, the MAP approach, (4.15) is modified to

$$\boldsymbol{\pi}, \boldsymbol{\mu}, \boldsymbol{\Sigma} = \arg \max \log \prod_{i=1}^N \hat{f}_t^{w,c}(g_{t-1,i}^w, g_{t,i}^w) + \log f(\boldsymbol{\pi}) + \log f(\boldsymbol{\mu}, \boldsymbol{\Sigma}), \quad (4.16)$$

In (4.16),  $f(\boldsymbol{\pi})$  and  $f(\boldsymbol{\mu}, \boldsymbol{\Sigma})$  are prior distributions on GMM parameters. In particular,  $f(\boldsymbol{\pi})$  is Dirichlet distribution and  $f(\boldsymbol{\mu}, \boldsymbol{\Sigma})$  is the Normal-Inverse-Wishart distribution. These prior

distributions act to regularize the parameters fitting and thus avoid overfitting and singularities. Using the expectation maximization method, the MAP estimates in (4.16) are obtained as [94]:

$$r_{i,k} = \frac{\pi_k \phi(g_{t-1,i}^w, g_{t,i}^w | \boldsymbol{\mu}_k, \Sigma_k)}{\sum_l \pi_l \phi(g_{t-1,i}^w, g_{t,i}^w | \boldsymbol{\mu}_l, \Sigma_l)}, \quad (4.17)$$

$$\pi_k = \frac{r_k + \alpha_k - 1}{N + \sum_k \alpha_k - K}, \quad (4.18)$$

$$\boldsymbol{\mu}_k = \frac{\sum_i r_{i,k} \mathbf{g}_i + v_0 \mathbf{m}_0}{r_k + v_0}, \quad (4.19)$$

$$\Sigma_k = \frac{\mathbf{S}_0 + \mathbf{S}_k + \left( \frac{v_0 r_k}{v_0 + r_k} \right) (\boldsymbol{\mu}_k - \mathbf{m}_0)(\boldsymbol{\mu}_k - \mathbf{m}_0)^T}{r_k + v_0 + D + 2}, \quad (4.20)$$

$$\mathbf{S}_k = \sum_i r_{i,k} (\mathbf{g}_i - \boldsymbol{\mu}_k)(\mathbf{g}_i - \boldsymbol{\mu}_k)^T, \quad (4.21)$$

where,  $r_k = \sum_i r_{i,k}$  and  $\mathbf{g}_i = [g_{t-1,i}^w, g_{t,i}^w]^T$ .  $\alpha_k$ 's are the parameters of Dirichlet distribution.  $\mathbf{m}_0$ ,  $v_0$ , and  $\mathbf{S}_0$  are the parameters of Normal-Inverse-Wishart distribution. Also,  $D$  is the number of dimensions in the data. Equation (4.17) represents the E-step and (4.18)–(4.21) correspond to the M-step of the expectation-maximization method. These two steps are conducted iteratively.

After obtaining the joint PDF, the conditional PDF for each cluster  $f_t^{w,c}(g_t^w | g_{t-1}^w)$  can be obtained. By the property of Gaussian PDFs, this conditional PDF is also a univariate GMM. Subsequently, this conditional PDF is employed in risk assessment.

## 4.5 Proposed short-term risk assessment method

In this section, the proposed operational risk assessment method is presented. The proposed method integrates the previously developed GMM model of wind power. As an example, the method is explained using the LOLP index. However, the method could easily be extended to estimate other reliability indices.

The risk in (4.1) is defined for a specific PDF  $f_t(\cdot)$ . As there are multiple PDFs for multiple clusters, (4.1) needs to be modified. The law of total expectation can be used to obtain the total risk considering different PDFs for different clusters. Using the law of total expectation

$$R = \sum_c \lambda_c \left( \int_{\Omega} H(\mathbf{x}) f_{t,c}(\mathbf{x}) d\mathbf{x} \right), \quad (4.22)$$

where  $f_{t,c}(\cdot)$  is similar to  $f_t(\cdot)$  in (4.2) with the exception that  $f_t^W(\cdot)$  is replaced by each cluster's PDF  $f_t^{W,c}(\cdot)$ .

Due to a large number of states in the state space  $\Omega$  and high dimensionality of the integral, it is difficult to evaluate (4.22) analytically [63]. Crude NSMCS could be used to estimate (4.22) as

$$\hat{R} = \sum_c \lambda_c \left( \frac{1}{N_s} \sum_{n=1}^{N_s} H(\mathbf{x}_n^c) \right), \quad (4.23)$$

where  $\{\mathbf{x}_1^c, \dots, \mathbf{x}_{N_s}^c\}$  are IID samples drawn from  $f_{t,c}(\cdot)$ , and  $N_s$  is the total number of samples. The test function  $H(\cdot)$  is defined as follows

$$H(\mathbf{x}) = \begin{cases} 0 & , S(\mathbf{x}) \geq L \\ 1 & , S(\mathbf{x}) < L \end{cases} \quad (4.24)$$

where,

$$S(\mathbf{x}) = \begin{cases} \sum_{b=1}^{N^B} P_b & , \sum_{b=1}^{N^B} P_b \geq L \\ \sum_{b=1}^{N^B} l_b & , \sum_{b=1}^{N^B} P_b < L \end{cases}. \quad (4.25)$$

In (4.24) and (4.25),  $L$  is the load demand during lead time,  $P_b$  is the cumulative available generation at bus  $b$ , and  $l_b$  is the load supplied to bus  $b$ . The DC OPF is used to evaluate  $P_b$  and  $l_b$ .

Because of low failure probabilities during power system operation, most of the samples correspond to  $H(\cdot)$  being zero. Thus, a larger number of samples is required to correctly estimate the risk indices. This would significantly increase the computational burden. To circumvent this issue, in the chapter, the IS technique is adopted. The IS technique proposes another joint PDF

$f_{t,c}^*(\cdot)$  that is biased to obtain samples for which  $H(\cdot)$  is non-zero. The risk index is then calculated using

$$\hat{R} = \sum_c \lambda_c \left( \frac{1}{N_s} \sum_{n=1}^{N_s} H(\mathbf{x}_n^c) W_{t,c}(\mathbf{x}_n^c) \right), \quad (4.26)$$

where,

$$W_{t,c}(\mathbf{x}) = \frac{f_{t,c}(\mathbf{x})}{f_{t,c}^*(\mathbf{x})} \quad (4.27)$$

In (4.26) the IID samples are now drawn from  $f_{t,c}^*(\cdot)$ . Similar to (4.2),  $f_{t,c}^*(\cdot)$  can be written as

$$f_{t,c}^*(\mathbf{x}) = f_t^{G,*}(\mathbf{x}^G) f_t^{L,*}(\mathbf{x}^L) f_t^{W,c,*}(\mathbf{x}^W). \quad (4.28)$$

The PDF  $f_{t,c}^*(\cdot)$ , which is also known as the importance sampling density, can be obtained using the widely-used CE optimization [56]. For CE optimization, closed-form analytical updating rules are available for the PDFs of  $f_t^{G,*}(\cdot)$  and  $f_t^{L,*}(\cdot)$  as these PDFs belong to the exponential family of distributions. However, for the GMMs of wind power, such closed-form analytical solution is not present. To mitigate this problem, in this work, a transformation strategy is adopted.

Consider the GMM PDF of wind farm  $w$  for cluster  $c$ ,  $f_t^{w,c}(\cdot)$ , the following transformation is used to obtain a new random variable  $\chi^w$  as

$$\chi^w = \Phi^{-1}(F_t^{w,c}(g_t^w | g_{t-1}^w)). \quad (4.29)$$

In (4.23),  $\Phi$  is the CDF of  $\phi(\chi^w | \mu_w, (\sigma_w)^2)$  and  $F_t^{w,c}(\cdot)$  is the CDF of  $f_t^{w,c}(\cdot)$ . After transformation, the PDF for  $\chi^w$  is distorted using the CE optimization. As  $\chi^w$  belongs to exponential family of distributions, analytical rules can be applied to obtain the CE parameters. In the calculation of (4.24) and (4.25), the random variable  $\chi^w$  is transformed back to actual wind power random variable using the distorted  $\phi^*(\cdot)$  via the inverse of (4.29). Thus  $\chi^w$  acts as a proxy random variable to distort the GMM. The complete CE algorithm is depicted as Algorithm 4.1. After obtaining  $f_{t,c}^*(\cdot)$  through Algorithm 4.1, NSMCS is employed to estimate (4.26).

---

**Algorithm 4.1:** CE Optimization for GMM-Integrated NSCMS

---

---

**Input:**  $p_s, \forall s; p_l, \forall l; f_t^{w,c}(\cdot); \phi(\cdot | \mu_w, (\sigma_w)^2), \forall w$

**Output:**  $p_s^*, \forall s; p_l^*, \forall l; \phi^*(\cdot | \mu_w^*, (\sigma_w^*)^2), \forall w$

- 1: Set CE parameters  $N_{\text{CE}}, \rho, \alpha$  and  $c^{\max}$
- 2: Set,  $\forall s, p_s^m = p_s; \forall l, p_l^m = p_l; \forall w, \phi^m(\cdot | \mu_w^m, (\sigma_w^m)^2) = \phi(\cdot | \mu_w, (\sigma_w)^2)$
- 3: **For**  $m = 1$  to  $m = m^{\max}$
- 4: Sample  $\{\mathbf{x}_1, \dots, \mathbf{x}_{N_{\text{CE}}}\}$  from (4.2) using  $p_s^m$  in (4.3),  $p_l^m$  in (4.6), and  $\mu_w^m$  and  $\sigma_w^m$  in inverse of (4.29)
- 5: For each sample, evaluate  $S(\mathbf{x})$  using (4.25) and sort  $S(\mathbf{x}_i)$  samples in ascending order to obtain order statistics,  $S[1] \leq S[2] \leq \dots \leq S[N_{\text{CE}}]$ .
- 6: **If**  $S[\rho N_{\text{CE}}] \geq L$ , set  $L^c = S[\rho N_{\text{CE}}]$ , otherwise set  $L^c = L$
- 7: For each sample, evaluate  $H(\mathbf{x})$  using (4.24) with  $L^c$  instead of  $L$ , also evaluate  $W(\mathbf{x})$  using (4.27)
- 8: Calculate the updated parameters of PDFs as follows  $\forall s, \forall l, \forall w$ :

$$p_s^{m+1} = \alpha \left( 1 - \frac{\sum_{i=1}^{N_{\text{CE}}} H(\mathbf{x}_i) W(\mathbf{x}_i) n_i^g}{N^s \sum_{i=1}^{N_{\text{CE}}} H(\mathbf{x}_i) W(\mathbf{x}_i)} \right) + (1 - \alpha) p_s^m$$

$$p_l^{m+1} = \alpha \left( 1 - \frac{\sum_{i=1}^{N_{\text{CE}}} H(\mathbf{x}_i) W(\mathbf{x}_i) \zeta_i^l}{\sum_{i=1}^{N_{\text{CE}}} H(\mathbf{x}_i) W(\mathbf{x}_i)} \right) + (1 - \alpha) p_l^m$$

$$\mu_w^{m+1} = \frac{\sum_{i=1}^{N_{\text{CE}}} H(\mathbf{x}_i) W(\mathbf{x}_i) \chi_i^w}{\sum_{i=1}^{N_{\text{CE}}} H(\mathbf{x}_i) W(\mathbf{x}_i)}$$

$$(\sigma_w^{m+1})^2 = \frac{\sum_{i=1}^{N_{\text{CE}}} H(\mathbf{x}_i) W(\mathbf{x}_i) (\chi_i^w - \mu_w^{m+1})^2}{\sum_{i=1}^{N_{\text{CE}}} H(\mathbf{x}_i) W(\mathbf{x}_i)}$$

- 9: **If**  $L^c = L$ , break the for loop.

- 10: The final parameters of PDFs are,

$$\forall s, p_s^* = p_s^{m+1}; \forall l, p_l^* = p_l^{m+1}; \forall w, \mu_w^* = \mu_w^{m+1}, \sigma_w^* = \sigma_w^{m+1}$$


---

## 4.6 Simulation Results

In this section, case studies are performed to depict the effectiveness of the proposed probabilistic modeling of wind power and the proposed operational risk assessment method. The simulations are performed on a modified 24-bus IEEE RTS (Appendix A) [77] and a modified 73-bus 3-area IEEE RTS. In the original 24-bus IEEE RTS, a wind farm with a total capacity of 1,000 MW is integrated at bus 19. A 155-MW conventional generating station at bus 16 is removed. The total wind power penetration is therefore equal to 23.5%. Ten years of real wind power data from the Sotavento wind farm in Spain is used [95]. All simulations are performed for the month of January. The operational risk is evaluated for a lead time of one hour. The particular time interval for the lead time is set to 03:00 – 04:00. The load is set to the peak values. For CE-optimization, the parameters are set according to [85], and the stopping criteria for NSCMS is set to 5%. For  $k$ -means clustering, the number of clusters is set to 3. This value of  $k$  was obtained by trial-and-error method to ensure that each cluster contains sufficient number of data points.

### 4.6.1 GMM Model

The efficacy of the GMM model is explained in this subsection. Figure 4.4 portrays the bivariate histogram of the dataset for a specific cluster. Figure 4.5 depicts GMM obtained for this cluster when parameters are obtained using MAP approach. By comparing Figure 4.4 with Figure 4.5, one can conclude that the GMM accurately captures the variability of wind power in the lead time. From close observation of Figure 4.5, two conclusions can be made. First, the PDF for wind power during the lead time are markedly different for different initial wind power. Second, the multimodality of PDF is evident. For instance, when the initial wind power lies in the interval  $[0.2, 0.4)$ , the wind power PDF in the lead time has three distinct modes. The effect of multimodality on operational risk indices will be discussed in the next subsection. Figure 4.6 represents the GMM model for the same dataset; however, the MLE approach is used to obtain the parameters. Some of the Gaussian components in Figure 4.7 have very low variance. This indicates overfitting. Finally, in Figure 4.7, a bivariate Gaussian PDF is estimated. It is clear from this figure that such a PDF cannot truly represent the distribution of wind power in the lead time.

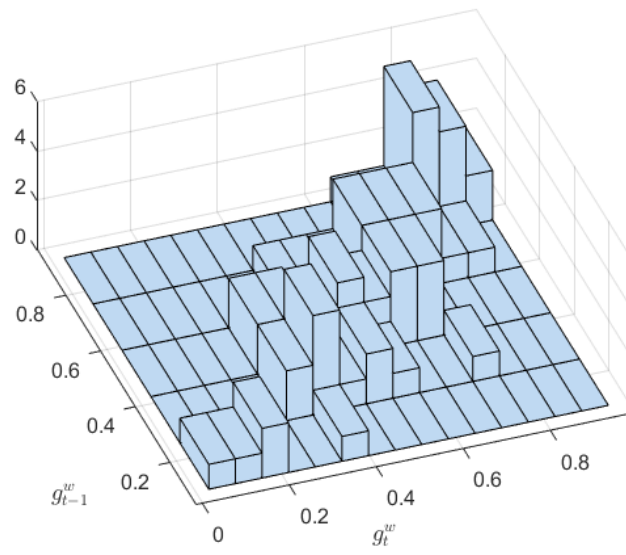


Figure 4.4 Bivariate histogram for the given dataset for one of the three clusters

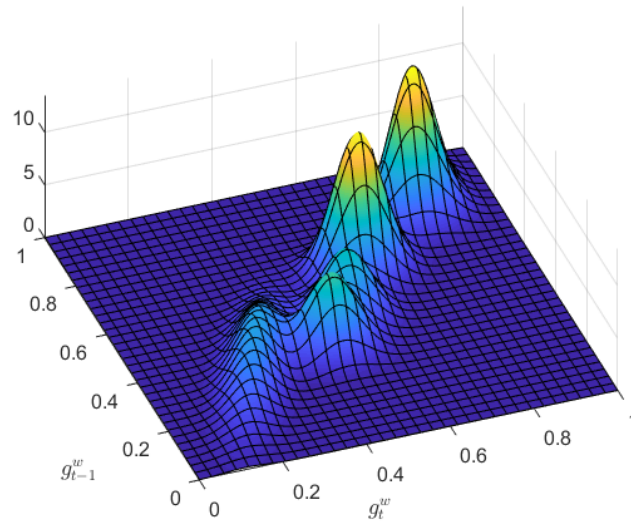


Figure 4.5 GMM for given dataset when MAP estimation is employed.

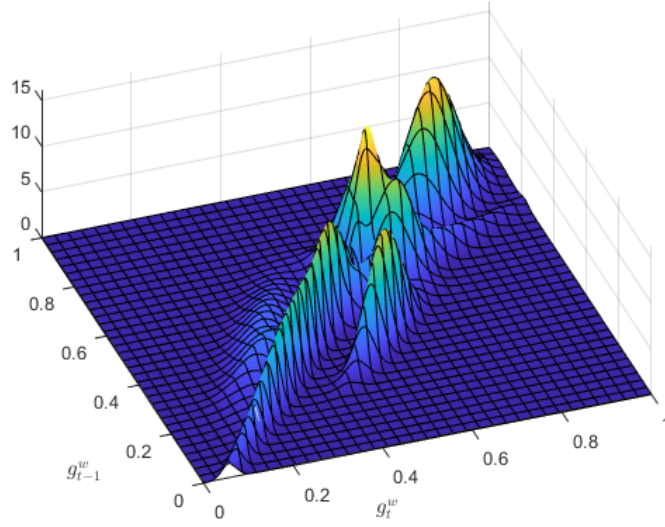


Figure 4.6 GMM for given dataset when MLE estimation is employed.

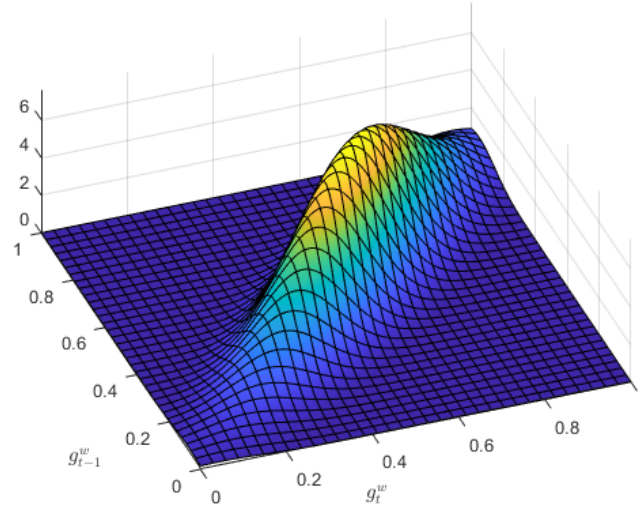


Figure 4.7 Bivariate Gaussian approximation to the given dataset.

#### 4.6.2 Operational risk indices for IEEE RTS

In this subsection, the operational risk indices are evaluated. The proposed method is compared with another method (Method B) in which the PDF of wind power is modeled using a bivariate Gaussian distribution as shown in Figure 4.7. The results are depicted in Table 4.1.

Table 4.1 Operational risk indices for 24-bus IEEE RTS

Initial wind power (p.u.)	Proposed Method	Method B
0.1	5.1417 E-6	2.0783 E-6
0.3	5.2571 E-6	2.2170 E-6
0.5	2.7805 E-6	2.0449 E-7
0.8	1.6245 E-6	7.5509 E-7
1.0	9.1727 E-7	4.3659 E-7

The results indicate there is a stark difference between the risks obtained from the two methods. For all values of initial wind power, the risk indices obtained by the proposed approach are higher than those obtained by Method B. A reason behind this observation can be deduced by investigating Figure 4.5 and Figure 4.7. As noted earlier, Method B is unable to capture the multiple modes of PDF of wind power. Some of these modes occur at lower values of wind power. For instance, as visible from Figure 4.5, there is a mode when next hour wind generation is around 0.2 p.u. By missing these modes, Method B assumes higher than actual wind generation and therefore overestimates the reliability of the power system. In the proposed approach, as these modes are captured, higher number of samples from low power states are also drawn during NSMCS, which contributes to higher risk indices.

#### 4.6.3 Computational Performance

This subsection examines the computational performance of the proposed method. Figure 4.8 pictorially describes the computational burden of the proposed method. From Figure 4.8, it can be observed that in this case, the operational risk indices are evaluated within 5,000 samples in NSMCS. On the contrary, for crude NSMCS, to evaluate the risk index which is in the order of  $10^{-6}$ , the total number of samples required are  $4 \times 10^8$  [63]. This high gain in computational performance has been achieved through adopting the CE-IS technique and modifying it for GMM-based modeling of wind power.

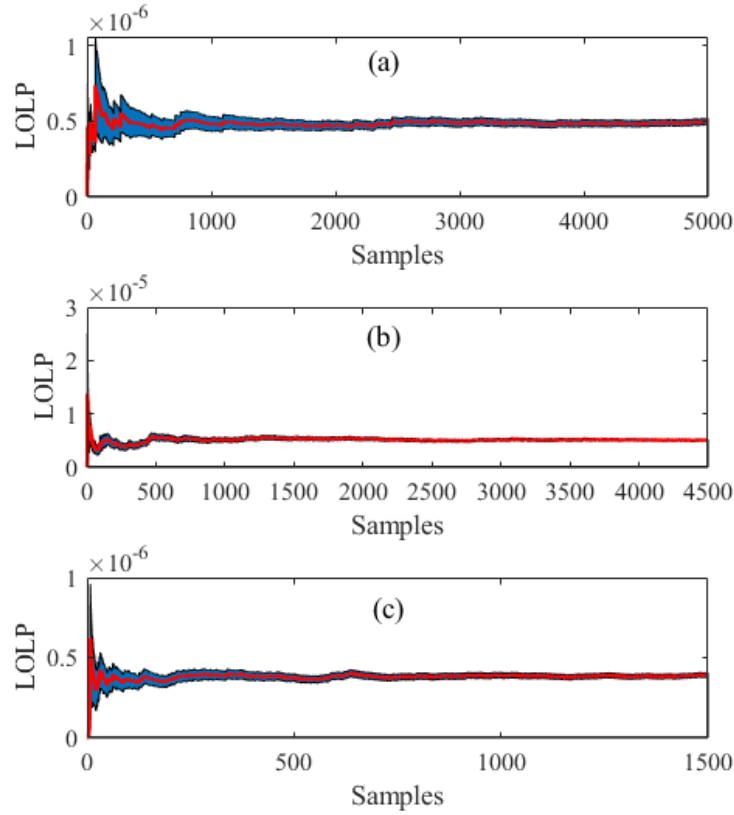


Figure 4.8 The convergence behavior of the proposed method for three clusters when the initial wind generation is 0.5 p.u. The confidence interval is also plotted.

#### 4.6.4 Impact of Wind Farm Location

In this subsection, the effect of the location of the wind farm on the operational risk indices is investigated to understand the impact of transmission system constraints. As can be observed from Table 4.2, the operational risk indices are markedly different for different buses. This variation stems from the difference in the total capacities of transmission lines connected to these buses. The operational risk indices for bus 4 are the highest as it has the lowest total capacity of transmission lines connected to it (i.e., 350 MW). Therefore, the output of the wind farm is highly constrained in this case. For bus 10, the total capacity of transmission lines is 1,545 MW. Ergo, the operational risk indices for this bus are lower than that of bus 4. Finally, for bus 19, the transmission capacity available to wind farm is 1,000 MW. Hence, the operational risk indices for this bus lie between those of bus 4 and bus 10. This effect is more pronounced for cases when the

wind power PDF for the lead time is skewed more toward the maximum capacity, e.g., when the initial wind power is 1.0. These results highlight the effects of transmission system on operational risk indices. These effects could only be considered through the risk assessment of composite power systems.

Table 4.2 Operational risk indices for different location of wind farm

Initial Wind power (p.u.)	Bus 4	Bus 10	Bus 19
0.1	5.2098 E-6	5.1127 E-6	5.1417 E-6
0.3	5.0623 E-5	5.3847 E-11	5.2571 E-6
0.5	1.8012 E-5	1.5909 E-9	2.7805 E-6
0.8	2.3407 E-6	1.5908 E-6	1.6245 E-6
1.0	1.4133 E-6	8.9567 E-7	9.1727 E-7

#### 4.6.5 Operational risk indices for 3-area IEEE RTS

This subsection performs studies on the 3-area RTS. Similar to previous case studies, a 155 MW conventional generator at bust 16 of each area is removed. A 500 MW wind farm is installed at bus 19 of each area. The load is set to the peak value of 8550 MW. The probabilistic model for wind power is similar to that in the previous studies. Table 4.3 display the risk indices obtained for this test system. Compared to the 24-bus IEEE RTS, the risk indices are expectedly lower. This is because the interconnection of three areas improves the overall reliability of the system. Figure 4.9 depicts the computational performance of the method for this test system. The maximum number of samples for NSMCS in this case is 10,000. Thus, the computational burden is expectedly higher than that for 24-bus IEEE RTS. However, it is still not as high as crude NSMCS.

Table 4.3 Operational risk indices for 3-area IEEE RTS

Initial wind power (p.u.)	Proposed Method
0.1	8.7893 E-11
0.3	3.7503 E-11
0.5	2.1835 E-11
0.8	1.2957 E-11
1.0	7.3894 E-12

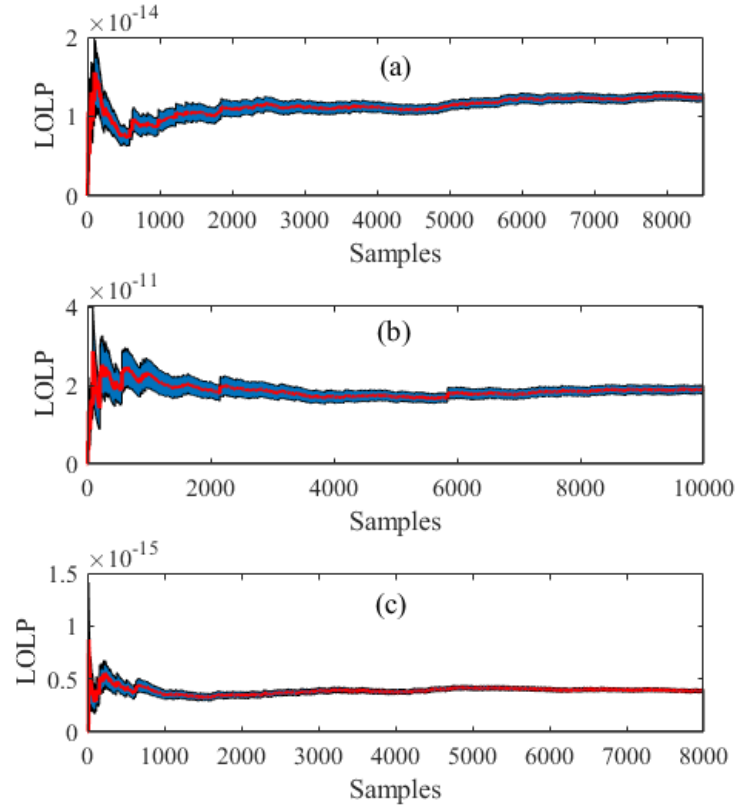


Figure 4.9 The convergence behavior of the proposed method for three clusters when 3-area IEEE RTS is employed. Initial wind generation is set to 0.5 p.u.

## 4.7 Conclusion

In this chapter, a new data-driven method for operational risk assessment of composite power systems considering wind power is proposed. The short-term uncertainty of wind power is directly modeled using GMMs. k-means clustering and MAP estimation are adopted to address the issue of limited data availability. The proposed GMM is then incorporated in the operational risk assessment framework using the total law of expectation. NSMCS is then applied to obtain the risk indices. The computational performance of NSMCS is improved by adapting the CE-IS.

Case studies have shown that the complex statistical features of wind power, which are modeled by GMM, are necessary to obtain accurate operational risk indices. In particular, the multimodality of wind power PDF affects the calculated operational risk indices. The computational performance

of the proposed data-driven method is also shown to be suitable for application in real power systems operation. It is also shown that the transmission system constraints significantly affect the operational risk indices. Therefore, it is crucial to include the transmission system in any operational risk studies. Compared to existing approaches, the proposed approach avoids the pitfalls of using wind speed data. Moreover, the extensive modeling of uncertainty of wind generation leads to more accurate estimation of risk indices.

# Chapter 5

## A Novel Framework for the Operational Reliability Evaluation of Integrated Electric Power-Gas Networks<sup>9</sup>

### 5.1 Abstract

This chapter proposes a new framework for the operational reliability evaluation of IEPGNs. First, a novel approach for modeling the failure modes of natural gas pipelines is presented. This approach utilizes the concept of virtual nodes and employs a gas release rate model to calculate the natural gas leaked from the pipelines. Thereafter, a four-state Markov model for NGFGs with dual-fuel capabilities is proposed. The area risk method is then extended to include the proposed reliability models, and the partial reliability indices of the area risk method are evaluated using a NSMCS. A nonlinear optimization model is also proposed to calculate electric and gas load curtailments for each system state. This optimization model is linearized to obtain a mixed-integer linear programming (MILP) model for reducing the computational burden. The computational performance of NSMCS is further improved by adopting CE-based IS. Finally, two test systems are employed to demonstrate the efficacy of the proposed framework. Case studies validate the importance of considering the proposed reliability models of IEPGNs for operational reliability evaluation. The impacts of operational strategies on the operational reliability indices are also demonstrated

---

<sup>9</sup> Reprinted without modification with permission from: O. A. Ansari, C. Y. Chung, and E. Zio, “A novel framework for the operational reliability evaluation of integrated electric power-gas networks (IEPGNs),” *IEEE Trans. Smart Grid*, (Early Access). Copyrights for future publication of this paper: © 2021 IEEE.

## 5.2 Introduction

The penetration of NGFGs in modern power systems has increased tremendously over the last decade owing to historically lower prices and the comparatively lower carbon intensity of natural gas [2]. Consequently, electric power systems and natural gas networks are becoming increasingly interdependent. This increased coupling poses considerable challenges to the reliable operation of IEPGNs. The impacts of component outages in one network can quickly propagate into the other, thereby jeopardizing the reliability of both networks [96]. Therefore, there is a heightened need to develop novel reliability evaluation tools to assist system operators in minimizing adequacy risks during the planning and operation of IEPGNs [7].

The existing literature on the reliability evaluation of IEPGNs can be broadly classified into two categories: long-term reliability evaluation and short-term, or operational reliability evaluation. In [97], the long-term reliability indices of IEPGNs are evaluated using a SMCS while considering power-to-gas and natural gas storage facilities. Reference [98] adopts reliability network equivalents to represent multi-state reliability models of IEPGN components and employs sequential MCS for reliability evaluation. The universal generating function technique is utilized in [99], where the multi-state models of gas injections to NGFGs are first calculated, followed by the reliability evaluation of power systems. In [100] and [101], the cascading effects of failures in IEPGNs are shown to decrease their long-term reliability. Although long-term reliability evaluation techniques are suitable for system planning purposes, operational reliability evaluation methods are required by system operators to schedule sufficient operating reserves to minimize adequacy risks in operational timescales [7], [20].

A very limited number of frameworks have been proposed in the literature to assess the operational reliability of IEPGNs. In [102], the worst N-1 contingencies in distribution-level IEPGNs are considered, and a heuristic tree search algorithm is proposed to solve the load restoration optimization problem for calculating operational reliability indices. In a multi-energy system setting, [103] models the dynamic behavior of thermal loads and adopts SMCS for operational reliability assessment. In [104], the customers' ability to substitute energy sources to meet their energy demands is included in the operational reliability assessment of multi-energy systems.

Despite their worthy contributions, the existing frameworks for operational reliability evaluation of IEPGNs suffer three key drawbacks. First, the reliability models of natural gas networks are simplified. In particular, the existing studies incorporate only one mode of failures for natural gas pipelines, i.e., ruptures, while neglecting the two more dominant failure modes, which are pinholes and holes in the pipelines [105], [106]. Second, modern NGFGs are equipped with dual-fuel capabilities that allow them to switch between natural gas supply and an alternate fuel supply to generate power in the event of supply shortages [107], [108]. Such a process entails a switching time, and probabilities are associated with the success and failure of this switching process. These characteristics of DF-NGFGs are not considered in existing frameworks. Third, following outages in IEPGNs, different operational strategies are not considered when determining the minimum load curtailment. For instance, NGFGs are treated as low-priority, non-human need gas loads, and thus are curtailed first by natural gas system operators in the case of outages [109]. The first two drawbacks could result in underestimation, whereas the third drawback could lead to overestimation, of operational reliability indices of IEPGNs.

The purpose of this work is therefore to extend the literature on operational reliability evaluation of IEPGNs by proposing a new framework that addresses the aforementioned limitations. A novel approach for reliability modeling of IEPGNs is first proposed that models all three failure modes of pipelines. To this end, a virtual node method is presented, and the natural gas released from the pipelines due to these failures is modeled. Additional PDFs are defined to complete the reliability modeling of pipelines and consider the uncertainties of failure locations and diameters of leaks. Furthermore, a four-state Markov model for DF-NGFGs is proposed that considers the probabilities of successful and failed switching of fuel supply.

Thereafter, the area risk method [17] is extended to include the proposed reliability models of IEPGNs. The partial reliability indices of the area risk method are evaluated using a NSMCS. A new optimization model for evaluating the amounts of electric and gas load curtailments is, then, presented. This optimization model embeds the gas release rate model and allows the incorporation of different operational strategies by system operators. The original non-linear optimization model is linearized into a MILP model to reduce the computational burden of the proposed framework. Finally, to mitigate the low computational performance of NSMCS for evaluating operational reliability indices, IS is adopted, whose parameters are obtained using CE optimization [73], [85].

The effectiveness of the proposed framework is demonstrated by its application to two test systems. The results clearly indicate the importance of including both the proposed reliability models of IEPGNs and the operational strategies of system operators. The good computational performance of the proposed framework is also shown in the case studies.

In summary, the main contributions of this work are as follows:

1. A novel approach for comprehensive reliability modeling of IEPGNs is proposed. The approach allows for the thorough investigation of the impacts of multiple failure modes of pipelines and dual-fuel capabilities of DF-NGFGs on the operational reliability of IEPGNs.
2. A novel framework, based on the area risk method and NSMCS, is proposed to integrate the proposed reliability models for the evaluation of the operational reliability of IEPGNs. To analyze the system state, a new optimization model is also formulated, which is linearized to reduce computational burden.
3. The CE-based IS technique is adopted to improve the computational efficiency of NSMCS in evaluating operational reliability indices.

### 5.3 Reliability Model of IEPGNs

Consider a power system with  $N^G$  generators,  $N^T$  transmission lines,  $N^B$  buses, and  $N^D$  electric loads. Also, among  $N^G$  generators, let  $N^{\text{NGFG}}$  be the number of NGFGs. Also, consider a gas network with  $N^W$  gas wells or sources,  $N^P$  pipelines,  $N^N$  nodes,  $N^L$  gas loads, and  $N^S$  natural gas storage facilities. Various reliability models of power systems for the operational reliability evaluation exist in the literature, e.g., [17], [34]. Specifically, the generators and transmission lines of power systems are modelled using the following ORRs, which represent the probabilities of failure during the future lead time  $T$ :

$$ORR_g^G = 1 - e^{-\lambda_g^G T} \approx \lambda_g^G T, \forall g \in \{1, \dots, N^G\}, \quad (5.1)$$

$$ORR_l^L = 1 - e^{-\lambda_l^L T} \approx \lambda_l^L T, \forall l \in \{1, \dots, N^T\}, \quad (5.2)$$

where  $ORR_g^G$  and  $\lambda_g^G$  represent the ORR and failure rate of the  $g$ th generator, respectively. Likewise,  $ORR_l^L$  and  $\lambda_l^L$  represent the ORR and failure rate of the  $l$ th transmission line,

respectively. Similar to power systems, also the gas sources and pipelines of gas networks can be modeled using ORRs.

$$ORR_w^W = 1 - e^{-\lambda_w^W T} \approx \lambda_w^W T, \forall w \in \{1, \dots, N^W\}, \quad (5.3)$$

$$ORR_p^P = 1 - e^{-\lambda_p^P T} \approx \lambda_p^P T, \forall p \in \{1, \dots, N^P\}. \quad (5.4)$$

In (5.3),  $ORR_w^W$  and  $\lambda_w^W$  describe the ORR and failure rate of the  $w$ th gas source, respectively. In (5.4),  $ORR_p^P$  and  $\lambda_p^P$  describe the ORR and failure rate of the  $p$ th pipeline, respectively.

### 5.3.1 Reliability Model of Natural Gas Pipelines

In the event of unplanned failures, power systems and natural gas networks are operated in different manners. Whereas an outage of a transmission line in a power system results in the line being completely out of service, a pipeline in a natural gas network can still operate with reduced service after it suffers from a failure [105], [110]. Moreover, due to the slower dynamics of natural gas networks, the impacts of pipeline failures are more localized in gas networks than that of transmission lines' failures in power systems. Thus, it becomes important to extend the ORR model of pipelines in (4) to consider these characteristics of natural gas networks.

To realistically model the reduced service of pipelines, multiple failure modes of pipelines need to be considered. Typically, pipeline failures can be classified into three categories: 1) pinhole or crack, 2) hole and 3) rupture [105], [106]. These categories are differentiated based on the size of the leak in the pipeline. For a pinhole, the effective diameter of the leak is less than or equal to 0.02 m. If the effective diameter of the leak is greater than 0.02 m but less than the diameter of the pipeline, the leak is classified as a hole. Finally, for a rupture, the effective diameter of the leak is greater than the pipeline diameter. Although a rupture causes a pipeline to be completely removed from service, a pipeline with a pinhole or a hole can operate with reduced service [111]. Note that the existing literature on reliability evaluation of IEPGNs only considers ruptures, while completely neglecting the other failure modes. Moreover, the data from actual pipeline incidents indicate that ruptures only represent less than 16% of all pipeline failures, with pinhole and hole failures contributing 63.97% and 20.58%, respectively [105]. Thus, it seems relevant to consider also pinhole and hole failures, which are the dominant failures modes of pipelines, to realistically

evaluate the operational reliability indices of IEPGNs. In what follows, a systematic approach is presented to incorporate all failure modes of pipelines for operational reliability evaluation.

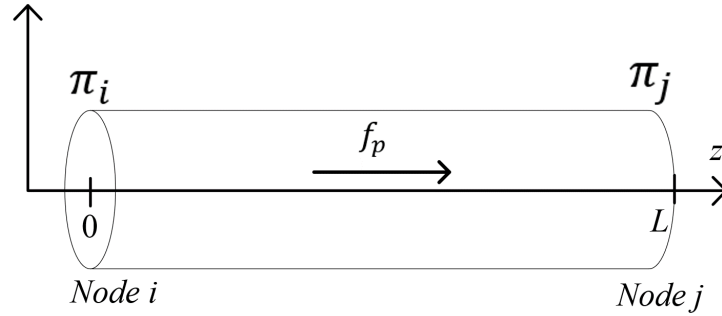


Figure 5.1 A natural gas pipeline of length  $L$  between nodes  $i$  and  $j$  of a natural gas network under normal operating conditions.

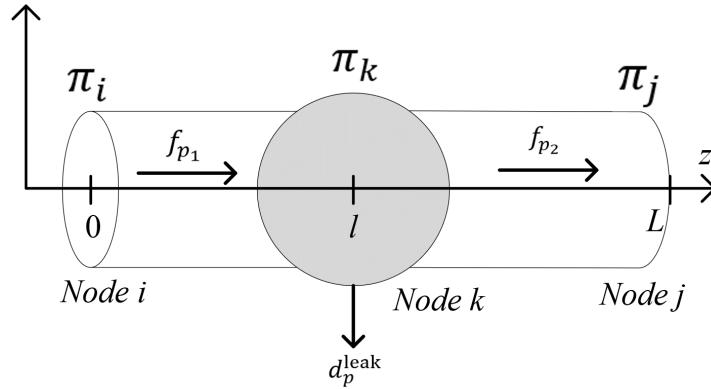


Figure 5.2 The natural gas pipeline of Fig. 5.1 in which a pinhole or hole failure occurs at a distance  $\ell$  from node  $i$ .

#### 5.3.1.1 Virtual Node Approach

The rupture of a pipeline can be modeled by eliminating that specific pipeline from the gas network model. To model pinhole and hole failures, instead a virtual node approach is here proposed. Consider Fig. 5.1, which represents the  $p$ th pipeline between nodes  $i$  and  $j$  of a gas network. In this figure,  $\pi_i$  and  $\pi_j$  represent the gas pressures at nodes  $i$  and  $j$ , respectively.  $f_p$  denotes the mass flow rate in the pipeline from node  $i$  to node  $j$ . Suppose a failure occurs at a distance  $\ell$  from node  $i$ , which results in a leak. To model the natural gas released from this leak, a virtual node  $k$  is introduced at a distance  $\ell$  from node  $i$ . As Fig. 5.2 shows, the gas released from this leak is modeled as an auxiliary gas load at this virtual node, which is represented by  $d_p^{\text{leak}}$ . This leak also modifies the original mass flow rate in the pipeline. Thus,  $f_p$  is replaced by two

mass flow rates  $f_{p_1}$  and  $f_{p_2}$ . Although, this virtual node physically represents a pinhole or hole, it is treated as an additional node in the gas network model with its nodal pressure  $\pi_k$ . The nodal balance equation at this virtual node is given by:

$$f_{p_1} = f_{p_2} + d_p^{\text{leak}}, \quad (5.5)$$

where

$$f_{p_1}|f_{p_1}| = \psi_{p_1}^2 (\pi_i^2 - \pi_k^2), \quad (5.6)$$

$$f_{p_2}|f_{p_2}| = \psi_{p_2}^2 (\pi_k^2 - \pi_j^2) \quad (5.7)$$

In (5.6) and (5.7),  $\psi_{p_1}$  and  $\psi_{p_2}$  are constants for the Weymouth equation, and are calculated using the pipeline lengths  $\ell$  and  $L - \ell$ , respectively.

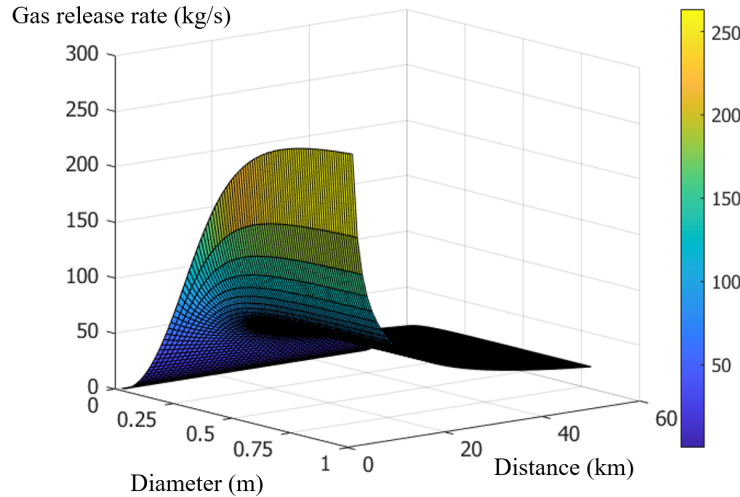


Figure 5.3 Gas release rate from a leak of varying diameter and distance from the starting node on a 60-km gas pipeline.

To calculate the auxiliary load  $d_p^{\text{leak}}$  representing the gas released from leak in the pipeline, the following gas release rate model is adopted [111].

$$d_p^{\text{leak}} = \alpha_p (1 + \beta_p \ell)^{-1/2} \sqrt{\pi_i}, \quad (5.8)$$

where  $\alpha_p$  and  $\beta_p$  are constants given in Appendix D that depend on the diameter of the leak and pipeline parameters. Fig. 5.3 portrays the auxiliary load for varying distance and diameter of the leak on a 60-km pipeline with a 1 m diameter. This figure demonstrates that the gas released from

the leak decreases as the distance from the starting node increases, and increases, as the diameter of the leak increases.

### 5.3.1.2 PDFs for Pipeline Failures

Apart from the ORR for pipelines given by (5.4), additional PDFs are required to complete the reliability model of the pipelines, considering multiple failure modes. The following categorical PDF  $f_p(z)$ , which is obtained from historical data, models the type of pipeline failure for the generic  $p$ th pipeline:

$$f_p(z) = \begin{cases} 0.6397 & z = 1 \\ 0.2058 & z = 2, \\ 0.1545 & z = 3 \end{cases} \quad (5.9)$$

where,  $z = 1, 2$ , and  $3$  denote pinhole, hole, and rupture failures, respectively. If the type of failure is a pinhole or hole, additional random variables need to be defined. For these types of failures, equation (5.8) and Fig. 5.3 show that the gas released from the leak depends on three factors: 1) the pressure at the starting node, 2) the distance of the leak from the starting node of the pipeline, and 3) the diameter of the leak. The pressure at the starting node is determined by solving the natural gas flow problem for gas networks or the combined power-gas flow problem for IEPGNs, as will be described later. The distance from the starting node and diameter of the leak after failure occurrence need to be probabilistically modeled. In this work, a continuous PDF  $f_p^{loc}(\ell)$  is defined for the distance of the leak from the starting node. For the diameter, two continuous PDFs are defined -  $f_p^{PH}(d_l)$  for pinhole and  $f_p^H(d_l)$  for hole, where  $d_l$  represents the diameter of the leak. Based on the definitions of pinhole and hole given above, the domains of  $f_p^{PH}(d_l)$  and  $f_p^H(d_l)$  are  $(0, 0.02]$  and  $(0.02, \mathcal{D}_p)$ , respectively, where  $\mathcal{D}_p$  is the diameter of the  $p$ th pipeline. The actual forms of these distributions are fitted on the available data. In this chapter, for the sake of simplicity, uniform distributions are assumed for  $f_{loc}(\ell)$ ,  $f_p^{PH}(d_l)$  and  $f_p^H(d_l)$  over their respective domains.

### 5.3.2 Reliability Modeling of DF-NGFGs

As mentioned in the Introduction, modern NGFGs are equipped with dual-fuel capabilities that allow them to switch from natural gas supply to an alternative fuel supply. This switching action is taken in the event of natural gas supply shortages. For instance, during the ‘‘Bomb Cyclone’’

event in the U.S. that led to curtailments of natural gas supply, a 1,218 MW NGFG was able to switch to oil to continue producing electric power [107]. This switching process requires a fixed number of hours to complete, and it entails the risk of unsuccessful switching leading to the outage of the NGFG [109]. This behavior is similar to the operation of rapid-start natural gas generating units [17].

To model DF-NGFGs, a four-state Markov model is proposed in this work, as depicted in Fig. 5.4. State 1 represents the normal operation mode of the DF-NGFG, where natural gas is used to generate electric power. State 2 represents the DF-NGFG outage. State 3 represents the operation of the DF-NGFG on alternate fuel. State 4 represents a temporary state when the switching action fails. After the failure of switching action, the DF-NGFG enters State 2 of outage. In Fig. 5.4,  $\mu_{ij}$  indicates the transition rate from state  $i$  to state  $j$ .

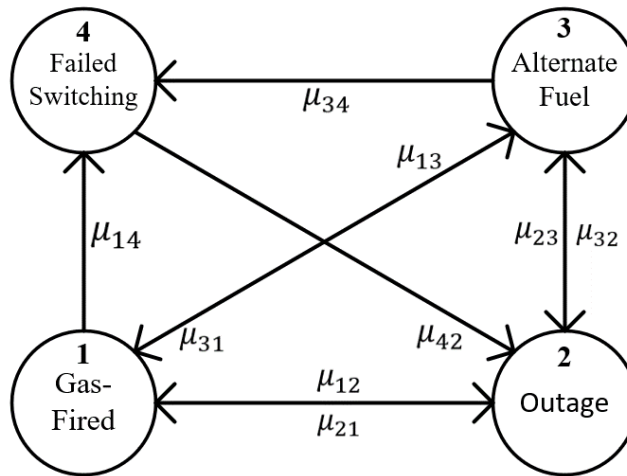


Figure 5.4 Four-state Markov model for NGFGs with dual fuel capabilities

## 5.4 Framework Proposed for Operational Reliability Evaluation of IEPGNs

This section presents the proposed framework for operational reliability evaluation of IEPGNs. The proposed framework, which is founded on the area risk method and NSMCS, evaluates the operational reliability indices for a given lead time considering the previously proposed reliability models of natural gas pipelines and DF-NGFGs. The proposed optimization model for evaluating electric and gas load curtailments considering the gas release rate model is also presented. In what

follows, the proposed framework for evaluating the probabilities of electric load curtailment (*PELC*) and gas load curtailment (*PGLC*) for a given lead time  $T$  is explained.

#### 5.4.1 Area Risk Method

The area risk method has been employed for operational reliability evaluation of power systems to consider rapid start generating units [17], wind generation [85], and energy storage. The area risk method splits the given lead time into several sub-periods, and the reliability indices in each sub-period are calculated. These reliability indices are then accumulated to obtain the operational reliability index for the given lead time. In this work, the area risk method is adopted to consider the switching time associated with the dual-fuel capabilities of DF-NGFGs.

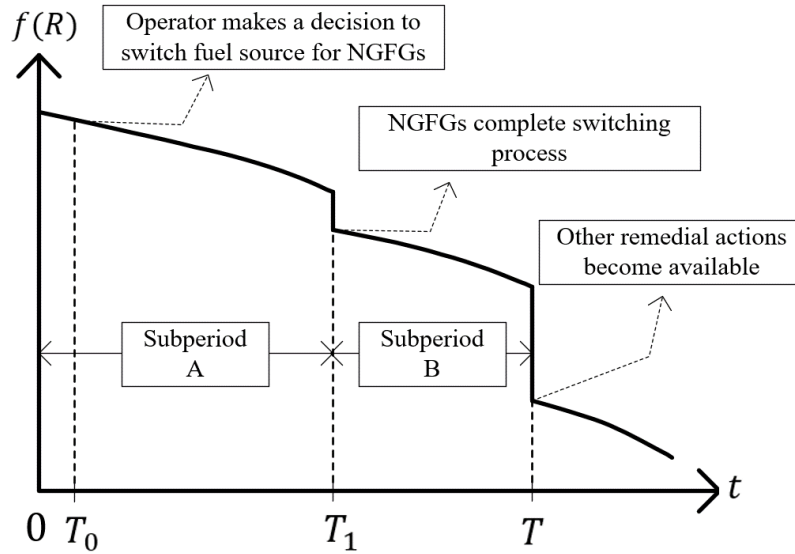


Figure 5.5 The area risk method with NGFGs with dual-fuel capabilities

The area risk method is pictorially sketched in Fig. 5.5 for a lead time  $T$ . For subperiod A, i.e., from 0 to  $T_1$ , the *PELC* and *PGLC* are given by:

$$PELC_A = \int_0^{T_1^-} H_{\text{Elect}}(\mathbf{x}) \mathcal{f}(\mathbf{x}) d\mathbf{x}, \quad (5.10)$$

$$PGLC_A = \int_0^{T_1^-} H_{\text{Gas}}(\mathbf{x}) \mathcal{f}(\mathbf{x}) d\mathbf{x}, \quad (5.11)$$

where  $H_{\text{Elect}}(\cdot)$  and  $H_{\text{Gas}}(\cdot)$  are test functions, which will be defined later.  $\mathcal{f}(\cdot)$  is the combined PDF of the random variables in IEPGNs. Assuming that the outages of different components are independent of each other,  $\mathcal{f}(\cdot)$  can be expressed as:

$$\mathcal{f}(\cdot) = \mathcal{f}_G(\cdot) \mathcal{f}_L(\cdot) \mathcal{f}_W(\cdot) \mathcal{f}_P(\cdot), \quad (5.12)$$

where  $\mathcal{f}_G(\cdot)$  and  $\mathcal{f}_L(\cdot)$  represent the product of binomial distributions of generators, and the product of Bernoulli distributions for the transmission lines, respectively.  $\mathcal{f}_W(\cdot)$  denotes the product of binomial distributions for natural gas sources.  $\mathcal{f}_P(\cdot)$  represents the product of multiple PDFs for the natural gas pipelines as defined in Section 5.3.1. In subperiod A, the DF-NGFGs in IEPGNs are dependent on gas supply from the natural gas network to generate power. Therefore, the ORRs defined in (1) are used in  $\mathcal{f}_G(\cdot)$  for DF-NGFGs.

Assuming that the system operator makes a decision at  $T_0$  to switch the fuel supply for DG-NGFGs, the DG-NGFGs would complete the switching process at  $T_1$ , where  $T_1 - T_0$  is the switching time for DG-NGFGs. After  $T_1$ , the DG-NGFGs that have been successfully switched, are no longer reliant on the natural gas network to generate power. Thus, they can still contribute to the power system if they are not in outage. Due to this switching action of DG-NGFGs, the evaluation of  $PELC$  and  $PGLC$  entail the calculation of two integrals:

$$PELC_B = \int_0^T H_{\text{Elect}}(\mathbf{x}) \mathcal{f}(\mathbf{x}) d\mathbf{x} - \int_0^{T_1^+} H_{\text{Elect}}(\mathbf{x}) \mathcal{f}(\mathbf{x}) d\mathbf{x}, \quad (5.13)$$

$$PGLC_B = \int_0^T H_{\text{Gas}}(\mathbf{x}) \mathcal{f}(\mathbf{x}) d\mathbf{x} - \int_0^{T_1^+} H_{\text{Gas}}(\mathbf{x}) \mathcal{f}(\mathbf{x}) d\mathbf{x}. \quad (5.14)$$

In above equations, the first integral evaluates the indices at the end of subperiod B, whereas the second integral does it indices at the start of subperiod B. For this subperiod, the proposed four-state model for DF-NGFGs is employed instead of using ORRs. Specifically, given a vector of initial state probabilities  $\mathbf{P}_0$  for the Markov model, the state probabilities of a DF-NGFG at a future lead time  $T_k$  can be evaluated by:

$$\mathbf{P}(T_k) = \mathbf{P}_0 \mathbf{P}_S^{T_k/\Delta T}, \quad (5.15)$$

where  $\mathbf{P}_S$  is the discretized stochastic transition probability matrix and  $\Delta T$  is the discretization time interval. The off-diagonal elements of  $\mathbf{P}_S$  are  $\mu_{ij}\Delta T$ , whereas the diagonal elements of  $\mathbf{P}_S$  are  $1 - \sum_{j,i \neq j} \mu_{ij}\Delta T$ .  $\mathbf{P}(T)$  and  $\mathbf{P}_0$  are then utilized to evaluate the first and second integrals, respectively. The total operational reliability indices for the given lead time are then given by:

$$PELC = PELC_A + PELC_B, \quad (5.16)$$

$$PELC = PELC_A + PELC_B, \quad (5.17)$$

For simple cases, the integrals in (5.10), (5.11), (5.13), and (5.14) are evaluated using analytical techniques, such as capacity outage probability tables [17]. In this work, these integrals are estimated using NSMCS. In particular, by using NSMCS, any integral of the form  $\int_0^{T_k} H_k(\mathbf{x}) f(\mathbf{x}) d\mathbf{x}$  can be estimated as:

$$\int_0^{T_k} H_k(\mathbf{x}) f(\mathbf{x}) d\mathbf{x} = \frac{1}{N_S} \sum_{i=1}^{N_S} H_k(\mathbf{x}_i), \quad (5.18)$$

where  $N_S$  is the number of NSMCS samples drawn from  $f(\cdot)$ .

#### 5.4.2 Proposed Optimization Model for Minimum Load Curtailments

The two test functions in Section 5.4.1 are defined as follows:

$$H_{\text{Elect}}(\mathbf{x}_i) = \begin{cases} 0 & S_{\text{Elect}}(\mathbf{x}_i) - \sum_{j=1}^{N^D} d_j \geq 0 \\ 1 & S_{\text{Elect}}(\mathbf{x}_i) - \sum_{j=1}^{N^D} d_j < 0 \end{cases}, \quad (5.19)$$

$$H_{\text{Gas}}(\mathbf{x}_i) = \begin{cases} 0 & S_{\text{Gas}}(\mathbf{x}_i) - \sum_{j=1}^{N^L} l_j \geq 0 \\ 1 & S_{\text{Gas}}(\mathbf{x}_i) - \sum_{j=1}^{N^L} l_j < 0 \end{cases}. \quad (5.20)$$

In (5.19),  $d_j$  denotes the  $j$ th electric load demand and  $S_{\text{Elect}}(\cdot)$  is the sum of electric loads supplied in system state  $\mathbf{x}_i$ . Similarly, in (5.20),  $l_j$  denotes the  $j$ th gas load demand and  $S_{\text{Gas}}(\cdot)$  is the sum of gas loads supplied in system state  $\mathbf{x}_i$ .

To find  $S_{\text{Elect}}(\cdot)$  and  $S_{\text{Gas}}(\cdot)$ , an optimization model is set up to determine the minimum values of the electric and gas loads curtailments. For this optimization model, the objective function is defined as:

$$\min \boldsymbol{\kappa}^T \mathbf{r} + \boldsymbol{\lambda}^T \mathbf{c}, \quad (5.21)$$

where  $\mathbf{r} = [r_1, \dots, r_{N^D}]^T$  and  $\mathbf{c} = [c_1, \dots, c_{N^L}]^T$  are vectors of the electric load and gas load curtailments, respectively.  $\kappa$ , and  $\lambda$  denote the vectors for the electric load and gas load curtailment costs, respectively.

The constraints for power systems are as follows:

$$\mathbf{A}_E \mathbf{g} - \mathbf{B}_E \mathbf{d} + \mathbf{B}_E \mathbf{r} = \mathbf{C}_E \mathbf{p}, \quad (5.22)$$

$$p_i = (\theta_{from(i)} - \theta_{to(i)})/x_i, \forall i \in \{1, \dots, N^T\}, \quad (5.23)$$

$$0 \leq \mathbf{g} \leq \bar{\mathbf{g}}, \quad (5.24)$$

$$0 \leq \mathbf{r} \leq \mathbf{d}, \quad (5.25)$$

Equation (5.22) represents the nodal power balance constraints, where  $\mathbf{g} = [g_1, \dots, g_{N^G}]^T$  and  $\mathbf{d} = [d_1, \dots, d_{N^D}]^T$  represent the vectors of generators and electric load demands, respectively.  $\mathbf{p} = [p_1, \dots, p_{N^T}]^T$  denotes the vector of power flows on the transmission lines.  $\mathbf{A}_E$ ,  $\mathbf{B}_E$ , and  $\mathbf{C}_E$  are incidence matrices that model the connections of generators, electric loads, and transmission lines, respectively, to buses in the power system. The DC power flow model, which is formulated in terms of bus angles  $\theta$ , is given by (5.23). Equations (5.24) and (5.25) set the limits on generator and electric load curtailments.

The constraints for the gas network are described as follows:

$$\mathbf{A}_G \mathbf{w} - \mathbf{B}_G \mathbf{l} + \mathbf{B}_G \mathbf{c} + \mathbf{D}_G \mathbf{s}_{dch} - \mathbf{D}_G \mathbf{s}_{ch} - \mathbf{E}_G \mathbf{n} = \mathbf{C}_G \mathbf{f}, \quad (5.26)$$

$$f_p |f_p| = \psi_p^2 (\Pi_{from(p)} - \Pi_{to(p)}), \forall p \in \{1, \dots, N^P\}, \quad (5.27)$$

$$\mathbf{m}_s - \mathbf{s}_{dch} \Delta T + \mathbf{s}_{ch} \Delta T = \mathbf{0}, \quad (5.28)$$

$$d_p^{\text{leak}} = \alpha_p (1 + \beta_p l)^{-\frac{1}{2}} \sqrt{\pi_i}, \forall p \in \Omega_{\text{leak}}, \quad (5.29)$$

$$\underline{\Pi} \leq \Pi \leq \bar{\Pi}, \quad (5.30)$$

$$\underline{\mathbf{f}} \leq \mathbf{f} \leq \bar{\mathbf{f}}, \quad (5.31)$$

$$\mathbf{0} \leq \mathbf{c} \leq \mathbf{l}, \quad (5.32)$$

$$\mathbf{0} \leq \mathbf{s}_{\text{dch}} \leq \bar{\mathbf{s}}_{\text{dch}}, \mathbf{0} \leq \mathbf{s}_{\text{ch}} \leq \bar{\mathbf{s}}_{\text{ch}}. \quad (5.33)$$

Equation (5.26) represents the nodal balance equation for the gas network, where  $\mathbf{w} = [w_1, \dots, w_{N^W}]^T$  and  $\mathbf{l} = [l_1, \dots, l_{N^L}]^T$ , represent the vectors of gas sources and gas load demands, respectively.  $\mathbf{s}_{\text{dch}} = [s_1^{\text{dch}}, \dots, s_{N^S}^{\text{dch}}]^T$  and  $\mathbf{s}_{\text{ch}} = [s_1^{\text{ch}}, \dots, s_{N^S}^{\text{ch}}]^T$  are vectors of discharge and charge mass flow rates, respectively, for gas storage facilities.  $\mathbf{n} = [n_1, \dots, n_{N^{\text{NGFG}}}]^T$  is a vector of NGFG gas consumptions.  $\mathbf{f}$  is a vector of gas flows in the pipelines. Similar to power systems,  $\mathbf{A}_G$ ,  $\mathbf{B}_G$ ,  $\mathbf{C}_G$ ,  $\mathbf{D}_G$ , and  $\mathbf{E}_G$  are incidence matrices, which denote the connections of gas sources, gas loads, pipelines, gas storages, and NGFGs, respectively, to nodes in the gas network. The Weymouth equations of the pipeline, which are formulated in terms of squared nodal pressure  $\Pi$ , are given by (5.27). The state-of-charge of gas storage facilities is modeled by (5.28). Equation (5.29) models the auxiliary load by using the gas release rate model, as described in Section 5.3.1 for the set of pipelines with failures  $\Omega_{\text{leak}}$ . Equations (5.30) – (5.33) represent the limits on gas network variables. Note that the matrices  $\mathbf{A}_G$ ,  $\mathbf{B}_G$ ,  $\mathbf{C}_G$ ,  $\mathbf{D}_G$ , and  $\mathbf{E}_G$  are modified when the cardinality of  $\Omega_{\text{leak}}$  is greater than zero to include virtual nodes.

The constraints coupling the power system and gas network are given by

$$n_i = \tau_i g_i, \forall i \in \Omega_{\text{NGFG}}, \quad (5.34)$$

where  $\tau_i$  is a constant representing the power conversion factor of the  $i$ th NGGF, and  $\Omega_{\text{NGFG}}$  is the set of NGFGs. This set contains both conventional NGFGs and DF-NGFGs. It is modified depending on whether DF-NGFGs are operating on natural gas supply or alternate fuel.

The optimization model given by (5.21) – (5.34) is nonlinear due to the inclusion of the gas release rate model and Weymouth equations. Nonlinear optimization models incur a large computational burden and therefore cannot be directly employed for operational reliability assessment. In this chapter, the nonlinear gas release rate model is linearized using a piecewise linearization method as given in Appendix B. After linearization, the optimization model is reduced to a MILP model.

### 5.4.3 CE-IS based NSCMS

The traditional NSMCS incurs a large computational burden when the values of *PELC* and *PGLC* being estimated are small. This is the case for operational reliability evaluation of IEPGNS.

Therefore, in this chapter, the widely used IS technique [112] is adopted to reduce the computational time. Using IS, the integral in (5.18) is evaluated using the following estimator:

$$\int_0^{T_k} H_k(\mathbf{x}) \mathcal{f}(\mathbf{x}) d\mathbf{x} = \frac{1}{N_s} \sum_{i=1}^{N_s} \frac{H_k(\mathbf{x}_i) \mathcal{f}(\mathbf{x}_i)}{\mathcal{f}^*(\mathbf{x}_i)}, \quad (5.25)$$

where the samples are now drawn from  $\mathcal{f}^*(\cdot)$ , which is called the IS density. In this chapter, the parameters of the IS density are obtained using the CE optimization. Interested readers are referred to [34], [73], [85] for a detailed explanation of CE-IS based NSCMS.

## 5.5 Simulation Results

This section presents the key results indicating obtained with the proposed framework. The simulations are performed on two test systems: 1) *Test System A*, which comprises the 6-bus power system integrated with the 7-node gas network [113] (Fig. 5.6), and 2) *Test System B*, which comprises the 24-bus IEEE reliability test system (RTS) [77] integrated with the 20-node Belgian gas network [114] (Fig. 5.7). The additional data, including failure rates, and the parameters of the CE-IS-based NSMCS, are provided in Appendix B. For NSMCS, the coefficient of variation of  $PGLC$  is selected, and the stopping criterion is set to 5%. All simulations are run on a PC with a 3.40 GHz Intel® Core i7-6700 CPU and 16 GB of RAM. The proposed framework is implemented in MATLAB 2019 and the GUROBI 9.0.1 solver is used to solve the optimization problem.

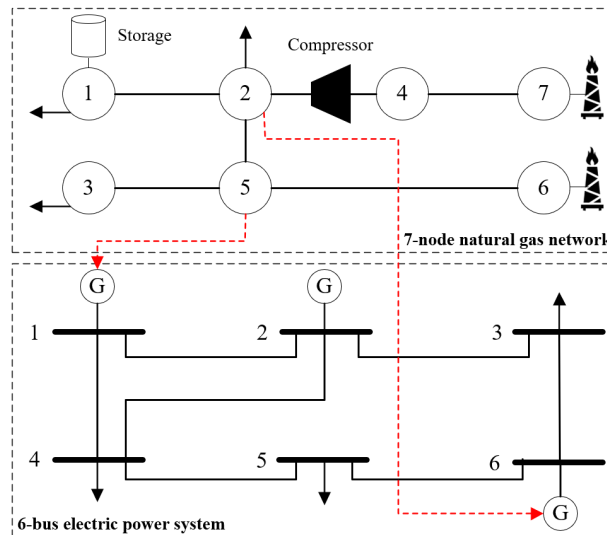


Figure 5.6 *Test System A* comprising a 6-bus power system and a 7-node gas network

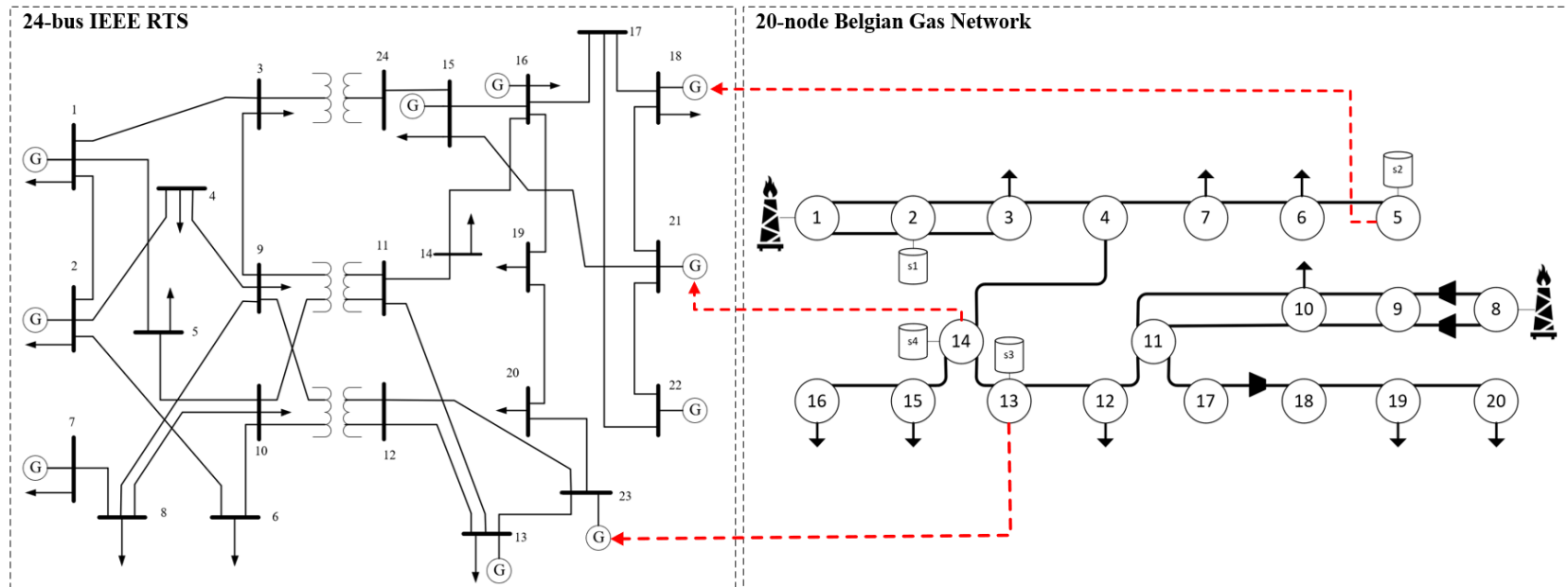


Figure 5.7 *Test System B* comprising the 24-bus IEEE RTS and the 20-node Belgian Gas Network

### 5.5.1 Demonstrative Cases

To demonstrate the importance of performing operational reliability assessment for IEPGNs, two cases are considered. In *Case A*, *Test System A* is decoupled. In *Case B*, the electric and gas networks of *Test System A* are coupled via NGFGs. For both cases, the total electric and gas load demands are set to 270 MW and 32.09 kg/s, respectively. The lead time is set to 2 hours.

Table 5.1 compares the *PELC* and *PGLC* indices for the two cases. The results show that the operational reliabilities of individual networks are lower for *Case B* than for *Case A*. The lower *PELC* for *Case A* is attributed to the supply of natural gas to NGFGs being significantly constrained in the event of pipeline outages. In particular, two pipelines connecting gas sources to other nodes in the gas network are crucial to maintain the supply of natural gas to NGFGs. Similarly, the *PGLC* in *Case B* is ~10% higher than in *Case A*. This is because the gas demands of NGFGs are not included in *Case A* and thus the probability of natural gas loads being supplied due to the absence of NGFG gas demands is higher. Also, for both cases, the *PGLC* is lower than the *PELC* due to higher reliabilities of individual gas sources and pipelines. To sum up, the results show that the need to consider the interactions between electric and gas networks to accurately evaluate the operational reliability indices of these networks.

The computational performance of the operational reliability evaluation framework is critical to facilitate its application during real system operation. Table 5.1 shows that the computational performance of the proposed method is clearly several orders of magnitude higher than that of traditional NSMCS.

Table 5.1 PELC and PGLC of IEPGNs for two demonstrative cases

Method	Indices	<i>Case A</i>	<i>Case B</i>	% Difference
Proposed	<i>PELC</i> ( $\times 10^{-3}$ )	6.570	9.039	37.57
	<i>PGLC</i> ( $\times 10^{-4}$ )	8.785	9.733	10.79
	Time (s)	562.92	404.87	-
Traditional NSMC	<i>PELC</i> ( $\times 10^{-3}$ )	6.488	9.124	40.62
	<i>PGLC</i> ( $\times 10^{-4}$ )	8.726	9.757	11.81
	Time (s)	215,892	151,333	-

Table 5.2 Operational reliability indices for varying gas loads and lead times

Increase in Gas Load		-10%		0%		10%		20%		30%	
Case	Lead Time (h)	PELC ( $\times 10^{-3}$ )	PGLC ( $\times 10^{-3}$ )	PELC ( $\times 10^{-3}$ )	PGLC ( $\times 10^{-3}$ )	PELC ( $\times 10^{-3}$ )	PGLC ( $\times 10^{-3}$ )	PELC ( $\times 10^{-3}$ )	PGLC ( $\times 10^{-3}$ )	PELC ( $\times 10^{-3}$ )	PGLC ( $\times 10^{-3}$ )
<i>Case C</i>	1	4.814	2.508	5.067	2.598	5.270	2.531	6.731	2.531	6.731	3.465
	2	9.183	4.801	9.666	4.975	10.053	5.270	12.085	5.269	12.085	7.484
	3	14.394	6.864	14.941	7.109	15.511	7.671	19.397	7.666	19.397	10.985
	4	20.047	9.276	21.751	9.624	22.044	10.345	25.992	10.335	25.992	14.339
<i>Case D</i>	1	4.353	0.268	4.291	0.262	4.595	0.283	5.416	0.303	5.199	1.709
	2	8.954	0.864	9.039	0.973	9.001	0.981	10.928	1.021	11.771	3.482
	3	12.569	1.155	14.174	1.157	1.264	1.351	15.966	1.478	17.041	5.216
	4	17.772	1.732	19.424	1.881	19.192	2.015	23.323	2.430	22.741	6.514

### 5.5.2 Impact of Failures of Natural Gas Pipelines

In this subsection, we demonstrate the efficacy of the proposed reliability model of natural gas pipelines. Two case studies are performed. In *Case C*, only gas pipeline ruptures are taken into account; whereas in *Case D*, the proposed reliability model is adopted to consider all three failure modes of gas pipelines.

Table 5.2 shows the *PELC* and *PGLC* indices for varying values of total natural gas load demands and lead times. From the Table, it can be deduced that the *PELC* and *PGLC* indices are overestimated in *Case C*. When all three failure modes of pipelines are treated in *Case D*, the *PELC* and *PGLC* indices are lower. With pinhole and hole failure modes, which are the two dominant failure modes of pipelines, the pipelines can be operated with reduced service which still allow the gas network to supply gas load demands to both the gas network and NGFGs in the power system. This leads to improved operational reliability of the gas network and power system. Table 5.2 also indicates that, as expected, this difference is higher for the gas network, i.e., the operational reliability of the gas network is more significantly improved than that of the power system. Furthermore, this improvement in the operational reliability of the gas network is greater at higher gas loads.

### 5.5.3 Impacts of DF-NGFGs

This subsection, the impacts of DF-NGFGs on the operational reliability of IEPGNs. Two case studies are performed. In *Case E*, the DF-NGFGs are not modeled and are treated as conventional NGFGs. In *Case F*, the proposed reliability model of DF-NGFGs is considered. For both cases, the total lead time is set to 3 hours. For *Case F*, the switching time of DF-NGFGs is set to 2 hours, and  $T_0$  in Fig. 5.5 is set to 10 minutes.

Table 5.3 provides the results for the two case studies. The dual-fuel switching capabilities of DF-NGFGs clearly improve the operational reliability of IEPGNs. As the switching process for DF-NGFGs completes in Subperiod B, these NGFGs are no longer constrained by the supply of gas from the gas network, thus shielding the power system from the impacts of gas network outages. The switching action of DF-NGFGs also slightly improves the reliability of the gas network as the total amount of gas load being served is reduced.

Table 5.3 Operational reliability indices with DF-NGFGs

Case	Indices	Subperiod	Subperiod	Total
		A	B	
<i>Case E</i>	$PELC (\times 10^{-3})$	9.039	5.135	14.174
	$PGLC (\times 10^{-4})$	9.733	1.840	11.573
<i>Case F</i>	$PELC (\times 10^{-3})$	9.039	4.128	13.168
	$PGLC (\times 10^{-4})$	9.733	1.688	11.421

### 5.5.4 Practical Considerations

In the optimization model of Section 5.4.2, the values of  $\kappa$  and  $\lambda$  significantly impact the amounts of electric and gas load curtailments and thus affect the operational reliability indices. In this work, three practical strategies are considered. In *Strategy 1*, the electric and gas loads are assumed to have equal priority, i.e., the per-unit electric and gas load curtailment costs are equal. In *Strategy 2*, the gas loads of gas networks have higher priority than the gas loads of NGFGs. In *Strategy 3*, the gas storage facilities in gas networks are only used to supply gas network loads. The lead time is set to 3 hours.

Table 5.4 compares the results for the three operational strategies. As expected, the operational reliability of the electric power system is highest for *Strategy 1* and lowest for *Strategy 3*. On the contrary, the operational reliability of the gas network is highest for *Strategy 3* and lowest for *Strategy 1*. In *Strategy 2*, the gas loads of NGFGs are considered as low priority loads and therefore are curtailed first, leading to reduced reliability of the power system. *Strategy 3* indicates that electric power system operators need to acquire access to gas storage facilities to improve the operational reliability of their networks. This is because these storage facilities are primarily developed to serve the non-electric gas load demands of the gas network.

Table 5.4 Operational reliability indices considering different operational strategies

Strategy	Indices	
<i>Strategy 1</i>	<i>PELC</i> ( $\times 10^{-3}$ )	14.174
	<i>PGLC</i> ( $\times 10^{-3}$ )	1.157
<i>Strategy 2</i>	<i>PELC</i> ( $\times 10^{-3}$ )	15.307
	<i>PGLC</i> ( $\times 10^{-3}$ )	1.133
<i>Strategy 3</i>	<i>PELC</i> ( $\times 10^{-3}$ )	16.301
	<i>PGLC</i> ( $\times 10^{-3}$ )	1.041

### 5.5.5 Case Studies for *Test System B*

In this subsection, we perform case studies on *Test System B* to indicate the scalability of the proposed framework. The results are shown in Table 5.5. For *Cases A* and *B*, the lead time is two hours; for the rest, the lead time is 3 hours. Generally, the operational reliability of *Test System B* is higher than that of *Test System A* due to the presence of multiple generating units in each generation station and redundant components in the gas network. The computational burden for this test system is expectedly higher than that of *Test System A*. The difference between the indices of *Cases C* and *D* reiterate the importance of considering all failure modes of the pipelines. The results presented in Table 5.5 also reinforce the importance of considering the dual-fuel capabilities of DF-NFGFs for operational reliability evaluation of IEPGNs and the impacts of the operational strategies on the reliability indices.

Table 5.5 Operational reliability indices for Test System B

Indices	<i>Case A</i>	<i>Case B</i>	<i>Case C</i>	<i>Case D</i>
<i>PELC</i> ( $\times 10^{-5}$ )	3.328	3.860	10.207	9.696
<i>PGLC</i> ( $\times 10^{-6}$ )	2.943	3.178	8.531	4.225
Time (s)	3,549.1	2,851.6	2,054.1	2,687.5
Indices	<i>Case E</i>	<i>Case F</i>	<i>Strategy 2</i>	<i>Strategy 3</i>
<i>PELC</i> ( $\times 10^{-5}$ )	9.696	9.221	10.471	10.859
<i>PGLC</i> ( $\times 10^{-6}$ )	4.225	4.203	3.975	3.802
Time (s)	2,687.5	2,889	2,456.8	2,994.7

## 5.6 Conclusion

This chapter proposes a novel framework for operational reliability evaluation of IEPGNs. Such framework includes a detailed reliability model of natural gas pipelines for realistically calculating reliability indices. It also accounts for the dual-fuel capabilities of DF-NGFGs, that are shown to improve the operational reliability of IEPGNs. The linear formulation of the proposed optimization model and the adoption of CE-based IS ensure high computational efficiency and make it feasible to adopt the proposed framework in practice. The results on the test cases analyzed indicate that the operational reliability indices of IEPGNs are improved when all three failure modes of pipelines are considered. In addition, the impacts of dual-fuel capabilities of DF-NGFGs and different operational strategies of system operators on operational reliability indices are demonstrated.

## Chapter 6

# Operational Reliability-Constrained Scheduling of Microgrids via Cross-Entropy Importance Sampling- based Sample Average Approximation<sup>10</sup>

### 6.1 Abstract

Microgrids are regarded as integral components of modern smart grids to facilitate higher utilization of distributed renewable energy resources (DRERs) and increase the reliability of supply to the customers. The presence of uncertainties originating from the unplanned outages of dispatchable generators and forecast errors of DRERs and loads complicates the optimal scheduling problem for microgrids. To this end, this chapter proposes a new optimization model for operational reliability-constrained optimal scheduling of microgrids. The proposed model first includes the hourly operational reliability indices as chance constraints in the model. Later, SAA technique is adopted to reformulate chance constraints as implicit linear constraints. Due to lower values of operational reliability indices, the direct application of SAA renders the model intractable. To circumvent this problem, an IS technique is adopted for SAA. The parameters of IS density are obtained using the CE optimization. Case studies are performed on a 15-bus microgrid to demonstrate the effectiveness of the proposed model. Sensitivity studies are then performed to examine the relationship of target operational reliability indices on the total operating costs of the microgrid.

---

<sup>10</sup> Reprinted without modifications and with from permission: O. A. Ansari, and C. Y. Chung, “Operational reliability-constrained scheduling of microgrids via cross-entropy importance sampling-based sample average approximation,” *to be submitted IEEE Trans. Smart Grid*. Copyrights for future publication of this paper: © 2021 IEEE.

## 6.2 Nomenclature

### *Indices and Sets*

$b, \Omega_B$	Index for buses, set of buses
$d, \Omega_D$	$d$ , set of load demands
$i, \Omega_G$	Index for generators, set of generators
$l, \Omega_L$	Index for lines, set of lines
$m, \Omega_R$	Index for distributed renewable energy sources (DRES), set of DRES
$s, \Omega_S$	Index for energy storage, set of energy storage
$t, \Omega_T$	Index for time, set of scheduling intervals $\Omega_T = \{1, 2, 3, \dots, T\}$

### *Constants*

$A_{b,l}$	Element of bus-line connection matrix
$d_{b,t}$	Load demand at $b$ th bus (MW)
$\underline{g}_i, \bar{g}_i$	Minimum/maximum power of $i$ th generator (MW)
$\overline{p_s^{\text{ch/dch}}}$	Maximum charging/discharging power of $s$ th energy storage (MW)
$\underline{p_s^{\text{ch/dch}}}$	Minimum charging/discharging power of $s$ th storage (MW)
$\bar{r}_{m,t}$	Predicted output power for $m$ th DRES (MW)
$rd_i$	Ramp down rate of $i$ th generator (MW/h)
$ru_i$	Ramp up rate of $i$ th generator (MW/h)
$su_i$	Startup cost of $i$ th generator (\$)
$sd_i$	Shutdown cost of $i$ th generator (\$)
$E_{s,0}$	Initial state-of-charge (SOC) of $s$ th energy storage (MWh)
$M$	Big M
$N_i$	Number of generating units for $i$ th generator
$N^{\text{SAA}}$	Number of samples for sample average approximation (SAA)
$N_t^*$	Number of samples for CE-IS-based SAA
$T_i^{\text{up/dn}}$	Minimum up/down time of $i$ th generator (h)
$\Delta t$	Time interval (1 h)
$\zeta_l$	Susceptance of $l$ th line (Siemens)

$\lambda_{g,t}$	Failure rate of $g$ th generator (outages/hour)
$\mu_i$	Running cost of $i$ th generator (\$)
$\rho_i$	Generation cost of $i$ th generator (\$/MW)
$\varrho_t$	Target probability of electric load curtailment <i>PELC</i> for $t$ th hour
$\sigma_t$	Approximate target probability of electric load curtailment <i>PELC</i> for $t$ th hour
$\tau_{i,t}$	Outage replacement rate (ORR) for $i$ th generator
$\omega_t$	Hourly cost of electricity from the upstream network (\$/MW)

*Variables*

$e_t$	Power imported from the upstream network (MW)
$g_{i,t}$	Output of $i$ th generator (MW)
$l_{l,t}$	Power flow on the $l$ th line (MW)
$p_{s,t}^{\text{ch/dch}}$	Charging/discharging power of $s$ th energy storage (MW)
$r_{m,t}$	Output of $m$ th DRES (MW)
$E_{s,t}$	SOC of $s$ th energy storage (MWh)
$\alpha_{i,t}$	Startup indicator for $i$ th generator
$\beta_{i,t}$	Shutdown indicator for $i$ th generator
$\gamma_{i,t}$	Unit commitment status for $i$ th generator
$n_{s,t}^{\text{ch/dch}}$	Charging/discharging indicator for $s$ th energy storage
$\theta_{l,t}^{\text{fr/to}}$	Bus angle at starting/ending bus of $l$ th line
$\pi_j$	Binary variable for SAA and CE-IS-based SAA
$\phi(), h(), y()$	Generic functions for objective function, linear constraints, and inequality constraints, respectively
$\varphi_t()$	Generic function for chance constraints

*Random Variables and Probability Distribution Functions (PDFS)*

$f_{D,t}$	PDF for load demand at time $t$
$f_{G,t}$	PDF for outages of generators at time $t$
$f_{R,t}$	PDF for DRES output at time $t$
$f_{i,t}$	PDF for outages of $i$ th generator
$f_t$	Combined PDF for the microgrid at time $t$

$X_{d,t}^D$	Random variable for $d$ th load
$X_{i,t}^G$	Random variable for $i$ th generator
$X_{m,t}^R$	Random variable for $m$ th DRES
$X_{s,t}^{\text{dch}}$	Random variable for discharging power of $s$ th energy storage

### 6.3 Introduction

Microgrids, which are integral components of smart grids, are touted as the most promising enablers to efficiently and reliably integrate a large penetration of DERs, including DRES, energy storage, and demand response, in existing power systems [115]. The reliability and economic benefits of microgrids are well established through theoretical research and practical demonstrations [3].

To maximize the reliability and economic benefits of microgrids, effective scheduling algorithms for optimal operation of such systems are required. However, the uncertainties associated with a high penetration of DRES in microgrids introduce considerable challenges to microgrid operators. To this end, in the existing literature, several models for optimal scheduling of microgrids have been proposed [116]. In [117], a two-stage model for optimal dispatch strategy is developed, where the second stage employs robust optimization to consider ramp events of solar photovoltaic (PV) generation. Reference [118] presents a two-stage robust optimization model to consider the uncertainties of DRES while considering the dispatch strategies for energy storage and direct load control. Apart from robust optimization, scenario-based stochastic programming has also been adopted, where a selected set of scenarios for DRES are included in the model [119], [120], [121]. Additionally, researchers have employed chance-constrained optimization to include uncertainties of DRES in the microgrid scheduling problem. For instance, reference [122] proposes a distributionally-robust chance-constrained model for islanded microgrids, where the proposed model is robust with respect to PDFs of DRES. In [123], unscented transformation is used to model DRES' uncertainties while also considering the reconfiguration capabilities of microgrids.

Although the uncertainties originating from DRES have been modeled in the previous work, the random unplanned outages of microgrid components, particularly dispatchable generators, have not been considered in [99], [117], [118], [119]. Due to a limited number of dispatchable

generators in microgrids, the outages of these generators can have devastating impacts leading to loss of supply to customers within those microgrids [124]. By ignoring such unplanned outages, the operational reliability of microgrids cannot be guaranteed through optimization models that only aim to maximize the economic benefits. In this regard, in [125], a tri-level two-stage robust optimization model for AC/DC hybrid microgrids is proposed. This model considers the  $N-1$  contingencies while minimizing the energy not served and DRES curtailment in a microgrid. In [126], a multi-objective optimization model is proposed that includes minimizing customers' outage costs as one of the objectives. In [127] the expected energy not supplied (EENS) index is considered, and a scenario-based stochastic programming model is presented. Reference [128] adopts chance constraints to model spinning reserve requirements, where PDFs for DRES and load demand are discretized to assist in the reformulation of chance constraints. Although the models of [126], [127], [128] have attempted to include reliability metrics in the form of outage costs and spinning reserve requirements based on DRES output and load, the outages of dispatchable generators are not modeled. In [129], generator outages are considered using long-term reliability parameters. However, the generators are assumed to be either available or unavailable for the entire optimization horizon, depending on their initial states in the first hour.

Within each hour of the optimization horizon, there is a finite risk of component outages that can lead to loss of load events. This risk is dependent on the time-conditional PDFs for generator outages, DRES, and loads. The existing models tend to ignore these operational reliability constraints in the scheduling problem. The microgrid operator should be able to set an acceptable level of risk for each hour of the optimization horizon while determining the optimal schedule to balance the tradeoff between reliability and cost.

To address the aforementioned issue, this chapter proposes a novel optimal scheduling model for microgrids that explicitly models the hourly operational reliability constraints. For this purpose, chance-constrained optimization is adopted to include the hourly probability of electric load curtailment *PELC* indices – an operational reliability metric. For determining the *PELC* at each hour, the uncertainties associated with generator outages, DRES output, and load demand are included. The resulting combined PDFs for the chance constraints are complicated mixed discrete-continuous PDFs that convolute the process of reformulating these explicit constraints into implicit constraints. To circumvent this issue, first, the chance constraints are represented as expectations.

Then, SAA is adopted to approximate the expectations by sample means. These sample means are included in the model using binary variables and additional constraints.

Due to the lower values of hourly *PELC*, the direct application of SAA renders the model computationally intractable [130]. Consequently, importance sampling (IS) is adopted to obtain an unbiased estimator of expectation that requires fewer samples to evaluate. To obtain the IS density, first, the decision variables are decoupled by using the microgrid conditions that lead to the lowest *PELC*, and hence, maximum number of samples, for each hour in the scheduling horizon. Then, IS density parameters are obtained using an iterative CE optimization. Finally, the CE-IS based sample means are reformulated using a reduced number of binary variables.

To indicate the effectiveness of the proposed model, case studies are performed on a synthetic 15-bus microgrid. Both intra-day and day-ahead scheduling problems are studied. The results indicate the importance of considering operational reliability constraints while determining the optimal schedule for microgrids. The tradeoff between the operational reliability and the total operating costs are also shown. The impacts of target *PELC* on the operating costs are also examined.

Chance-constrained optimization has been adopted previously for operational scheduling of power systems to consider various uncertainties [131], [132], [133]. Compared to these worthy research works, the proposed model differs in three key aspects: 1) the outages of dispatchable generators are included in the chance constraints, 2) the operational reliability index, i.e. the *PELC*, is considered for each hour of the scheduling horizon, 3) no restrictions on the definitions of PDFs for chance constraints are assumed, and 4) CE-IS-based SAA is adopted to render the model tractable.

## 6.4 Deterministic Model Formulation

This section presents the deterministic version of the optimal scheduling problem for microgrids. The objective of this problem is to minimize the total operation cost of the microgrid. This operation cost consists of three components, (i) the generation costs of dispatchable generators in the microgrid, (ii) the startup and shutdown costs of dispatchable generators in the microgrid, and (iii) the cost of electricity purchased from the upstream network.

$$\begin{aligned} \min \sum_{t=1}^T \sum_{i \in \Omega_G} (\rho_i g_{i,t} + \mu_i \gamma_{i,t}) \\ + \sum_{t=1}^T \sum_{i=1}^{N^G} (s u_{i,t} \alpha_{i,t} + s d_{i,t} \beta_{i,t}) + \sum_{t=1}^T \omega_t e_t \end{aligned} \quad (6.1)$$

The optimal scheduling problem is constrained by following equations:

$$\begin{aligned} \sum_{l \in \Omega_L(b)} A_{b,l} l_{l,t} + \sum_{i \in \Omega_G(b)} g_{i,t} + \sum_{m \in \Omega_R(b)} r_{m,t} \\ + \sum_{s \in \Omega_S(b)} (p_{s,t}^{\text{dch}} - p_{s,t}^{\text{ch}}) - d_{b,t} = 0, \quad \forall b \in \Omega_B \setminus 1, \forall t, \end{aligned} \quad (6.2)$$

$$l_{l,t} = \zeta_l (\theta_{l,t}^{\text{fr}} - \theta_{l,t}^{\text{to}}), \quad \forall l \in \Omega_L, \forall t, \quad (6.3)$$

$$\gamma_{i,t} \underline{g}_i \leq g_{i,t} \leq \gamma_{i,t} \bar{g}_i, \quad \forall i \in \Omega_G, \forall t, \quad (6.4)$$

$$\alpha_{i,t} - \beta_{i,t} = \gamma_{i,t} - \gamma_{i,t-1}, \quad \forall i \in \Omega_G, \forall t, \quad (6.5)$$

$$\sum_{j=t-T_i^{\text{up}}+1}^t \alpha_{i,t} \leq \gamma_{i,t}, \quad \forall i \in \Omega_G, \forall t, \quad (6.6)$$

$$\sum_{j=t-T_i^{\text{dn}}+1}^t \beta_{i,t} \leq 1 - \gamma_{i,t}, \quad \forall i \in \Omega_G, \forall t, \quad (6.7)$$

$$g_{i,t} - g_{i,t-1} \leq r u_i, \quad \forall i \in \Omega_G, \forall t, \quad (6.8)$$

$$g_{i,t-1} - g_{i,t} \leq r d_i, \quad \forall i \in \Omega_G, \forall t, \quad (6.9)$$

$$E_{s,t} = E_{s,t-1} - p_{s,t}^{\text{dch}} \Delta t + p_{s,t}^{\text{ch}} \Delta t, \quad \forall s \in \Omega_S, \forall t, \quad (6.10)$$

$$\eta_{s,t}^{\text{dch}} \underline{p_s^{\text{dch}}} \leq p_{s,t}^{\text{dch}} \leq \eta_{s,t}^{\text{dch}} \overline{p_s^{\text{dch}}}, \quad \forall s \in \Omega_S, \forall t \quad (6.11)$$

$$\eta_{s,t}^{\text{ch}} \underline{p_s^{\text{ch}}} \leq p_{s,t}^{\text{ch}} \leq \eta_{s,t}^{\text{ch}} \overline{p_s^{\text{ch}}}, \quad \forall s \in \Omega_S, \forall t \quad (6.12)$$

$$E_{s,T} = E_{s,0}, \quad \forall s \in \Omega_S \quad (6.13)$$

$$\eta_{s,t}^{\text{dch}} + \eta_{s,t}^{\text{ch}} \leq 1, \quad \forall s \in \Omega_S, \forall t \quad (6.14)$$

$$r_{m,t} \leq \bar{r}_{m,t}, \quad \forall m \in \Omega_R, \forall t, \quad (6.15)$$

Equation (6.2) represents the power balance constraints for all buses except the bus connected to point of common coupling, which is labelled as Bus 1. For the point of common coupling bus,  $e_t$  is added to the power balance equation. The power flow equations are given by (6.). Equation (6.4) constraints the power generated by generating stations. Equation (6.5) models the relationships between the three unit commitment status variables for generators. Equation (6.6) and (6.7) model the minimum up time, and minimum down time, respectively, for generators. Equation (6.8) and (6.9) limit the ramping capabilities of generators. The state-of-charge (SOC) equation for storage is provided by (6.10). In (6.11) and (6.12), the constraints on the maximum charging and discharging power of storage are set. Equation (6.13) sets the cycling constraint for energy storage, which ensures that energy storage maintains the initial SOC at the end of scheduling horizon. Equation (6.14) ensures energy storage is not charged and discharged simultaneously. Finally, the constraints on DRES output are provided by (6.15).

## 6.5 Proposed Chance-Constrained Optimization Formulation

The deterministic formulation presented in the previous section ignores the uncertainties associated with the unplanned outages of dispatchable generators, the output of DRERs and the load forecast errors. The outages of dispatchable generators coupled with uncertainties of DRES, in particular, can lead to loss of load events, thus threatening the operational reliability of the microgrid. Ignoring these uncertainties may lead to an operation schedule, which, although, maximizes the economic benefit of the microgrid but could increase the risk of loss of load events. Therefore, it is important to consider the operational reliability constraints to minimize this risk. Moreover, the microgrid operator should be able to set a preferable level of risk for each hour while scheduling the microgrid. Consequently, in this chapter, chance-constrained optimization is adopted to model the operational reliability constraints in the scheduling problem.

To represent these uncertainties, random variables are introduced. Specifically, let  $X_{i,t}^G$  be a random variable representing the available number of generating units of the  $i$ th generator, which comprises total  $N_i$  identical units. Let  $X_{m,t}^R$  and  $X_{d,t}^D$  represent the random variables for the  $m$ th DRER and the  $d$ th load, respectively. Similarly, let  $X_{s,t}^{\text{dch}}$  denote the random variable for available discharging power for the  $s$ th storage. Employing these random variables, the power balance equation in (6.2) is then replaced by the following constraint:

$$\begin{aligned}
& \sum_{l \in \Omega_{L(b)}} A_{b,l} l_{l,t} + \sum_{i \in \Omega_{G(b)}} g_{i,t} + \sum_{m \in \Omega_{R(b)}} \mathbb{E}_{f_{R,t}} X_{m,t}^R \\
& + \sum_{s \in \Omega_{S(b)}} (p_{s,t}^{\text{dch}} - p_{s,t}^{\text{ch}}) - \sum_{d \in \Omega_{D(b)}} \mathbb{E}_{f_{D,t}} X_{d,t}^D = 0, \quad (6.16) \\
& \forall b \in \Omega_B \setminus 1, \forall t,
\end{aligned}$$

where  $\mathbb{E}_f$  denotes the expectation taken with respect to the PDF  $f$ . In order to quantify the risk of loss of load events, the operational reliability indices can be employed. In this work, the *PELC* index is considered [85]. In particular, the *PELC* index is given by:

$$\begin{aligned}
& \mathbb{P}_{f_t} \left\{ \sum_{i \in \Omega_G} \gamma_{i,t} \bar{g}_i X_{i,t}^G + \sum_{m \in \Omega_R} X_{m,t}^R - \sum_{d \in \Omega_D} X_{d,t}^D + \sum_{s \in \Omega_S} X_{s,t}^{\text{dch}} \leq 0 \right\} \\
& \leq \varrho_t, \quad \forall t, \quad (6.17)
\end{aligned}$$

where  $f_t$  represents the combined PDF for the system. Also, in (6.17), it is assumed that the energy storage is always discharged in the event of outages to improve the operational reliability of the microgrid. Such practical operation strategy of energy storage is commonly assumed in the operational reliability literature [27].

In (6.17), the PDF  $f_t$  should be defined for each hour of the scheduling horizon. Assuming that the random variables are independent, this PDF can be decomposed as follows:

$$f_t(\mathbf{X}) = f_{G,t} f_{R,t} f_{D,t}. \quad (6.18)$$

The PDF for generator outages at each hour can be formulated in terms of outage replacement rates (ORRs) [85] as follows. Specifically,  $X_{i,t}^G$  follows a binomial distribution

$$f_{i,t}(X_{i,t}^G) = \binom{N_i}{X_{i,t}^G} (1 - \tau_{i,t})^{X_{i,t}^G} (\tau_{i,t})^{N_i - X_{i,t}^G}, \quad (6.19)$$

Where the ORR is given by

$$\tau_{i,t} = \lambda_{i,t} \Delta t. \quad (6.20)$$

Then,

$$f_{G,t} = \prod_{i \in \Omega_G} f_{i,t}. \quad (6.21)$$

The PDFs for DRES  $f_{R,t}$  and load demand  $f_{D,t}$  are fitted on historical forecast errors data. For simplicity, in this chapter, these PDFs are modeled as Gaussian distributions centered on forecasted values. However, it should be noted that the proposed approach of this chapter does not restrict the definition of these PDFs. In fact, any forms of PDFs can be employed as long as samples can be generated from those PDFs and appropriate IS density can be obtained. Interested readers are referred to [34] for an example of using GMM models for renewable energy sources in the operational reliability evaluation.

The constraints given by (6.16) and (6.17) along with the associated definitions of PDFs are included in the optimization model presented in the previous subsection. The proposed chance-constrained formulation is then given by:

$$\min(6.1) \text{ s.t. } \{(6.3) - (6.15), (6.16) - (6.21)\}. \quad (6.22)$$

The inclusion of the explicit constraints requires reformulation strategies to convert them into implicit constraints. The reformulation strategy employed in this chapter is explained in the next section.

## 6.6 Model Reformulation via CE-IS Based SAA

### 6.6.1 IS-Based SAA

The chance-constrained formulation of (6.22) can be rewritten in the following concise format:

$$\min \phi(\mathbf{x}). \quad (6.23)$$

$$\text{s.t.} \quad h(\mathbf{x}) = 0, \quad (6.24)$$

$$y(\mathbf{x}) \leq 0, \quad (6.25)$$

$$\mathbb{P}_{f_t}\{\varphi_t(\mathbf{x}, \boldsymbol{\xi}) \leq 0\} \leq \varrho_t, \quad \forall t \in \Omega_T, \quad (6.26)$$

where  $\boldsymbol{\xi}$  is a random vector with PDF given by  $f(\cdot)$ , and  $\mathbf{x}$  is the vector of decision variables.  $\varrho_t$  represent the target *PELC* index for each hour set by the microgrid operator. Note that, in the above

formulation, the chance constraints are applied to each hour of the scheduling period. These chance constraints can also be written in the form of expectation of an indicator function as follows:

$$\mathbb{E}_f\{\mathbf{1}\{\varphi_t(\mathbf{x}, \xi) \leq 0\}\} \leq \varrho_t, \quad \forall t \in \Omega_T. \quad (6.27)$$

The model given by (6.23)–(6.27) cannot be directly solved due to the implicit chance constraints. Thus, it is necessary to reformulate the implicit chance constraints into explicit constraints. Typically, existing studies reformulate these chance constraints into linear constraints by assuming a standard PDF for  $f_t$ , e.g., Gaussian distribution. Such assumptions cannot be applied as  $f_t$  in (6.18) represents a mixed discrete-continuous PDF. Also, depending on the definitions of  $f_R$  and  $f_D$ , the form of  $f_t$  can be very complicated.

An approach to reformulate the above chance constraints is to employ approximation techniques. SAA falls under the category of these approximation techniques. Using SAA, the expectation in (6.27) is replaced by the sample means as follows:

$$\frac{1}{N^{SAA}} \sum_{j=1}^{N^{SAA}} \mathbf{1}\{\varphi_t(\mathbf{x}, \xi_j) \leq 0\} \leq \sigma_t, \quad \forall t \in \Omega_T. \quad (6.28)$$

where  $\xi_j$  is the  $j$ th sample drawn from  $f_t(\cdot)$ , and  $N^{SAA}$  is the total number of independent and identically distributed (IID) samples from  $f_t(\cdot)$ . Note that due to the approximation,  $\varrho_t$  is modified to  $\sigma_t$ , where  $\sigma_t > \varrho_t$ . Using binary variables, the constraints of (6.28) can be reformulated as follows:

$$\frac{1}{N^{SAA}} \sum_{j=1}^{N^{SAA}} \pi_j \leq \sigma_t, \quad \forall t \in \Omega_T, \pi_j \in [0,1], \quad (6.29)$$

$$\varphi_t(\mathbf{x}, \xi_j) + M\pi_j \geq 0, \quad \forall j \in \{1, \dots, N^{SAA}\}, \forall t \in \Omega_T, \quad (6.30)$$

where big-M method is used to allow constraint violations for samples when  $\pi_j$  is 1.

A major drawback of SAA lies in the inclusion of a large number of additional constraints of the form (6.30). In particular, when (6.27) represents a rare event, the number of samples  $N^{SAA}$  required for (6.28) would be very large. This is the situation for the operational reliability constraints as the operational reliability indices are very small. For instance, for the hourly *PELC* equal to  $10^{-4}$ ,  $N^{SAA}$  should be set to at least  $10^4$  to have one sample on average that causes the

violation of (6.27). Otherwise, all other samples will always satisfy (6.27). Consequently, to reformulate these chance constraints, for each hour  $10^4$  binary variables and  $10^4$  additional constraints need to be added to the model. The model quickly becomes intractable and difficult to solve as the number of hours in the scheduling horizon increase from one. To address this issue, in this chapter, IS is adopted [130]. The idea of IS is to distort the original PDF  $f_t(\cdot)$  to obtain a different PDF  $f_t^*(\cdot)$  that is biased to generate more samples that are of interest [73]. That is, more samples are generated that violate the operational reliability constraints. Using IS, (6.28) is replaced by the following unbiased estimator:

$$\frac{1}{N_t^*} \sum_{j=1}^{N_t^*} \mathbf{1}\{\varphi_t(\mathbf{x}, \xi_j) \leq 0\} W_t(\mathbf{x}, \xi_j) \leq \varrho_t, \quad \forall t \in \Omega_T. \quad (6.31)$$

where  $N_t^*$  IID samples are drawn from  $f_t^*(\cdot)$  and  $W_j$  is the likelihood ratio, which is given by:

$$W_t(\mathbf{x}, \xi_j) = \frac{f_t(\mathbf{x}, \xi_j)}{f_t^*(\mathbf{x}, \xi_j)}, \quad \forall t \in \Omega_T. \quad (6.32)$$

After adopting IS, (6.29)–(6.30) are reformulated using the following binary variables as follows [Ref]:

$$\sum_{j=1}^{N_t^*} W_t(\mathbf{x}, \xi_j) \pi_j \leq \sigma_t, \quad \forall t \in \Omega_T, \pi_j \in [0,1], \quad (6.33)$$

$$\varphi_t(\mathbf{x}, \xi_j) + M\pi_j \geq 0, \quad \forall j \in \{1, \dots, N_t^*\}, \forall t \in \Omega_T. \quad (6.34)$$

## 6.6.2 CE-IS-based SAA

The challenge now becomes finding the IS density  $f_t^*$  for each hour. To do so, first, we fix the decision variables  $\mathbf{x}$  for selecting an appropriate IS density. Specially, we select  $\mathbf{x}$  such that the *PELC* is lowest for each hour. This corresponds to all generators being committed in each hour and the energy storage discharged at the maximum power. Second, we assume a parametric form of  $f_t$  and  $f_t^*$ . In particular,  $f_t(\cdot | \mathbf{u})$  and  $f_t^*(\cdot) = f_t(\cdot | \mathbf{v})$  belong to the same parametric PDF family with parameters  $\mathbf{u}$  and  $\mathbf{v}$ , respectively. To obtain  $\mathbf{v}$ , CE optimization is used in this work. CE optimization is an iterative technique that minimizes the Kullback-Leibler divergence between the ideal IS density  $f_t(\cdot | \mathbf{v}^*)$  and approximate IS density  $f(\cdot | \mathbf{v})$  [73]. The advantage of using CE

optimization in this work lies in the fact that closed-form analytical expressions are readily available to obtain  $\nu$  for many PDFs that are typically used in the operational reliability studies [34], [85]. Interested readers are referred to [34], [85] for these expressions and the CE optimization process.

After adopting the CE-IS-based SAA, the model is reformulated into a tractable MILP model that can be solved by multiple off-the-shelf solvers. The reformulated model is given by:

$$\min(6.23) \text{ s. t. } \{(6.24), (6.25), (6.33), (6.34)\}. \quad (6.35)$$

The complete framework for solving the model is given by Fig. 6.1.

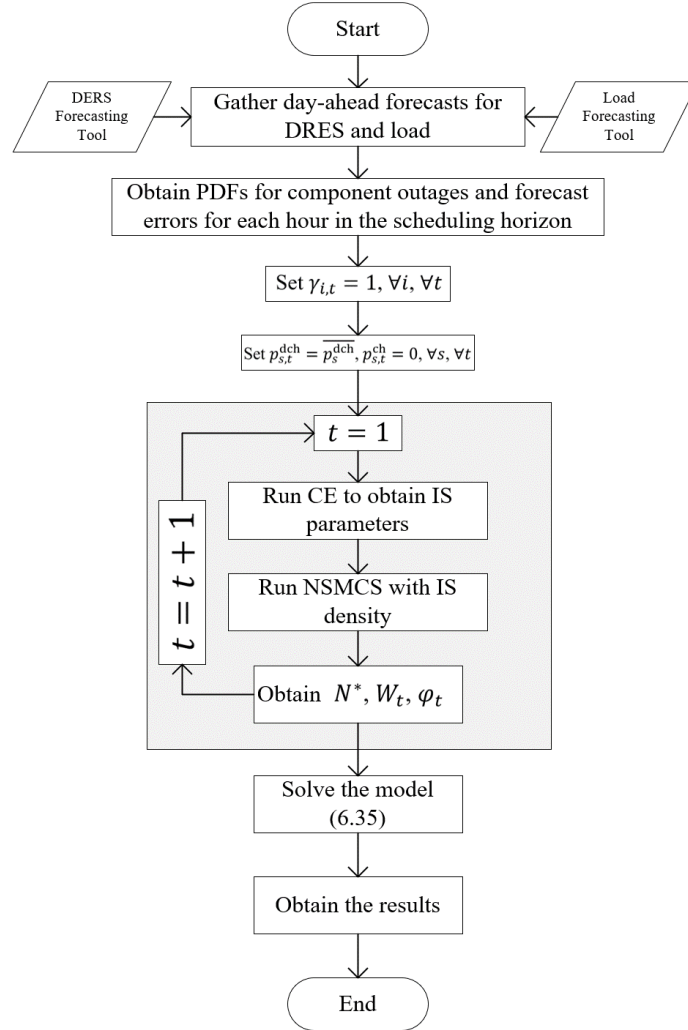


Figure 6.1 Framework for the proposed microgrid scheduling problem

## 6.7 Case Studies

This section performs case studies to depict the effectiveness of the proposed model. The case studies are performed on a synthetic 15-bus microgrid as shown in Fig. 6.2. The microgrid comprises 2 dispatchable generators. The maximum capacities of the 2 dispatchable generators are 0.5 MW and 1.4 MW, respectively. The first generator comprises a single unit, whereas the second generator includes two identical units of 0.7 MW. The microgrid also includes a 1.1 MW wind turbine, 1 MW solar PV and a 0.4 MW/2.4MWh energy storage. The peak load for this system is 2.53 MW. The CE-IS based SAA method is implemented in MATLAB 2019 and the GUROBI 9.0.1 solver is used to solve the optimization problem.

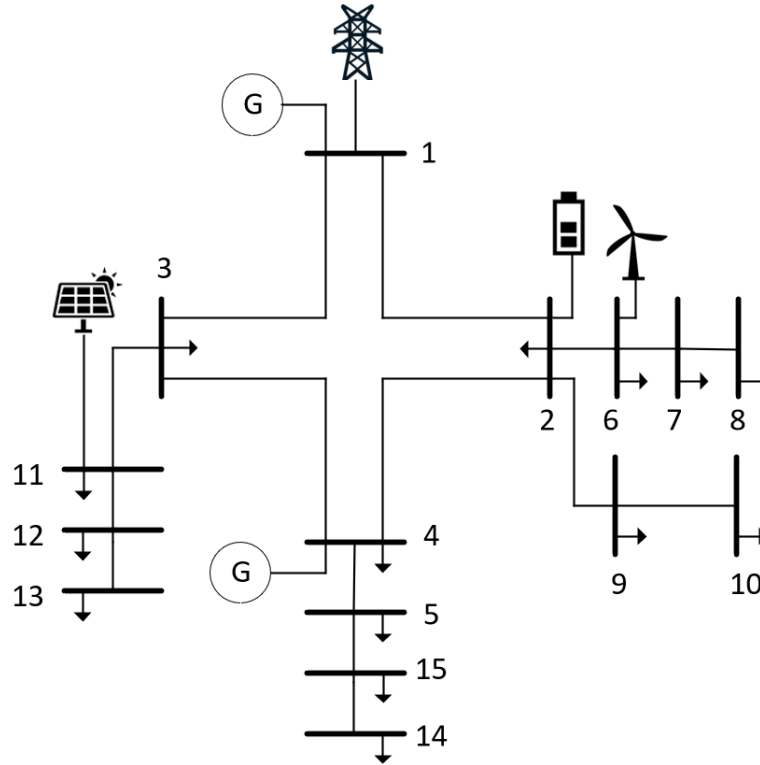


Figure 6.2 A 15-bus synthetic microgrid for case studies

### 6.7.1 Demonstrative Case

This subsection performs case studies by using the following two optimization models. In *Model A*, the operational reliability constraints are ignored and the microgrid is scheduled solely based on the operation costs. In *Model B*, the proposed model is used to include the operational reliability constraints in the form of hourly *PELC* indices, which are set to  $1 \times 10^{-5}$  for each hour. For

demonstration purposes, the scheduling horizon is limited to 6 hours for the intra-day scheduling of the microgrid. In a later section, this scheduling horizon is extended to 24 hours for the day-ahead scheduling problem.

Table 6.1 depicts the commitment statuses of the dispatchable generators obtained by *Model A* and *Model B*. In the results, G1 represents the power received from the upstream network. The results indicate that the optimal schedule is evidently different for the two models. To explain why this is the case, consider Fig. 6.3 and Fig. 6.4. Fig. 6.3 portrays the total committed generation capacities, expected load demands, expected renewable generation, and energy storage operation for each hour in the scheduling horizon for the two models. Fig. 6.4 shows the log of hourly *PELC* indices for the two models. During hours 1–3, both models satisfy the target *PELC* indices. In fact, the risk for *Model B* is higher than that of *Model A* due to the lower total committed capacity in *Model B*, as shown in Fig. 6.3. In *Model A*, the committed capacity is higher due to the scheduling of a larger but cheaper generator G4 instead of a smaller but more expensive generator G2. During hours 4–6, the *PELC* for *Model A* increases after the decommitment of G4, which happens due to increased output from the renewable generation as shown in Fig. 6.3. Consequently, during these hours, the target *PELC* indices are violated. On the contrary, for *Model B*, no units are decommitted during these hours, thus, ensuring that the target *PELC* indices are satisfied for all hours. This is also shown in Fig. 6.4. The *PELC* indices decrease significantly during hours 4–6. The increase in operational reliability for *Model B* comes at an increase in the operating costs. In fact, the value of objective function for *Model A* and *Model B* are \$527.1 and \$657.36, respectively.

Table 6.1 Scheduling of dispatchable generators for demonstrative cases

Model	Generator	Hour 1	Hour 2	Hour 3	Hour 4	Hour 5	Hour 6
<b>Model A</b>	G1	1	1	1	1	1	1
	G2	0	0	0	0	0	0
	G3	1	1	1	1	1	1
	G4	1	1	1	0	0	0
<b>Model B</b>	G1	1	1	1	1	1	1
	G2	1	1	1	1	1	1
	G3	1	1	1	1	1	1

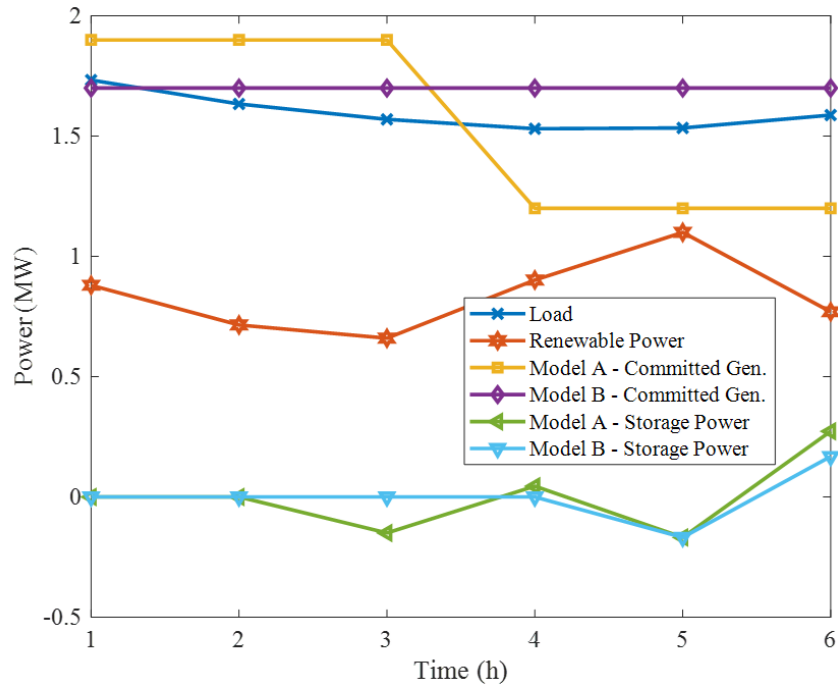


Figure 6.3 Load, renewable power, committed generation, and storage power for *Model A* and *Model B*

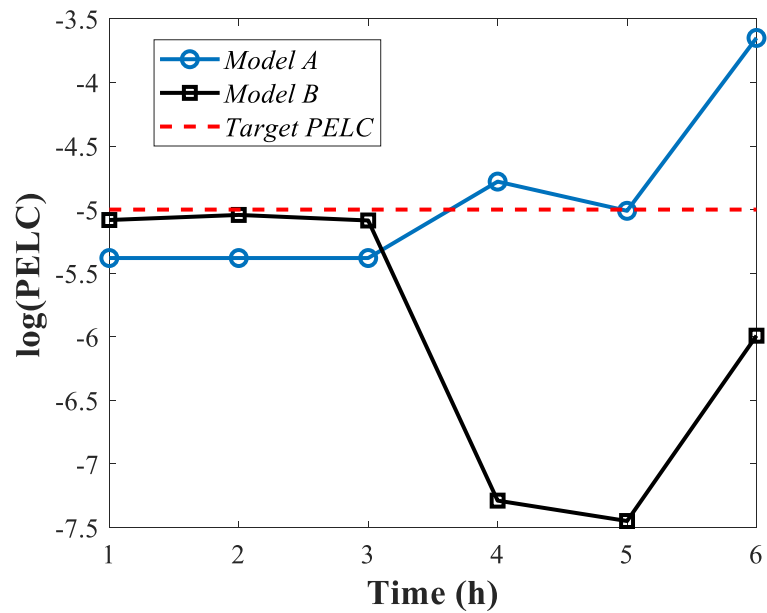


Figure 6.4  $\text{PELC}$  indices for *Model A* and *Model B*

### 6.7.2 24-hour Day-Ahead Scheduling

The results for the 24-hour day-ahead scheduling of microgrids are presented here. For *Model B*, the target hourly *PELC* indices are set to  $5 \times 10^{-3}$  for each hour. Table 6.2 on the next page shows the commitment statuses of the generators for the two models. As observed previously, the introduction of operational reliability constraints modifies the commitment schedules. In particular, during hours 17-24, *Model B* commits G2 to reduce the *PELC* indices. The *PELC* indices are shown in Fig. 6.5. Note that the target *PELC* indices are satisfied for all hours until hour 16 for *Model A*. For hours 17-24, the *PELC* indices increase due to the reduction in the output of solar power. This is shown in Fig. 6.6, which portrays the hourly load demand and DRES output for the 24 hours. On the other hand, for *Model B*, the *PELC* indices are satisfied for hours 17-24 as well due to the commitment of G2. The total operation costs for *Model A* and *Model B* are \$16,686 and \$17,188, again indicating an increase in the operating cost as the operational reliability constraints are included in the model.

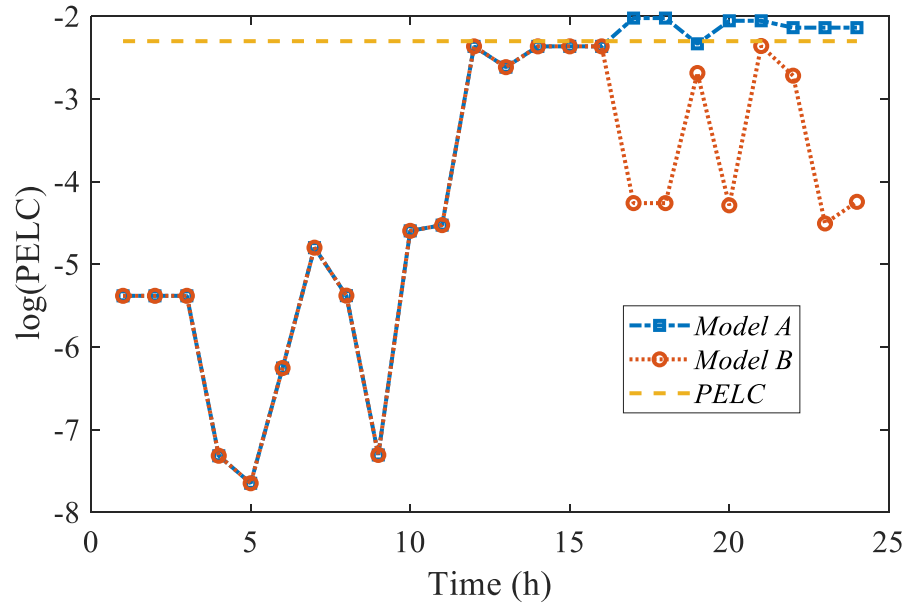


Figure 6.5 *PELC* indices for *Model A* and *Model B* for day-ahead scheduling

Table 6.2 Scheduling of dispatchable generators for 24-hour day-ahead scheduling

<b>Model</b>	<b>Gene rator</b>	<b>1</b>	<b>2</b>	<b>3</b>	<b>4</b>	<b>5</b>	<b>6</b>	<b>7</b>	<b>8</b>	<b>9</b>	<b>10</b>	<b>11</b>	<b>12</b>	<b>13</b>	<b>14</b>	<b>15</b>	<b>16</b>	<b>17</b>	<b>18</b>	<b>19</b>	<b>20</b>	<b>21</b>	<b>22</b>	<b>23</b>	<b>24</b>
<b><i>Model A</i></b>	G1	1	1	1	1	1	1	1	1	1	1	1	1	1	1	1	1	1	1	1	1	1	1	1	1
	G2	0	0	0	0	0	0	0	0	0	0	0	0	0	0	0	0	0	0	0	0	0	0	0	0
	G3	1	1	1	1	1	1	1	1	1	1	1	1	1	1	1	1	1	1	1	1	1	0	0	0
	G4	1	1	1	1	1	1	1	1	1	1	1	1	1	1	1	1	1	1	1	1	1	1	1	1
<b><i>Model B</i></b>	G1	1	1	1	1	1	1	1	1	1	1	1	1	1	1	1	1	1	1	1	1	1	1	1	1
	G2	0	0	0	0	0	0	0	0	0	0	0	0	0	0	0	0	1	1	1	1	1	1	1	1
	G3	1	1	1	1	1	1	1	1	1	1	1	1	1	1	1	1	1	1	1	1	1	0	0	0
	G4	1	1	1	1	1	1	1	1	1	1	1	1	1	1	1	1	1	1	1	1	1	1	1	1

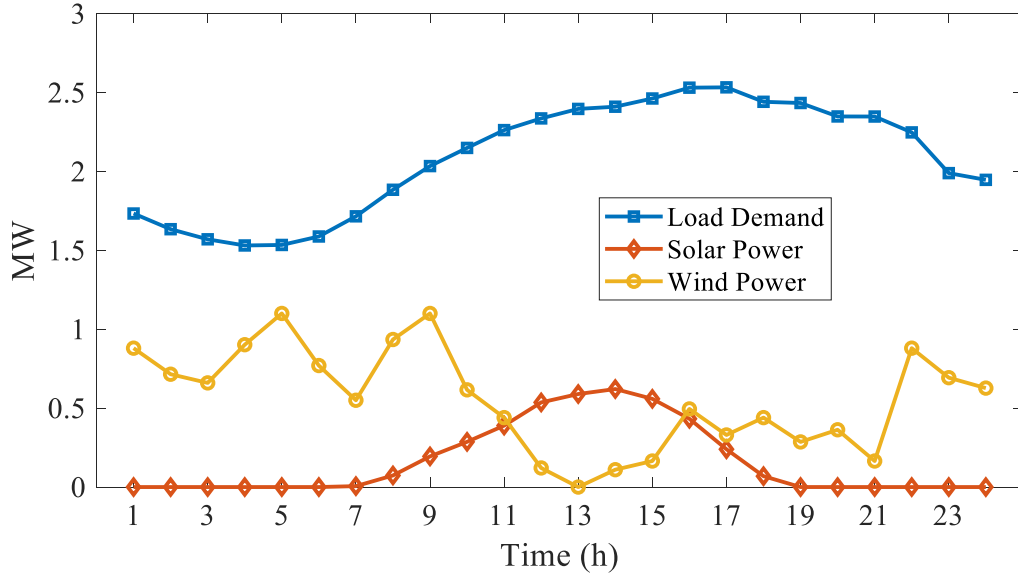


Figure 6.6 Hourly load demand and DRES output for day-ahead scheduling

### 6.7.3 Impacts of Target *PELC* on the Operating Costs

In this subsection, the impacts of changing the target *PELC*, which is set by the microgrid operator on the operating costs of the microgrid, are analyzed. For these studies, the 24-hour day ahead scheduling is considered. A single *PELC* is set for all hours of the scheduling horizon. Fig. 6.7 shows the variation in the operating costs as the target *PELC* is changed. As expected, as the target *PELC* is reduced, which means stricter operational reliability constraints are enforced, the operating costs for the microgrid increase. This increase continues until a certain *PELC* is reached. After that, the model becomes infeasible as the microgrid commits all available generation capacity. This is shown by a zero operating cost in Fig. 6.7. Also, from Fig. 6.7, note that the microgrid satisfies the criterion of  $1 \times 10^{-2}$  when the reliability constraints are not included. In particular, the operating costs remain the same from  $1 \times 10^{-2}$  to 1.

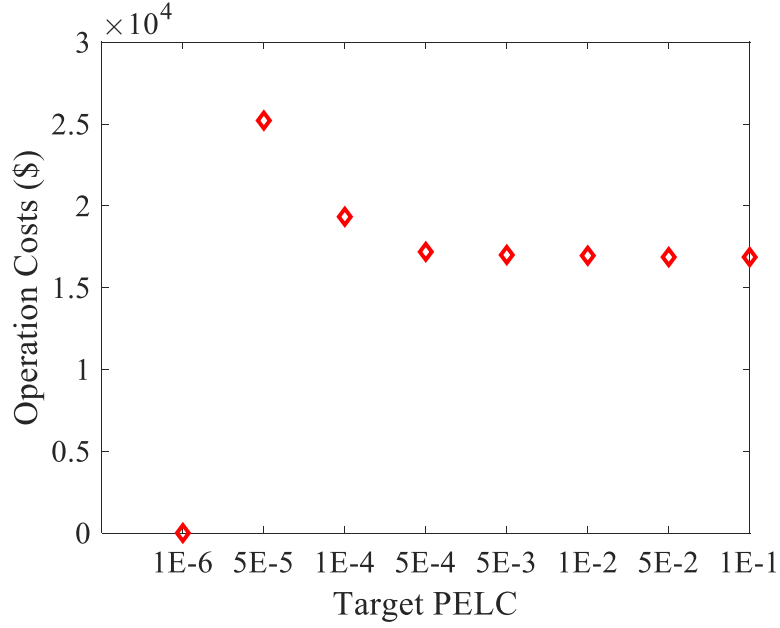


Figure 6.7 Variation in the total operating costs of microgrids with varying target *PELC*

## 6.8 Conclusion

This chapter proposes a new optimization model for the operational reliability-constrained scheduling of microgrids. To this end, chance-constrained optimization is adopted to include hourly *PELC* indices in the scheduling problem of microgrids. The explicit chance constraints in the model are reformulated using SAA. To render the model tractable, IS is adopted to distort the PDFs, and CE was used to obtain IS parameters. Case studies performed on a synthetic microgrid showed that the schedule obtained from the proposed model satisfies the operational reliability constraints set by the microgrid operator. Intra-day and day-ahead scheduling problems are solved to explain the results. The impacts of target *PELC* on the operation costs are also examined

## **Chapter 7**

### **Conclusion**

#### **7.1 Conclusion**

In this thesis, a new set of comprehensive tools for the operational reliability and risk evaluation of sustainable electric power systems and IEPGNs are proposed and developed. In the first step, a new computationally efficient simulation technique called FECS is adapted for the operational reliability of generating systems. The proposed simulation technique has two advantages: 1) it is able to integrate complicated PDFs of different components of power systems, e.g., wind power, and 2) it requires a significantly lower computational burden compared to CMCS. The simulation results have verified the advantages of the proposed approach. Additional case studies have indicated the impact of uncertainties of load and wind generation on the short-term reliability of generating systems.

Regarding the second step of the project, a novel hybrid analytical-simulation framework is proposed for the short-term risk assessment of wind-integrated composite power systems. The proposed framework has three key merits: first, it comprehensively models the uncertainty of wind speed during power systems operation; second, it includes the contingencies and constraints of transmission systems and therefore estimates more accurate risk indices; and third, it estimates short-term risk indices with a very low computational burden. The simulation results show that the proposed framework outperforms existing state-of-the-art approaches in capturing the impact of uncertainty of wind speed on the short-term risk indices. The results also indicate the excellent computational performance of the framework. Furthermore, for the first time, the short-term risk indices at individual buses are also calculated. The results also show the drawbacks of utilizing deterministic techniques to ensure the operational reliability of power systems.

The third step of the research builds upon the work performed in the second step. In particular, the third step aims to improve the uncertainty modeling of wind generation for operational reliability studies. To this end, a new data-driven approach to model the wind generation

uncertainty for the operational reliability studies is presented. The proposed modeling approach avoids the drawbacks of overfitting to limited wind generation data and includes the temporal correlation and multimodality of wind generation PDF. An IS technique is also modified to integrate the proposed modeling of wind generation. Case studies on two test systems indicate the impact of considering complex statistical features of wind generation on the operational risk indices of composite power systems.

In the fourth step, a novel framework for the operational reliability evaluation of IEPGNS is proposed. The framework has three notable features. First, it includes a detailed reliability model of natural gas pipelines to realistically evaluate the reliability indices. Second, it models the dual-fuel capabilities of DF-NGFGs that have been shown to improve the operational reliability of IEPGNS. Third, the linear formulation of the proposed optimization model and the adoption of CE-based IS ensures high computational efficiency of the proposed framework. The results indicate that the operational reliability indices of IEPGNS are improved when all three failure modes of pipelines are considered. In addition, the impacts of dual-fuel capabilities of DF-NGFGs and the different operational strategies of system operators on operational reliability indices are also demonstrated.

Finally, in the last step, a new optimization model for the operational reliability-constrained scheduling of microgrids is proposed. To this end, chance-constrained optimization is adopted to embed the hourly operational reliability indices in the scheduling problem of microgrids. The explicit chance constraints in the model are reformulated using SAA. IS is adopted to render the model tractable. The parameters of IS are obtained after making realistic assumptions and using CE optimization. Case studies performed on a synthetic microgrid showed that the schedule obtained from the proposed model satisfies the operational reliability constraints set by the microgrid operator. Intra-day and day-ahead scheduling problems are solved to explain the results in detail. The impacts of target *PELC* on the operating costs are also examined.

## 7.2 Suggestions for Future Work

For the future extension of this study, the following research works are recommended:

- The FEGS approach can be extended for calculating other reliability indices of sustainable electric power systems, such as EENS. In addition, this approach can also be applied to generate lists of cascading contingencies that lead to a specific event of interest. Multiple cascading paths can be generated, and their probabilities can be assessed.
- The conditional PDF models for wind speed in the operational reliability framework can be extended. In particular, dependence structure modeling can be employed to model the dependencies between multiple wind farms in power systems. For this purpose, copulas, such as C-Vine copulas, can be employed. This will lead to a more realistic evaluation of the operational reliability indices.
- To further improve the data-driven modeling of wind power uncertainty, advanced machine learning models can be implemented. In particular, generative adversarial networks can be used to provide a completely model-free method for generating wind power samples in the operational reliability evaluation process. Moreover, the application of Bayesian belief networks to incorporate the dependencies of wind power on wind speed, temperature, and other meteorological factors can be examined.
- The framework of the operational reliability evaluation of IEPGNs can be extended by including more detailed reliability models of gas sources. Also, the relationship of the output gas sources with important factors, such as temperature, can also be modeled and included in the reliability evaluation process.
- The operational reliability-constrained optimal scheduling model for microgrids can also incorporate advanced uncertainty models of DRES. Furthermore, multistate models for dispatchable generators and time-dependent failure rates can be included to extend the model. Theoretical work can also be performed to study the global optimality of the obtained solutions.

## **Appendix A**

### **Author's Vita**

Osama Aslam Ansari received the Bachelor of Electrical Engineering (B.E.E.) from the National University of Sciences and Technology (NUST), Islamabad, Pakistan, in 2015 with a CGPA of 3.95 out of 4.00. He received the Master of Science (M.Sc.) in Electrical Engineering from the University of Saskatchewan, Saskatoon, Canada, in 2017 with a grade of 96.25%. He is currently a Ph.D. candidate in Electrical Engineering at the University of Saskatchewan, Saskatoon, Canada.

Osama's research interests include power systems reliability, power systems operation, energy storage systems, and integration of renewable energy sources in power systems. Osama is a recipient of multiple scholarships and awards, including the "Top 25 under the age of 25 in Pakistan", Excellence in Sustainable Energy Leadership Award, 2014 and 2015 NUST Rector's High Achiever's Awards, Departmental Devolved Scholarships, Saskatchewan Innovation and Opportunity Scholarship, Russell William Haid Memorial Scholarship, Commendation Award at Hong Kong Polytechnic University Global Student Challenge and others. His complete profile can be accessed at <https://oaansari.com/>

## Appendix B

### Author's Bibliography

#### List of Publications

##### Peer-Reviewed Journal Papers

1. **O. A. Ansari**, and C. Y. Chung, “A hybrid framework for short-term risk assessment of wind-integrated composite power systems”, *IEEE Trans. Power Syst.*, vol. 34, no. 3, pp. 2334-2344, May 2019.
2. J. Zhan, **O. A. Ansari**, W. Liu, and C. Y. Chung, “An accurate bilinear cavern model for compressed air energy storage,” *Applied Energy*, vol. 272, pp. 752-768, May 2019.
3. **O. A. Ansari**, Y. Z. Gong, W. Liu, and C. Y. Chung, “Data-driven operational risk assessment of wind-integrated power systems via mixture models and importance sampling”, *Journal of Modern Power System and Clean Energy*, vol. 8, no. 3, pp. 437-445, May 2020.
4. **O. A. Ansari**, C. Y. Chung, and E. Zio, “A novel framework for operational reliability evaluation of integrated electric power-gas networks (IEPGNs)”, *IEEE Trans. Smart Grid*, (Early Access).
5. **O. A. Ansari**, and C. Y. Chung, “Operational reliability-constrained scheduling of microgrids via cross entropy-importance sampling-based sample average approximation”, *To be submitted to IEEE Trans. Smart Grid*.

##### Peer-Reviewed Conference Papers

1. **O. A. Ansari**, S. Mahdi Mazhari, Yuzhong Gong, and C. Y. Chung, “Short-term reliability evaluation of generating systems using fixed-effort generalized splitting”, *2020 IEEE Power and Energy Society General Meeting*, Montreal, 2020. (selected among “**Best Conference Papers**”)
2. **O. A. Ansari**, S. Bhattarai, R. Karki, and C. Y. Chung, “Reliability evaluation of bulk power system considering compressed air energy storage,” in *2017 IEEE Electrical Power and Energy Conference (EPEC)*, Saskatoon, 2017.

3. N. Safari, **O. A. Ansari**, A. Zare, and C. Y. Chung, “A novel decomposition-based localized short-term tidal current speed and direction prediction model,” in *2017 IEEE Power and Energy Society General Meeting*, Chicago, 2017.
4. **O. A. Ansari**, N. Safari, and C. Y. Chung, “Reliability assessment of microgrid with renewable generation and prioritized loads,” in *2016 IEEE Green Energy and Systems Conference (IGSEC)*, Long Beach 2016.
5. N. Safari, **O. A. Ansari**, and C. Y. Chung, “A predictive direct power control technique for transformerless grid connected PV systems application,” in *2016 IEEE Electrical Power and Energy Conference (EPEC)*, Ottawa, 2016.
6. D. Hameed, S. Hamayoon, A. A. Malik, and **O. A. Ansari**, “Solar grid-tied inverter with battery back-up for efficient solar energy harvesting,” in *2016 IEEE Smart Energy Grid Engineering (SEGE)*, Oshawa, 2016.

## Appendix C

### IEEE Reliability Test System (RTS)

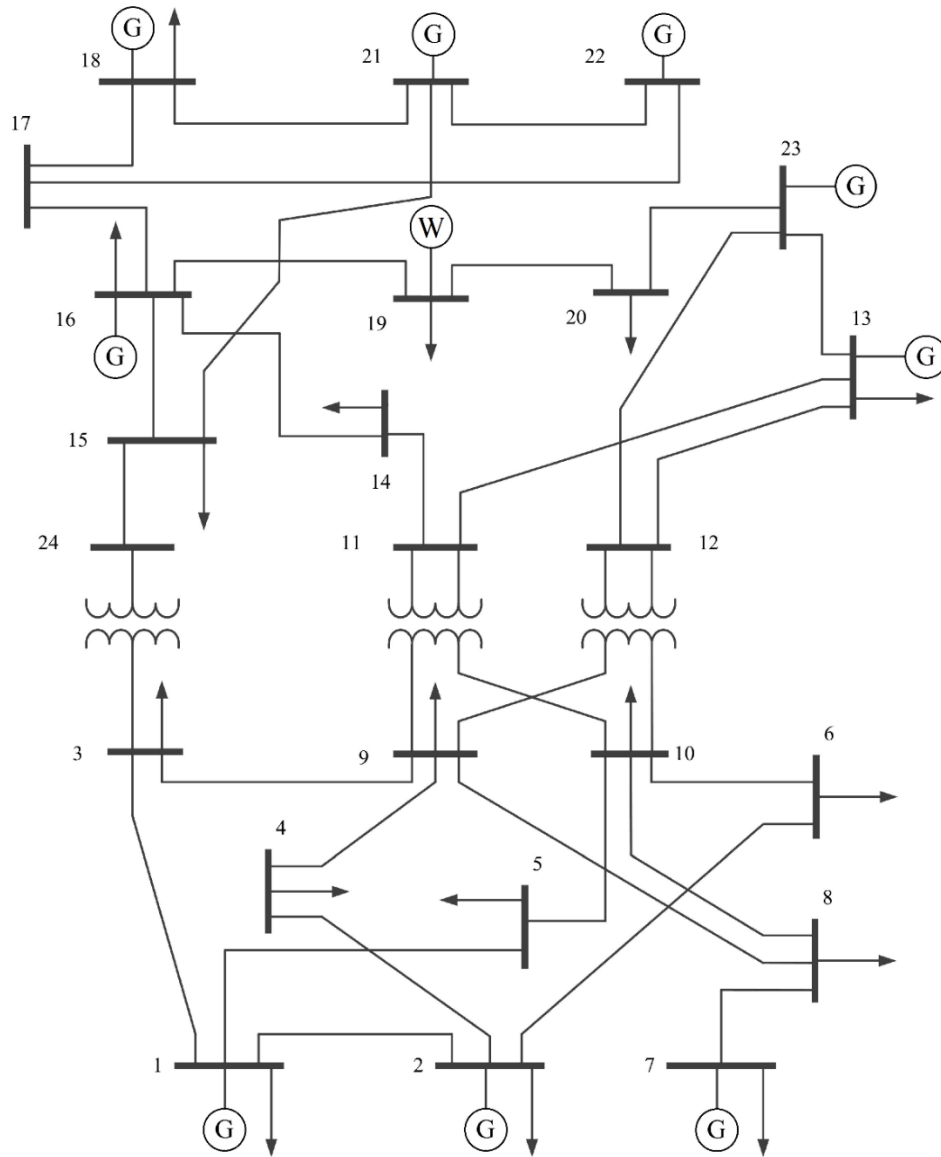


Figure C.1 Modified IEEE RTS with wind generation

## Appendix D

### Supplementary Data for IEPGNs

Table D.1 General parameters for natural gas networks

Parameter	Value
Specific gas constant $R$	$5.1828 \times 10^{-3} \text{ m}^3 \text{ bar} / \text{kgK}$
Gas temperature $T$	281.85 K
Gas compressibility $Z$	0.8
Speed of sound $c$	380 m/s
Natural gas density $\rho_0$	$0.68 \text{ kg} / \text{m}^3$
Specific heat ratio $\gamma$	1.32
Effective leak area factor $\omega$	0.9

Table D.2 CE optimization parameters

Parameter	Value
Multi-level parameter for cross entropy optimization	0.01
Number of samples for cross entropy optimization	10,000
Maximum number of cross entropy optimization iterations	10

Table D.3 Optimization parameters

Parameter	Value
Number of linearization points for Weymouth Equation (7-node gas network) per pipeline	20
Number of linearization points for Weymouth Equation (20-node Belgian gas network) per pipeline	60
Number of linearization points for Gas Release Rate Model	5

**Data for the 7-node gas network:**

Table D.4 Node data

<b>Bus</b>	<b>Type</b>	<b>Gas load (factor)</b>	<b>Minimum pressure (bar)</b>	<b>Maximum pressure (bar)</b>
<b>1</b>	Load	0.5	7.23	10.34
<b>2</b>	Load	0.15	9.65	11.72
<b>3</b>	Load	0.35	10.34	13.44
<b>4</b>	Node	0	4.82	6.89
<b>5</b>	Node	0	10.34	13.78
<b>6</b>	Source	0	11.03	16.54
<b>7</b>	Source	0	6.89	9.65

Table D.5 Pipeline data

<b>From</b>	<b>To</b>	<b><math>\psi</math></b>	<b>Active Pipe- line</b>	<b>Compres- sion Factor</b>	<b>Diameter (m)</b>	<b>Length (m)</b>	<b>Friction</b>	<b>MTTF (hour/outage)</b>
2	1	0.03925	0	0	0.8	82733	0.01098	1176
2	5	0.02909	0	0	0.8	150633	0.01098	1176
6	5	0.03514	0	0	0.8	103225	0.01098	1176
5	3	0.03374	0	0	0.8	111945	0.01098	1176
7	4	0.03886	0	0	0.8	84393	0.01098	1176
4	2	0.03886	1	2.5	0.8	84393	0.01098	1764

Table D.6 Gas generation data

<b>Node</b>	<b>Maximum Generation (kg/s)</b>	<b>Minimum Generation (kg/s)</b>	<b>MTTF (hour/outage)</b>
<b>6</b>	32.0924	0	1100
<b>7</b>	28.3483	0	950

Table D.7 Gas storage data

Node	Maximum Discharge (kg/s)	Maximum Charge (kg/s)	Current SOC (kg)	Minimum SOC (kg)	Maximum SOC (kg)
1	10.6975	10.6975	96277.12	38510.848	192554.24

Table D.8 NGFGs data

Electrical Bus	Gas Node	Maximum Power	Conversion Factor	MTTF (hour/outage)
1	5	220	0.04033	1100
6	2	20	0.05011	950

Table D.9 Parameters for the 4-state model of DF-NGFGs

Parameter	Value
$\mu_{12}$	0.033 transitions/hour
$\mu_{13}$	0.008 transitions/hour
$\mu_{14}$	$\lambda$ transitions/hour
$\mu_{21}$	0
$\mu_{23}$	0
$\mu_{24}$	$2\lambda$
$\mu_{31}$	0
$\mu_{32}$	0
$\mu_{34}$	0.025 transistions/hour
$\mu_{41}, \mu_{42}, \mu_{43}$	0

Where  $\lambda$  is the failure rate of the NGFG.

**Data for the 20-node Belgian gas network:**

The complete data for this network is available in: D. De Wolf, and Y. Smeers, “The gas transmission problem solved by an extension of the simplex algorithm,” *Management Science*, vol. 46, no. 11, pp. 1454-1465, Nov. 2000.

For the 20-node Belgian Gas Network, the MTTFs of all pipelines are assumed to be 1176 hours/outage. For compressors, the MTTFs are assumed to 1764 hours/outage.

Table D.10 NGFGs data

Electrical Bus	Gas Node	Maximum Power	Conversion Factor	MTTF (hour/outage)
18	5	400	0.04033	1100
23	13	350	0.05011	1150
21	14	400	0.05011	1100

No changes are made to the test systems’ data for the 6-bus power system and the 24-bus IEEE RTS.

For efficiency purposes, natural gas flows on pipelines are scaled down by a factor of 100. Corresponding equations are modified to include this scale factor.

### Gas Release Rate Model:

The coefficients of the gas release rate model in (8) are given as follows [23]:

$$\alpha_p = \frac{\pi \mathcal{D}_p^2 \sigma_p}{4} \sqrt{\gamma \rho_0 \left( \frac{2}{\gamma + 1} \right)^{(\gamma+1)(\gamma-1)}}, \quad (\text{D.1})$$

$$\beta_p = (4\sigma_p^2 \zeta_p / d_p) (2/(\gamma + 1))^{2/(\gamma-1)}. \quad (\text{D.2})$$

In (A.B.1) and (A.B.2),  $\mathcal{D}_p$  and  $\zeta_p$  represent the diameter and friction factor of the  $p$ th pipeline, respectively.  $\gamma$  and  $\rho_0$  are the specific heat ratio and density of natural gas at operating conditions.  $\sigma_p$  models the ratio of the effective hole area to the cross-sectional area of the pipeline, or

$$\sigma_p = \omega d_l^2 / \mathcal{D}_p^2, \quad (\text{D.3})$$

where  $d_l$  is the diameter of the leak and  $\omega$  is a constant modeling the irregular shape of the leak.

**Linearization Method:**

Let  $h(y)$  be a non-linear function of  $y$ , then using the incremental model,  $h(y)$  is linearized as

$$h(y) = h(y_1) + \sum_{i=1}^P (h(y_{i+1}) - h(y_i))\delta_i, \quad (\text{D.4})$$

$$y = y_1 + \sum_{i=1}^P (y_{i+1} - y_i)\delta_i, \quad (\text{D.5})$$

$$\delta_{i+1} \leq \alpha_i, \alpha_i \leq \delta_i \quad \forall i \in \{1, \dots, P-1\}, \quad (\text{D.6})$$

$$0 \leq \delta_i \leq 1, \quad \forall i \in \{1, \dots, P\}, \quad (\text{D.7})$$

where  $P$  is the number of points for linearization and  $\alpha$  is a binary variable.

## **Appendix E**

### **Copyright Permission Letters**

To Whom It May Concern:

I, Chi Yung Chung, hereby grant permission to Mr. Osama Aslam Ansari to reuse the following articles in his thesis titled “Operational Reliability and Risk Evaluation Frameworks for Sustainable Electric Power Systems”.

- O. A. Ansari, and C. Y. Chung, “A hybrid framework for short-term risk assessment of wind-integrated composite power systems”, *IEEE Trans. Power Syst.*, vol. 34, no. 3, pp. 2334-2344, May 2019.
- O. A. Ansari, Y. Z. Gong, W. Liu, and C. Y. Chung, “Data-driven operational risk assessment of wind-integrated power systems via mixture models and importance sampling”, *Journal of Modern Power System and Clean Energy*, vol. 8, no. 3, pp. 437-445, May 2020
- O. A. Ansari, C. Y. Chung, and E. Zio, “A novel framework for operational reliability evaluation of integrated electric power-gas networks (IEPGNs)”, *IEEE Trans. Smart Grid*, (Early Access).
- O. A. Ansari, and C. Y. Chung, “Operational reliability-constrained scheduling of microgrids via cross entropy-importance sampling-based sample average approximation”, *To be submitted to IEEE Trans. Smart Grid*.
- O. A. Ansari, S. Mahdi Mazhari, Yuzhong Gong, and C. Y. Chung, “Short-term reliability evaluation of generating systems using fixed-effort generalized splitting”, *2020 IEEE Power and Energy General Meeting, Montreal*.

I am aware that Mr. Ansari has made additions to the work “Short-term reliability evaluation of generating systems using fixed-effort generalized splitting”.

I am aware that all University of Saskatchewan theses are also posted in the digital USask eCommons thesis repository, making the thesis openly available on the internet.

Date:

Signature:

To Whom It May Concern:

I, Yuzhong Gong, hereby grant permission to Mr. Osama Aslam Ansari to reuse the following articles in his thesis titled “Operational Reliability and Risk Evaluation Frameworks for Sustainable Electric Power Systems”.

- O. A. Ansari, Y. Z. Gong, W. Liu, and C. Y. Chung, “Data-driven operational risk assessment of wind-integrated power systems via mixture models and importance sampling”, *Journal of Modern Power System and Clean Energy*, vol. 8, no. 3, pp. 437-445, May 2020
- O. A. Ansari, S. Mahdi Mazhari, Yuzhong Gong, and C. Y. Chung, “Short-term reliability evaluation of generating systems using fixed-effort generalized splitting”, *2020 IEEE Power and Energy General Meeting*, Montreal

I am aware that Mr. Ansari has made additions to the work “Short-term reliability evaluation of generating systems using fixed-effort generalized splitting”.

I am aware that all University of Saskatchewan theses are also posted in the digital USask eCommons thesis repository, making the thesis openly available on the internet.

Date:

Signature:

To Whom It May Concern:

I, W. Liu, hereby grant permission to Mr. Osama Aslam Ansari to reuse the following articles in his thesis titled “Operational Reliability and Risk Evaluation Frameworks for Sustainable Electric Power Systems”.

- O. A. Ansari, Y. Z. Gong, W. Liu, and C. Y. Chung, “Data-driven operational risk assessment of wind-integrated power systems via mixture models and importance sampling”, *Journal of Modern Power System and Clean Energy*, vol. 8, no. 3, pp. 437-445, May 2020

I am aware that all University of Saskatchewan theses are also posted in the digital USask eCommons thesis repository, making the thesis openly available on the internet.

Date:

Signature:

To Whom It May Concern:

I, S. Mahdi Mazhari, hereby grant permission to Mr. Osama Aslam Ansari to reuse the following articles in his thesis titled “Operational Reliability and Risk Evaluation Frameworks for Sustainable Electric Power Systems”.

- O. A. Ansari, S. Mahdi Mazhari, Yuzhong Gong, and C. Y. Chung, “Short-term reliability evaluation of generating systems using fixed-effort generalized splitting”, *2020 IEEE Power and Energy General Meeting, Montreal*

I am aware that all University of Saskatchewan theses are also posted in the digital USask eCommons thesis repository, making the thesis openly available on the internet.

I am aware that Mr. Ansari has made additions to the work “Short-term reliability evaluation of generating systems using fixed-effort generalized splitting”.

Date:

Signature:

To Whom It May Concern:

I, Enrico Zio, hereby grant permission to Mr. Osama Aslam Ansari to reuse the following articles in his thesis titled “Operational Reliability and Risk Evaluation Frameworks for Sustainable Electric Power Systems”.

- O. A. Ansari, C. Y. Chung, and E. Zio, “A novel framework for operational reliability evaluation of integrated electric power-gas networks (IEPGNs)”, *IEEE Trans. Smart Grid*, (Early Access).

I am aware that all University of Saskatchewan theses are also posted in the digital USask eCommons thesis repository, making the thesis openly available on the internet.

Date:

Signature:

## References

- [1] International Energy Agency (IEA), "Renewables 2019: Market analysis and forecast from 2019 to 2024," IEA, Oct. 2019. [Online]. Available: <https://www.iea.org/reports/renewables-2019>. [Accessed 10 Sep. 2020].
- [2] International Energy Agency (IEA), "Natural gas-fired power," 2020. [Online]. Available: [www.iea.org/reports/natural-gas-fired-power](http://www.iea.org/reports/natural-gas-fired-power). [Accessed 20 Sep. 2020].
- [3] J. Giraldez, F. Flores-Espino, S. MacAlpine and P. Asmus, "Phase I microgrid cost study: Data collection and analysis of microgrid costs in the United States," National Renewable Energy Laboratory (NREL), Golden, CO, USA, Oct. 2018.
- [4] H. Farhangi, "The path of the smart grid," *IEEE Power and Energy Magazine*, vol. 8, no. 1, pp. 18-28, Jan.-Feb. 2010.
- [5] K. Moslehi and R. Kumar, "A reliability perspective of the smart grid," *IEEE Trans. Smart Grid*, vol. 1, no. 1, pp. 57-64, Jun. 2010.
- [6] North American Electric Reliability Corporation, "Task 1.6 Probabilistic Methods," NERC, Atlanta, GA, USA, Jul. 2014.
- [7] North American Electric Reliability Corporation, "Short-Term Special Assessment: Operational Risk Assessment with High Penetration of Natural Gas-Fired Generation," NERC, Atlanta, GA, USA, May 2016.
- [8] P. Pourbeik, P. S. Kundur and C. W. Taylor, "The anatomy of a power grid blackout - root causes and dynamics of recent major blackouts," *IEEE Power and Energy Magazine*, vol. 4, no. 5, pp. 22-29, Sept.-Oct. 2006.
- [9] North American Electric Reliability Corporation (NERC), "Probabilistic adequacy and measures," NERC, Atlanta, GA, USA, Jul. 2018.

- [10] R. Billinton and W. Li, Reliability Assessment of Electrical Power Systems Using Monte Carlo Methods, New York, USA: Plenum, 1994.
- [11] A. J. Wood and B. F. Wollenberg, Power Generation, Operation, and Control, Hoboken, NJ, USA: Wiley, 1984.
- [12] North American Reliability Corporation (NERC), "RCR-35 Reliability coordinator reliability plan for the SaskPower subregion of the Midwest Reliability Organization," NERC, Atlanta, USA, 2008.
- [13] C. Thompson and J. Gilbertson, "Real-Time Transmission Congestion Management & Market Effects," 2020. [Online]. Available: [http://www.ercot.com/content/wcm/training\\_courses/109626/Constraint\\_Management.pptx](http://www.ercot.com/content/wcm/training_courses/109626/Constraint_Management.pptx). [Accessed 23 Sep. 2020].
- [14] T&D World, "California ISO adds real-time contingency analysis software," T&D World, 13 Apr. 2016. [Online]. Available: <https://www.tdworld.com/smart-grid/california-iso-adds-real-time-contingency-analysis-software>. [Accessed 21 October 2019].
- [15] J. Baranowski and D. J. French, "Operational use of contingency analysis at PJM," in *2012 IEEE PES General Meeting*, San Diego, CA, USA, 2012.
- [16] H. Holttinen, M. Milligan, E. Ela, N. Menemenlis, J. Dobschinski, B. Rawn, R. J. Bessa, D. Flynn, E. Gómez-Lázaro and N. K. Detlefsen, "Methodologies to determine operating reserves due to increased wind power," *IEEE Trans. Sustain. Energy*, vol. 3, no. 4, pp. 713-723, Oct. 2012.
- [17] R. Billinton and R. N. Allan, Reliability Evaluation of Power Systems, 2nd ed., New York, USA: Springer US, 1996.
- [18] C. L. T. Borges, "An overview of reliability models and methods for distribution systems with renewable energy distributed generation," *Renewable and Sustain. Energy Reviews*, vol. 16, no. 6, pp. 4008-4015, Aug. 2012.

- [19] R. N. Allan, R. Billinton, A. M. Breipohl and C. H. Grigg, "Bibliography on the application of probability methods in power system reliability evaluation," *IEEE Trans. Power Syst.*, vol. 14, no. 1, pp. 51-57, Feb. 1999.
- [20] W. Li, Risk Assessment of Power Systems - Models, Methods, and Applications, New York, NY, USA: IEEE Press, 2005.
- [21] R. Billinton and W. Wangdee, "Reliability-based transmission reinforcement planning associated with large-scale wind farms," *IEEE Trans. Power Syst.*, vol. 22, no. 1, pp. 34-41, Feb. 2007.
- [22] R. Billinton and D. Huang, "Incorporating wind power in generating capacity reliability evaluation using different models," *IEEE Trans. Power Syst.*, vol. 26, no. 4, pp. 2509-2517, Mar. 2011.
- [23] R. Billinton, B. Karki, R. Karki and G. Ramakrishna, "Unit commitment risk analysis of wind integrated power systems," *IEEE Trans. Power Syst.*, vol. 24, no. 2, pp. 930-939, May 2009.
- [24] X. Chen, J. Tang and W. Li, "Probabilistic operational reliability of composite power systems considering multiple meteorological factors," *IEEE Trans. Power Syst.*, pp. 1-1, 2019 (Early Access).
- [25] Y. Wang, "An adaptive importance sampling method for spinning reserve risk evaluation of generating systems incorporating virtual power plants," *IEEE Trans. Power Syst.*, vol. 33, no. 5, pp. 5082-5091, Sept. 2018.
- [26] A. Moshari, A. Ebrahimi and M. Fotuhi-Firuzabad, "Short-term impacts of DR programs on reliability of wind integrated power systems considering demand-side uncertainties," *IEEE Trans. Power Syst.*, vol. 31, no. 3, pp. 2481-2490, May 2016.
- [27] Z. Parvini, A. Abbaspour, M. Fotuhi-Firuzabad and M. Moeini-Aghaie, "Operational reliability studies of power systems in presence of energy storage systems," *IEEE Trans. Power Syst.*, vol. 33, no. 4, pp. 3691-3700, Jul. 2018.

- [28] Y. Ding, L. Cheng and Y. Zhang, "Operational reliability evaluation of restructured power systems with wind power penetration utilizing reliability network equivalent and time-sequential simulation approaches," *Journal of Modern Power Systems and Clean Energy*, vol. 2, no. 4, pp. 329-340, Dec. 2014.
- [29] F. Tagliaferri, B. P. Hayes, I. M. Viola and S. Z. Djokić, "Wind modeling with nested Markov chains," *Journal of Wind Engineering and Industrial Aerodynamics*, vol. 157, pp. 118-124, Aug. 2016.
- [30] T. Ackermann, *Wind Power in Power Systems*, Hoboken, NJ, USA: Wiley, 2012.
- [31] X. Han, Y. Qu, P. Wang and J. Yang, "Four-dimensional wind speed model for adequacy assessment of power systems with wind farms," *IEEE Trans. Power Syst.*, vol. 28, no. 3, pp. 2978-2985, Aug. 2013.
- [32] G. Valverde, A. T. Saric and V. Terzija, "Probabilistic load flow with non-Gaussian correlated random variables using Gaussian mixture models," *IET Genr., Trans., and Distrib.*, vol. 6, no. 7, pp. 701-109, Jul. 2012.
- [33] D. Ke, C. Y. Chung and Y. Sun, "A novel probabilistic optimal power flow model with uncertain wind power generation described by customized Gaussian mixture model," *IEEE Trans. Sustain. Energy*, vol. 7, no. 1, pp. 200-212, Jan. 2016.
- [34] O. A. Ansari, Y. Z. Gong, W. Liu and C. Y. Chung, "Data-driven operational risk assessment of wind-integrated power systems via mixture models and importance sampling," *Journal of Modern Power System and Clean Energy*, vol. 8, no. 3, pp. 437-445, May 2020.
- [35] R. Doherty and M. O'Malley, "A new approach to quantify reserve demand in systems with significant installed wind capacity," *IEEE Trans. Power Syst.*, vol. 20, no. 2, pp. 587-595, May 2005.
- [36] S. Tewari, C. J. Geyer and N. Mohan, "A statistical model for wind power forecast error and its application to the estimation of penalties in liberalized markets," *IEEE Trans. Power Syst.*, vol. 20, no. 3, pp. 1440-1446, Aug. 2005.

- [37] H. Bludszuweit, J. Dominguez-Navarro and A. Llombart, "Statistical analysis of wind power forecast error," *IEEE Trans. Power Syst.*, vol. 23, no. 3, pp. 983-991, Aug. 2008.
- [38] C. Tang, J. Xu, Y. Sun, J. Liu, X. Li, D. Ke, J. Yang and X. Peng, "A versatile mixture distribution and its application in economic dispatch with multiple wind farms," *IEEE Trans. Sustain. Energy*, vol. 8, no. 4, pp. 1747-1762, Oct. 2017.
- [39] K. Bruninx and E. Delarue, "A statistical description of the error on wind power forecasts for probabilistic reserve sizing," *IEEE Trans. Sustain. Energy*, vol. 5, no. 3, pp. 995-1002, Jul. 2014.
- [40] H. A. Nielsen, H. Madsen and T. S. Nielsen, "Using quantile regression to extend an existing wind power forecasting system with probabilistic forecasts," *Wind Energy*, vol. 9, pp. 95-108, 2006.
- [41] B. Khorramdel, C. Y. Chung, N. Safari and G. C. D. Price, "A fuzzy adaptive probabilistic wind power prediction framework using diffusion kernel density estimators," *IEEE Trans. Power Syst.*, vol. 33, no. 6, pp. 7109-7121, Nov. 2018.
- [42] R. Billinton and R. N. Allan, *Reliability Evaluation of Engineering Systems*, 2nd ed., New York, NY, USA: Springer, 1992.
- [43] L. T. Anstine, R. E. Burke, J. E. Casey, R. Holgate, R. S. John and H. G. Stewart, "Application of probability methods to the determination of spinning reserve requirements for the Pennsylvania-New Jersey-Maryland interconnection," *IEEE Trans. Power App. Syst.*, vol. 82, no. 68, pp. 726-735, Oct. 1963.
- [44] R. Billinton and A. V. Jain, "Unit derating levels in spinning reserve studies," *IEEE Trans. Power Apparatus and Systems*, Vols. PAS-90, no. 4, pp. 1677-1687, Jul. 1971.
- [45] R. Billinton and A. V. Jain, "The effect of rapid start and hot reserve units in spinning reserve studies," *IEEE Trans. Power Apparatus and Systems*, Vols. PAS-91, no. 2, pp. 511-516, Mar. 1972.

- [46] S. Thapa, R. Karki and R. Billinton, "Utilization of the area risk concept for operational reliability evaluation of a wind-integrated power system," *IEEE Trans. Power Syst.*, vol. 28, no. 4, pp. 4771-4779, Nov. 2013.
- [47] M. Fotuhi-Firuzabad, R. Billinton and S. Aboreshaid, "Response health constraints in economic load dispatch considering standby bunits, interruptible loads and postponable outages," *IEEE Proceedings - Genr., Trans., and Distrib.*, vol. 143, no. 6, pp. 599-607, Nov. 1996.
- [48] S. Thapa and R. Karki, "Reliability benefit of energy storage in wind integrated power system operation," *IET Generation, Transmission and Distribution*, vol. 10, no. 3, pp. 807-814, Mar. 2016.
- [49] N. Z. Xu and C. Y. Chung, "Well-being analysis of generating systems considering electric vehicle charging," *IEEE Trans. Power Syst.*, vol. 29, no. 5, pp. 2311-2320, Sep. 2014.
- [50] N. Z. Xu and C. Y. Chung, "Uncertainties of EV charging and effects on well-being analysis of generating systems," *IEEE Trans. Power Syst.*, vol. 30, no. 5, pp. 2547-2557, Sep. 2015.
- [51] C. Liang, P. Wang, X. Han, W. Qin, R. Billinton and W. Li, "Operational reliability and economics of power systems with considering frequency control processes," *IEEE Trans. Power Syst.*, vol. 32, no. 4, pp. 2570-2580, Jul. 2017.
- [52] Y. Sun, P. Wang, L. Cheng and H. Liu, "Operational reliability assessment of power systems considering condition-dependent failure rate," *IET Genr., Trans., and Distrib.*, vol. 4, no. 1, pp. 60-72, Jan. 2010.
- [53] Y. Ding, C. Singh, L. Goel, J. Østergaard and P. Wang, "Short-term and medium-term reliability evaluation for power systems with high penetration of wind power," *IEEE Trans. Sustain. Energy*, vol. 5, no. 3, pp. 896-906, Jul. 2014.
- [54] D. P. Kroese, T. Taimre and Z. I. Botev, *Handbook of Monte-Carlo Methods*, Hoboken, NJ, USA: Wiley, 2011.

- [55] A. M. Leite da Silva, J. F. Costa Castro and R. A. González-Fernández, "Spinning reserve assessment under transmission constraints based on cross-entropy method," *IEEE Trans. Power Syst.*, vol. 31, no. 2, pp. 1624-1632, Mar. 2016.
- [56] A. M. Leite da Silva, J. F. Costa Castro and R. Billinton, "Probabilistic assessment of spinning reserve via cross-entropy method considering renewable sources and transmission restrictions," *IEEE Trans. Power Syst.*, vol. 33, no. 4, pp. 4574-4582, Jul. 2018.
- [57] Y. Wang, C. Guo and Q. H. Wu, "A cross-entropy-based three-stage sequential importance sampling for composite power system short-term reliability evaluation," *IEEE Trans. Power Syst.*, vol. 28, no. 4, pp. 4254-4263, Nov. 2013.
- [58] W. Wadman, D. Crommelin and J. Frank, "Applying a splitting technique to estimate electrical grid reliability," in *Proceedings of the 2013 Winter Simulation Conference*, Washington, DC, USA, 2013.
- [59] T. Ding, C. Li, C. Yan, F. Li and Z. Bie, "A bilevel optimization model for risk assessment and contingency ranking in transmission system reliability evaluation," *IEEE Trans. Power Syst.*, vol. 32, no. 5, pp. 3803-3813, Sep. 2017.
- [60] H. Liu, Y. Sun, L. Cheng, P. Wang and F. Xiao, "Online short-term reliability evaluation using a fast sorting technique," *IET Genr., Trans., and Distrib.*, vol. 2, no. 1, pp. 139-148, Jan. 2008.
- [61] R. Billinton, "Criteria used by Canadian utilities in the planning and operation of generating capacity," *IEEE Trans. Power Syst.*, vol. 3, no. 4, pp. 1488-1493, Nov. 1988.
- [62] A. Papoulis and S. U. Pillai, *Probability, Random Variables and Stochastic Processes*, 4th ed., New York, NY, USA: McGraw-Hill, 2002.
- [63] R. Y. Rubinstein and D. P. Kroese, *Simulation and the Monte Carlo Methods*, 2nd ed., New York, NY, USA: Wiley, 2007.

- [64] R. Billinton and A. Jonnavithula, "Composite system adequacy assessment using sequential Monte Carlo simulation with variance reduction techniques," *IEE Proc. Genr., Transm., Distrib.*, vol. 144, no. 1, pp. 1-6, Jan. 1997.
- [65] P. L'Ecuyer, V. Demers and B. Tuffin, "Rare events, splitting, and quasi-Monte Carlo," *ACM Trans. on Modeling and Computer Simulation*, vol. 17, no. 2, pp. 1-44, Apr. 2007.
- [66] N. J. J. Garveks, "The splitting method in rare event simulation," University of Twente, The Netherlands, 2000.
- [67] Z. I. Botev and D. P. Kroese, "Efficient Monte Carlo simulation via the generalized splitting method," *Statistics and Computing*, vol. 22, no. 1, pp. 1-16, Jan. 2012.
- [68] B. Hua, Z. Bie, S. K. Au and X. Wang, "Extracting rare failure events in composite system reliability evaluation via subset simulation," *IEEE Trans. Power Syst.*, vol. 30, no. 2, pp. 753-762, Mar. 2015.
- [69] R. Karki, S. Thapa and R. Billinton, "A simplified risk-based method for short-term wind power commitment," *IEEE Trans. Sustain. Energy*, vol. 3, no. 3, pp. 498-504, Jul. 2012.
- [70] P. Wang, Z. Gao and L. B. Tjernberg, "Operational adequacy studies of power systems with wind farms and energy storages," *IEEE Trans. Power Syst.*, vol. 27, no. 4, pp. 2377-2384, Nov. 2012.
- [71] Y. Wang, C. Guo, Q. Wu and S. Dong, "Adaptive sequential importance sampling technique for short-term composite power system adequacy evaluation," *IET Gener., Transm., and Distrib.*, vol. 8, no. 4, pp. 730-741, Apr. 2014.
- [72] Y. Feng, W. Wu, B. Zhang and W. Li, "Power system operation risk assessment using credibility theory," *IEEE Trans. Power Syst.*, vol. 23, no. 3, pp. 1309-1318, Aug. 2008.
- [73] R. Y. Rubinstein and D. P. Kroese, *The Cross-Entropy Method*, 1st ed., New York, NY, USA: Springer, 2004.

- [74] A. M. Leite da Silva, R. A. González-Fernández and C. Singh, "Generating capacity reliability evaluation based on Monte Carlo simulation and cross-entropy methods," *IEEE Trans. Power Syst.*, vol. 28, no. 4, pp. 4598-4606, Nov. 2013.
- [75] R. A. González-Fernández, A. M. Leite da Silva, L. C. Resendé and M. T. Schilling, "Composite systems reliability evaluation based on Monte Carlo simulation and cross-entropy methods," *IEEE Trans. Power Syst.*, vol. 28, no. 4, pp. 4598-4606, Nov. 2013.
- [76] E. Tómasson and L. Söder, "Improved importance sampling for reliability evaluation of composite power systems," *IEEE Trans. Power Syst.*, vol. 32, no. 3, pp. 2426-2434, May 2017.
- [77] Reliability Test System Task Force of the IEEE Subcommittee on the Application of Probability Methods, "IEEE reliability test system," *IEEE Trans. Power App. Syst.*, vol. 1, pp. 2047-2054, 1979.
- [78] S. Babicki, D. Arndt, A. Marcu, Y. Liang, J. R. Grant, A. Maciejewski and D. S. Wishart, "Heatmapper: web-enabled heat mapping for all," *Nucleic Acids Res.*, May 2016.
- [79] M. A. Ortega-Vazquez, "Optimizing the spinning reserve requirements," 2006.
- [80] H. B. Gooi, D. P. Mendes, K. R. W. Bell and D. S. Kirschen, "Optimal scheduling of spinning reserve," *IEEE Trans. Power Syst.*, vol. 14, no. 4, pp. 1485-1492, Nov. 1999.
- [81] Global Wind Energy Council, "Global wind report: Annual market update 2017," 2017.
- [82] M. Liu, W. Li, J. Yu and Z. Ren, "Reliability evaluation of tidal and wind power generation system with battery energy storage," *Journal of Modern Power System and Clean Energy*, vol. 4, no. 4, pp. 636-647, Oct. 2016.
- [83] R. Billinton, R. Karki, Y. Gao, D. Huang, P. Hu and W. Wangdee, "Adequacy assessment considerations in wind integrated power systems," *IEEE Trans. Power Syst.*, vol. 27, no. 4, pp. 2297-2305, Nov. 2012.

- [84] S. Sulaeman, M. Benidris, J. Mitra and C. Singh, "A wind farm reliability model considering both wind variability and turbine forced outages," *IEEE Trans. Sustain. Energy*, vol. 8, no. 2, pp. 629-637, Apr. 2017.
- [85] O. A. Ansari and C. Y. Chung, "A hybrid framework for short-term risk assessment of wind-integrated composite power systems.," *IEEE Trans. Power Syst.*, vol. 34, no. 3, pp. 2334-2344, May 2019.
- [86] Y. Wang, Q. Hu and S. Pei, "Wind power curve modeling with asymmetric error distribution," *IEEE Trans. Sustain. Energy*, pp. 1-1, 2019 (Early Access).
- [87] L. Geng, Y. Zhao and W. Li, "Enhanced cross entropy method for composite power system reliability evaluation," *IEEE Trans. Power Syst.*, vol. 34, no. 4, pp. 3129-3139, Jul. 2019.
- [88] J. Cai, Q. Xu, M. Cao and B. Yang, "A novel importance sampling method of power system reliability assessment considering multi-state units and correlation between wind speed and load," *International Journal of Electrical Power and Energy Syst.*, vol. 109, pp. 217-226, Jul. 2019.
- [89] F. Ge, Y. Ju, Z. Qi and Y. Lin, "Parameter estimation of a Gaussian mixture model for wind power forecast error by Riemann L-BFGS optimization," *IEEE Access*, vol. 6, pp. 38892-38899, Jul. 2018.
- [90] C. M. Bishop, *Pattern Recognition and Machine Learning*, 1st ed., New York, NY, USA: Springer, 2006.
- [91] D. W. Scott, *Multivariate Density Estimation: Theory, Practice and Visualization*, 2nd ed., Hoboken, NJ, USA: Wiley, 2015.
- [92] A. L. Rojas, "Conditional density estimation using finite mixture models with an application to astrophysics," *Center for Automatic Learning and Discovery, Department of Statistics, Carnegie Mellon University*, 2005.

- [93] G. McLachlan and D. Peel, *Finite Mixture Models*, 1st ed., New York, NY, USA: Wiley, 2000.
- [94] K. P. Murphy, *Machine Learning: A Probabilistic Approach*, Cambridge, USA: The MIT Press, 2012.
- [95] P. E. E. Sotavento, "Wind Power Data," 2011. [Online]. Available: <http://www.sotaventogalicia.com/es>. [Accessed 20 Aug. 2019].
- [96] North American Electric Reliability Corporation (NERC), "Special reliability assessment: Potential bulk power system impacts due to severe disruptions on the natural gas system," NERC, Atlanta, GA, USA, Nov. 2017.
- [97] Z. Zeng, T. Ding, X. Xu, Y. Yang and Z. Dong, "Reliability evaluation for integrated power-gas systems with power-to-gas and gas storages," *IEEE Trans. Power Syst.*, vol. 35, no. 1, pp. 571-583, Jan. 2020.
- [98] S. Wang, Y. Ding, C. Ye and C. Wan, "Reliability evaluation of integrated electricity-gas system utilizing network equivalent and integrated optimal power flow techniques," *J. Mod. Power Syst. Clean Energy*, vol. 7, no. 6, pp. 1523-1535, Nov. 2019.
- [99] M. Bao, Y. Ding, C. Singh and C. Shao, "A multi-state model for reliability assessment of integrated gas and power systems utilizing universal generating function techniques," *IEEE Trans. Smart Grid*, vol. 10, no. 6, pp. 6271-6283, Nov. 2019.
- [100] M. Bao, Y. Ding, C. Shao, Y. Yang and P. Wang, "Nodal reliability evaluation of interdependent gas and power systems considering cascading effects," *IEEE Trans. Smart Grid*, vol. 11, no. 5, pp. 4090-4104, Sep. 2020.
- [101] Z. Bao, JiangZ and L. Wu, "Evaluation of bi-directional cascading failure propagation in integrated electricity-natural gas system," *Int. J. Elect. Power and Energy Syst.*, vol. 121, Oct. 2020.

- [102] Y. Liu, Y. Su, Y. Xiang, J. Liu, L. Wang and W. Wu, "Operational reliability assessment for gas-electric integrated distribution feeders," *IEEE Trans. Smart Grid*, vol. 10, no. 1, pp. 1091-1100, Jan. 2019.
- [103] M. H. Shariatkah, M. R. Haghifam, M. Parsa-Moghaddam and P. Siano, "Modeling the reliability of multi-carrier energy systems considering dynamic behavior of thermal loads," *Energy and Buildings*, vol. 103, pp. 375-383, Sep. 2015.
- [104] S. Wang, C. Shao, Y. Ding and J. Yan, "Operational reliability of multi-energy customers considering service-based self-scheduling," *Applied Energy*, vol. 254, Nov. 2019.
- [105] European Gas Pipeline Incident Data Group (EGIG), "10th report of the European Gas Pipeline Incident Data Group (period 1970-2016)," EGIG, Groningen, Netherlands, Mar. 2018.
- [106] H. Su, J. Zhang, E. Zio, N. Yang, X. Li and Z. Zhang, "An integrated systemic method for supply reliability assessment of natural gas pipeline networks," *Applied Energy*, vol. 209, pp. 489-501, Jan. 2018.
- [107] U.S. Energy Information Administration (EIA), "Natural gas-burning power plant operations vary during periods of cold weather," U.S. EIA, Jan. 2019. [Online]. Available: <https://www.eia.gov/todayinenergy/detail.php?id=37992>. [Accessed 25 Sep. 2020].
- [108] X. Zhang, M. Shahidepour, A. Alabdulwahab and A. Abusorrah, "Security-constrained co-optimization planning of electricity and natural gas transportation infrastructures," *IEEE Trans. Power Syst.*, vol. 30, no. 6, pp. 2954-2993, Nov. 2015.
- [109] North American Electric Reliability Corporation (NERC), "2013 special reliability assessment: Accommodating an increased dependence on natural gas for electric power: Phase-II: A vulnerability and scenario assessment for the North American bulk power system," NERC, Atlanta, GA, USA, May 2013.
- [110] Z. Han and G. W. Weng, "An overview of quantitative risk analysis methods for natural gas pipelines," *J. China Safety Science*, vol. 19, pp. 154-164, Jan. 2009.

- [111] Y.-D. Jo and D. A. Crowl, "Individual risk analysis of high-pressure natural pipelines," *J. Loss Prevention in the Process Industries*, vol. 21, no. 6, pp. 589-595, Nov. 2008.
- [112] E. Zio, *The Monte Carlo Simulation Method for System Reliability and Risk Analysis*, London, UK: Springer, 2013.
- [113] C. Liu, M. Shahidehpour, Y. Fu and Z. Li, "Security-constrained unit commitment with natural gas transmission constraints," *IEEE Trans. Power Syst.*, vol. 24, no. 3, pp. 1523-1536, Aug. 2009.
- [114] D. De Wolf and Y. Smeers, "The gas transmission problem solved by an extension of the simplex algorithm," *Management Science*, vol. 46, no. 11, pp. 1454-1465, Nov. 2000.
- [115] N. Hatziargyriou, H. Asano, M. R. Iravani and C. Marnay, "Microgrids: An overview of ongoing research, development and demonstration projects," *IEEE Power and Energy Mag.*, vol. 5, no. 4, pp. 78-94, Jul./Aug. 2007.
- [116] A. Khodaei, "Microgrid optimal scheduling with multi-period islanding constraints," *IEEE Trans. Power Syst.*, vol. 29, no. 3, pp. 1383-1392, May 2014.
- [117] J. Zhao and Z. Xu, "Ramp-limited optimal dispatch strategy for PV-embedded microgrid," *IEEE Trans. Power Syst.*, vol. 32, no. 2, pp. 4155-4157, Sep. 2017.
- [118] C. Zhang, Y. Xu, Z. Y. Dong and J. Ma, "Robust operation of microgrids via two-stage coordinated energy storage and direct load control," *IEEE Trans. Power Syst.*, vol. 32, no. 4, pp. 2858-2868, Jul. 2017.
- [119] S. Esmaili, A. Anvari-Moghaddam and S. Jadid, "Optimal operation scheduling of a microgrid incorporating battery swapping stations," *IEEE Trans. Power Syst.*, vol. 34, no. 6, pp. 5063-5072, Nov. 2019.
- [120] Z. Bao, Q. Zhou, Q. Yang, L. Xu and T. Wu, "A mult time-scale and multi energy-type coordinated microgrid scheduling solution - Part I: Model and methodology," *IEEE Trans. Power Syst.*, vol. 30, no. 5, pp. 2257-2266, Sep. 2015.

- [121] F. Farzan, M. A. Jafari, R. Masiello and Y. Lu, "Toward optimal day-ahead scheduling and operation control of microgrids under uncertainty," *IEEE Trans. Smart Grid*, vol. 6, no. 2, pp. 499-507, Mar. 2015.
- [122] Z. Shi, H. Liang, S. Huang and V. Dinavahi, "Distributionally-robust chance-constrained energy management for islanded microgrids," *IEEE Trans. Smart Grid*, vol. 10, no. 2, pp. 2234-2244, Mar. 2019.
- [123] A. Kavousi-Fard, A. Zare and A. Khodaei, "Effective dynamic scheduling of reconfigurable microgrids," *IEEE Trans. Power Syst.*, vol. 33, no. 5, pp. 5519-5530, Sep. 2018.
- [124] O. A. Ansari, N. Safari and C. Y. Chung, "Reliability assessment of microgrid with renewable generation and prioritized loads," in *2016 IEEE Green Energy and Systems Conference (IGESC)*, Long Beach, CA, USA, Nov. 2016.
- [125] H. Qiu, W. Gu, Y. Xu, W. Yu, G. Pan and P. Liu, "Tri-level mixed-integer optimization for two-stage microgrid dispatch with multi-uncertainties," *IEEE Trans. Power Syst.*, vol. 35, no. 5, pp. 3636-3647, Sep. 2020.
- [126] V. Sarfi and H. Livani, "An economic-reliability security-constrained optimal dispatch for microgrids," *IEEE Trans. Power Syst.*, vol. 33, no. 6, pp. 6776-6786, Nov. 2018.
- [127] M. Vahedipour-Dahraie, H. Rashidizadeh-Kermani, A. Anvari-Moghaddam and J. M. Guerrerreo, "Stochastic risk-constrained scheduling of renewable-powered autonomous microgrids with demand response actions: Reliability and economic implications," *IEEE Trans. Ind. Appl.*, vol. 56, no. 2, pp. 1882-1895, Mar./Apr. 2020.
- [128] Y. Li, Z. Yang, G. Li, D. Zhao and W. Tian, "Optimal scheduling of an isolated microgrid with battery storage considering load and renewable generation uncertainties," *IEEE Trans. Ind. Elect.*, vol. 66, no. 2, pp. 1565-1575, Feb. 2019.
- [129] A. A. Bashir, M. Pourakbari-Kasmaei, J. Contreras and M. Lehtonen, "A novel energy scheduling framework for reliable and economic operation of islanded and grid-connected microgrids," *Electric Power Syst. Research*, vol. 171, pp. 85-96, Jun. 2019.

- [130] J. Barrera, T. Homem-de-Mello, E. Moreno, B. K. Pagnoncelli and G. Canessa, "Chance-constrained problems and rare events: an importance sampling approach," *Math. Program.*, vol. 157, pp. 153-189, Sep. 2016.
- [131] H. Wu, M. Shahidehpour, Z. Li and W. Tan, "Chance-constrained day-ahead scheduling in stochastic power system operation," *IEEE Trans. Power Syst.*, vol. 29, no. 4, pp. 1583-1591, Jul. 2014.
- [132] A. Kargarian, Y. Fu and H. Wu, "Chance-constrained system of systems based operation of power systems," *IEEE Trans. Power Syst.*, vol. 31, no. 5, pp. 3404-3413, Sep. 2016.
- [133] Q. Wang, Y. Guan and J. Wang, "A chance-constrained two-stage stochastic program for unit commitment with uncertain wind power output," *IEEE Trans. Power Syst.*, vol. 27, no. 1, pp. 206-215, Feb. 2012.
- [134] J. Kim, A. Bucklew and I. Dobson, "Splitting method for speedy simulation of cascading blackouts," *IEEE Trans. Power Syst.*, vol. 28, no. 3, pp. 3010-3017, Aug. 2013.
- [135] S.-P. Wang, A. Chen, C.-W. Liu, C.-H. Chen and J. Shortle, "Efficient splitting simulation for blackout analysis," *IEEE Trans. Power Syst.*, vol. 30, no. 4, pp. 1775-1783, Jul. 2015.